Dipeptidyl peptidase 4 inhibitors and Glucagon-like peptide-1 receptor agonist mitigate inflammation and fibrosis in models of Non-alcoholic steatohepatitis and biliary fibrosis

A Thesis for the award of the degree of

DOCTOR OF NATURAL SCIENCES

Submitted at

Faculty of Chemistry, Pharmacy and Geoscience

Johannes Gutenberg-University Mainz

By

Xiaoyu Wang

Born in Liaoning, China

On 12.20.1985

Mainz, October 2016

Dean:

1. Reviewer:

2. Reviewer:

Day of defense:

Declaration

“I hereby declare that I wrote the dissertation submitted without any unauthorized external assistance and used only sources acknowledged in the work. All textual passages which are appropriated verbatim or paraphrased from published and unpublished texts as well as all information obtained from oral sources are duly indicated and listed in accordance with bibliographical rules. In carrying out this research, I complied with the rules of standard scientific practice as formulated in the statutes of Johannes Gutenberg-University Mainz to insure standard scientific practice.”

Xiaoyu Wang

Summary

Non-alcoholic fatty liver disease (NAFLD) is currently the most common cause of chronic liver disease. 10-15% of patients with NAFLD present with non-alcoholic steatohepatitis (NASH), characterized by hepatocyte apoptosis, severe liver inflammation, steatosis, and fibrosis, with a high risk of progression to cirrhosis and primary liver cancer. Notably, morbidity and mortality in earlier stages of NAFLD/NASH are largely due to complications of the metabolic syndrome. However, studies that explore therapeutic modalities that address both liver inflammation and the metabolic syndrome are limited.

The incretin glucagon-like peptide-1 (GLP-1) is secreted postprandially from intestinal L-cells, pancreatic α-cells and from neurons of the caudal solitary tract. While it controls food intake in the central nervous system (CNS), intestinal GLP-1 stimulates pancreatic insulin secretion and inhibits glucagon release via the GLP-1 receptor (GLP-1R) leading to improved insulin signaling and glucose uptake in liver, adipose tissue, and muscle which in turn reduces hepatic gluconeogenesis. Options for pharmacological modulation of GLP-1 function include GLP-1 mimetics that directly increase the action of GLP-1, or alternatively the inhibition of the ubiquitously expressed cell surface enzyme dipeptidyl peptidase-4 (DPP-4) that induces the proteolytic inactivation of GLP-1. GLP-1 mimetics and DPP-4 inhibitors are increasingly used to manage type 2 diabetes (T2D). In animal models of NAFLD and NASH, GLP-1 mimetics and DPP-4 inhibitors have anti-inflammatory and anti-oxidative effects. However, till now *in vivo* liver studies with DPP-4 inhibitors and GLP-1R agonists were largely limited to hepatocyte damage or steatosis and in-depth studies of liver inflammation and fibrosis with these agents are generally missing. Moreover, the assessment of GLP-1 mimetics and DPP-4 inhibitors on macrophage polarization has not been properly addressed.

Here, I present a detailed *in vivo* study of two major DPP-4 inhibitors (Linagliptin and Sitagliptin) and also the long-acting GLP-1R agonist Bydureon (BY). The therapeutic efficacy of these agents was tested using the methionine choline deficient (MCD) diet model of severe lipoapoptotic liver injury, and the Mdr2$^{-/-}$ model of biliary fibrosis, both of which represent key pathologies of advanced NASH. Moreover, I determined the distinct role of pro-inflammatory versus anti-inflammatory

monocytes/macrophages in vitro and during initiation and progression of liver damage in vivo, and thus established a mechanistic link between macrophage polarization and disease activity.

MCD mice developed pronounced hepatic steatosis, inflammation, fibrosis and apoptosis compared to methionine and choline sufficient (MCS) controls. Here, the use of the MCD model which lacks insulin resistance, an important comorbidity in human NASH, proved advantageous, since it rules out insulin resistance/T2D as an indirect contributor to vascular inflammation and endothelial dysfunction, which is relevant in view of the current discussion if and how far the liver, the pre-diabetic/diabetic state, or both need to be addressed to treat the disease. The here presented study provides clear evidence for a beneficial role of DPP-4 inhibitors and the GLP-1R agonist BY in the treatment of key aspects of NASH (monocyte-macrophage infiltration and unfavorable polarization, hepatocyte lipoapoptosis) and resultant liver fibrosis. In addition, these therapies ameliorated hepatic inflammation and exerted a modest direct anti-fibrotic effect, as demonstrated in the $Mdr2^{-/-}$ model of biliary fibrosis.

Interestingly, my data demonstrated that the beneficial actions of DPP-4 inhibitors are a class effect, since Linagliptin and Sitagliptin showed similar efficacy across all parameters measured. Moreover, the analysis of M1 and M2 macrophage subtypes in the NASH and $Mdr2^{-/-}$ models, revealed for the first time a mechanistic role of these populations in hepatic inflammation and fibrosis. In particular, I found that GLP-1R agonist action induced the activation of M2 macrophage polarization, which was associated with anti-inflammatory effects, wound repair and angiogenesis. Moreover, the therapeutic benefit of the BY GLP-1R agonist was closely associated with inhibition of unfavorable JNK/ ERK1/2 signaling. Therefore, this study provides the first evidence that GLP-1/GLP-1R activation via inhibition of JNK/ ERK1/2 activation induce a beneficial M2-macrophage polarization.

Taken together, this work shows that DPP-4 inhibitors and GLP-1R agonists decrease overall liver steatosis, (macrophage-mediated) inflammation and apoptosis in a rodent model of sever NASH and exert modest intrinsic anti-fibrotic properties. These findings demonstrate a close mechanistic link between GPL-1/GPL-1R modulation, M2 polarization and fibrosis and qualify DPP-4-inhibitors and GLP-1R agonists as promising drugs for the treatment of NASH and the prevention of liver

fibrosis. These extend the beneficial effect of gliptins and direct GLP-1 agonists towards NASH, drugs that are effective in patients with T2D and the metabolic syndrome, both comorbidities of most patients with this important chronic liver disease.

Zusammenfassung

Die nicht-alkoholische Fettlebererkrankung (non-alcoholic fatty liver disease, NAFLD) ist mittlerweile die häufigste Ursache chronischer Lebererkrankungen. 10-15% aller NAFLD-Patienten zeigen das klinische Bild der nicht-alkoholischen Steatohepatitis (NASH), welches durch Steatose, Apoptose von Leberzellen, Leberentzündung, und Fibrosierung charakterisiert ist und ein großes Risiko einer Leberzirrhose und der malignen Progression zu primärem Leberkrebs birgt. Morbidität und Mortalität sind in den Frühstadien der NAFLD/NASH größtenteils auf Komplikationen eines metabolischen Syndroms zurückzuführen. Detaillierte Studien zu effektiven Therapeutika, die die chronische Leberentzündung und –fibrose sowiedas metabolische Syndrom adressieren, existieren kaum.

Das Inkretin Glucagon-like Peptide-1 (GLP-1) wird nach der Nahrungsaufnahme von intestinalen L-Zellen, den α-Zellen der Bauspeicheldrüse und den Neuronen des Tractus solitarius des zentralen Nervensystems (ZNS) sezerniert. Während GLP-1 im ZNS die Nahrungsaufnahme kontrolliert, stimuliert intestinales GLP-1 die Insulinsekretion der Bauspeicheldrüse und verhindert die Glukagon-Freisetzung über den GLP-1-Rezeptor (GLP-1R), was zu einer verbesserten Insulinsekretion der Bauchspeicheldrüse und Glukose-Aufnahme in die Leber, dem Fettgewebe und den Muskeln führt, ein Mechanismus, der wiederum die diabetogene hepatische Glukoneogenese reduziert. Um die Wirkung von GLP-1 pharmakologisch zu modulieren, gibt es verschiedene Optionen: Einerseits kann mit Hilfe von GLP-1-Mimetika die Wirkung von GLP-1 am GLP-1R verstärkt werden, andererseits kann die proteolytische Wirkung der Dipeptidylpeptidase-4 (DPP-4), welche ubiquitär auf Zelloberflächen exprimiert ist und GLP-1 enzymatisch abbaut, pharmakologisch gehemmt werden. Tatsächlich werden GLP-1-Mimetika und DPP-4-Hemmer bereits zunehmend für die Behandlung des Typ 2 Diabetes (T2D) eingesetzt. Darüber hinaus zeigten Tiermodelle, daß GLP-1 Mimetika und DPP-4 Hemmer eine anti-entzündliche und anti-oxidative Wirkung besitzen. Studien zur Erforschung von GLP-1 Mimetika und DPP-4 Hemmern bei NAFLD und NASH beschränkten sich jedoch bisher auf ihren Einfluß auf die Apoptose von Hepatozyten und die Steatose der Leber. Es gab bisher jedoch keine Untersuchungen über ihren Einfluß auf die zentralen Mechanismen der Entzündung und Fibrose. U.a. war ist nicht bekannt, ob und auf welche Weise GLP-1 Mimetika und DPP-4 Hemmer die Polarisierung von Makrophagen, zentrale Zellen in der Pathogenese von NAFLD/NASH und dem metabolischen Syndrom, beeinflussen.

In der vorliegenden Doktorarbeit wurde eine detaillierte *in vivo* Studie zur therapeutischen Wirkung und zugrunde liegende Mechanismen der zwei bereits klinisch eingesetzten DPP-4-Hemmer Linagliptin und Sitagliptin durchgeführt und darüber hinaus die therapeutische Wirkung des lang-wirksamen GLP-1R-Agonisten Bydureon (BY) untersucht. Um diese Wirkstoffe in Tiermodellen zu testen, welche die bei Patienten gefundene Pathologie der fortgeschrittenen NASH widerspiegeln, wurde sowohl das Methionin- und Cholin-defiziente (MCD) Diätmodell der akuten lipo-apoptotischen Leberschädigung als auch das Mdr2$^{-/-}$ Mausmodell der biliären Leberfibrose eingesetzt. Ferner wurde die Rolle von pro- versus anti-inflammatorischen Makrophagen/Monozyten während der Initiation und der Progression der NASH untersucht und es konnte in dieser Arbeit erstmals eine direkte mechanistische Beziehung zwischen der therapeutischen Regulierung der GPL-1-Aktivität, NASH und der Makrophagen/Monozyten-Polarisation hergestellt werden.

Die MCD Mäuse entwickelten eine ausgeprägte Hepatosteatose, Entzündung, Apoptose und Fibrose verglichen mit den Methionine-Choline suffizienten (MCS) Kontrolltieren. Hierbei erwies sich der Einsatz des MCD Modells, welches keine Insulinresistenz entwickelt, eine wichtige Komorbidität der humanen NASH, als vorteilhaft, da damit indirekte Effekte der GLP-1-Pharmaka auf die NASH (über eine Verbesserung der Insulinresistenz) von einer direkten Wirkung auf die hepatische Entzündung/Entzündungszellen und die Leberfibrose zu separieren. . Die hier durchgeführte Studie lieferte deutliche Hinweise auf eine effektive therapeutische Wirkung der beiden getesteten DPP-4-Inhibitoren und des GLP-1R Agonisten auf die Monozyten-Makrophagen-Infiltration und Polarisierung, die Hepatozyten-Lipoapoptose und sekundär die Leberfibrose. Ferner an Mdr2$^{-/-}$ Mäusen ein direkter sowie ein über Makrophagen vermittelter anti-fibrotischer Effekt nachgewiesen werden.

Die Arbeiten zeigten auch, daß dieser therapeutische Effekt der DPP-4-Inhibitoren klassenspezifisch ist, da Linagliptin und Sitagliptin bei allen durchgeführten Untersuchungen ähnliche wirksam waren. Die Analyse der M1- vs M2-Makrophagen in den beiden in vivo Mausmodellen belegte darüber hinaus erstmals eine zentrale mechanistische Rolle der Makrophagen polarisiertung bei der Leberentzündung und fibrose. So induziert die vermehrte GPL-1-Aktivität eine anti-entzündliche und anti-fibrotische M2-Makrophagen-Polarisation. . Arbeiten anderer Gruppen hatten bereits

gezeigt, daß der GPL-1R auf unterschiedlichen Zelltypen exprimiert wird und daß die GLP-1/GLP-1R Signalkaskade über PI3K und cAMP vermittelt werden kann. Allerdings wurden bisher keine Studien, die eine mögliche Assoziation zwischen GLP-1/GLP-1R und dem JNK/ERK1/2 Signalweg untersuchten, durchgeführt. Unsere ursprüngliche Arbeitshypothese, daß die agonistische Verstärkung der GPL-1 Funktion durch BY zu einer M2-Makrophagen-Polarisation führt, welche die Entzündung der Leber und die Fibrogenese dämpft, mit der Aktivierung des JNK/ERK1/2 Signalweges assoziiert ist, konnte durch die hier durchgeführten Experimente bestätigt werden.

Zusammenfassend zeigen die hier beschreibenen *in vivo* Ergebnisse erstmals, daß die DPP-4-Hemmer Linagliptin und Sitagliptin und der lang-wirksame GLP-1 Agonist BY in Mausmodellen der NASH und Leberfibrose die Lebersteatose, Hepatozyten-Lipoapoptose, die Entzündung inhibieren und gleichzeitig eine geringe direkte anti-fibrotische Wirkung besitzen. Die hier dokumentierte enge mechanistische Verknüpfung zwischen GPL-1/GPL-1R-Modulation, M2-Makrophagenpolarisierung, NASH und Fibrogenese belegen somit, daß DPP-4-Hemmer und GPL-1-Agonisten vielversprechende pharmakologische Kandidaten zur Behandlung von NASH und zur Therapie der assoziierten Leberfibrose. Diese günstigen Effekte der direkten und indirekten GLP-1-Pharmaka bereichern neben den bekannten Wirkungen auf Typ 2 Diabetes und das metabolische Syndrom, beide Komorbiditäten der NASH, das medikamentöse Armamentarium für diese wichtige Lebererkrankung.

Abbreviations

ACC	acetyl-CoA carboxylase
Akt	protein kinase B
Akt1	RAC-alpha serine/threonine-protein kinase 1
ALT	alanine aminotransferase

AMPK	5' adenosine monophosphate-activated protein kinase
Arg1	arginase 1
AST	aspartate aminotransferase
AP	alkaline phosphatase
α-SMA	alpha-smooth muscle actin
BMI	body mass index
BY	Bydureon
CCL2	chemokine (C-C motif) ligand 2
CCL3	chemokine (C-C motif) ligand 3
CCL5	chemokine (C-C motif) ligand 5
CCR1	C-C chemokine receptor type 1
CCR2	C-C chemokine receptor type 2
CCR3	C-C chemokine receptor type 3
CCR5	C-C chemokine receptor type 5
COL1α1	procollagen α1 (I)
COL3	procollagen type III
CYP	cytochrome P
DPP-4	dipeptidyl peptidase-4
DCs	dendritic cells
ECM	extracellular matrix
ER	endoplasmic reticulum
ERK1/2	extracellular signal–regulated kinases
EQW	exenatide once-weekly (exendin-4, Bydureon™,)
FAS	fatty acid synthase
GIP	glucose-dependent insulinotropic peptide
GLP-1	glucagon like peptide -1
GRP	gastrin-releasing peptide

Gliptins	e.g. Linagliptin, Sitagliptin
HDL	high density lipoprorein
HFD	high fat diet
Hg	mercury
HSC	hepatic stellate cell
HSCs	hepatic stellate cells
Hyp	hydroxyproline
ICAM-1	intercellular adhesion-1 molecule-1
IKKb	inhibitor of kappa B kinase
IFNγ	interferon gamma
IL-2	interleukin 2
IL-10	interleukin-10
IL-1β	interleukin-1β
IL-1Ra	IL-1 receptor antagonist
iNOS	inducible nitric oxide synthase
IR	insulin resistance
IRS	insulin receptor substrate
JNK	c-Jun N-terminal kinases
LDH	lactate dehydrogenase
LPL	lipoprotein lipase
MGL 1	macrophage galactose-type lectin 1
MCD	methionine choline deficient
MCP-1	macrophage chemotactic protein-1
MCS	methionine choline sufficient
MMP	matrix metalloprotease
mRNA	messenger RNA
NAFLD	non-alcoholic fatty liver disease

NAS	NAFLD activity score
NASH	non-alcoholic steatohepatitis
PKCζ	protein kinase C, zeta
PPARα	peroxisome proliferator-activated receptor alpha
PPARγ	peroxisome proliferator-activated receptor gamma
PPARδ	peroxisome proliferator-activated receptor delta
PKC-ζ	protein kinase C, zeta
qPCR	quantitative real-time PCR
RANTES	regulated on activation, normal T cell expressed and secreted
SCD-1	stearoyl-CoA desaturase-1
SREBP	sterol regulatory element-binding protein
Sirt1	sirtuin 1
SCD-1	stearoyl-CoA desaturase 1
SREBP-1c	sterol-regulatory binding protein-1c
T2D	type 2 diabetes
TGFβ1	transforming growth factor beta 1
TIMP-1	tissue inhibitor of metalloproteinases-1
TNFα	tumor necrosis factor α
VCAM-1	vascular cell adhesion molecule-1
VLDL	very-low-density lipoprotein
Ym1	beta-N-acetylhexosaminidase

Units

%	percent
°C	degree centigrade
D	day
Dl	0.1 liter

g	grams
h	hour
min	minute
mg	milligrams
mm	millimeter
µg	micrograms
µm	micrometer
U/L	units per liter

Table of Contents

1. Introduction

1.1 NAFLD/NASH

Nonalcoholic fatty liver disease (NAFLD) is associated and overlaps with obesity, dyslipidemia, cardiovascular disease, insulin resistance (IR), type 2 diabetes (T2D) and the metabolic syndrome, which is a significant cause of morbidity and mortality in developed and developing countries[1]. Presently, NAFLD is the most general cause of chronic liver disease and affects 20%-30% of people living in the United States[2]. In Europe, NAFLD prevalence is equally estimated at 10-30%[3], while in Asia, the prevalence of NAFLD is reported to be 12%-24%[4].

NAFLD is characterized as steatosis, i.e., excess lipid accumulation in hepatocytes and occurs without alcohol abuse[5]. Simple steatosis is the primary and most common form of NAFLD, which is a prevalent and largely benign state of liver injury. However, human studies showed that various factors causing fatty liver are leading to steatohepatitis[6], the inflammatory variant of NAFLD, therefore dramatically raising the susceptibility to increased liver-related morbidity and mortality[7]. NAFLD has a high prevalence in the obese population and thus can be considered to be one of the manifestations directly linked to the metabolic syndrome including hyperglycemia, hypertension, hyperlipidemia, obesity, and T2D[8]. Additional causes also contribute directly to the progression of NAFLD, such as a sedentary lifestyle and beverages with a super-normal content of fructose as well as increased consumption of high-fat content foods[9].

In Asian populations that historically had a low prevalence of NAFLD and metabolic risk factors, the incidence and prevalence of NAFLD has increased dramatically[10,11]. Additionally, there is a marked difference between urban and rural areas, indicating that education and lifestyle are contributing to NAFLD in Asia[11]. Not surprisingly, in the wealthy areas of China the number of cases of NAFLD doubled in a decade to affect 15% of the population today, mostly driven by the marked increase in average body mass[12].

Recent studies suggest that nearly 30% of the US population have NAFLD and up to 75% of patients with diabetes and obesity are prone to NAFLD. Regarding the increasing prevalence of NAFLD in children, up to 50% of obese children and 2.6-9.6% of children in United States and Asia are thought to be affected[13]. Thus NAFLD is becoming a pediatric problem. Nearly 90% of NAFLD patients have at least one

characteristic feature of the metabolic syndrome, which is characterized by at least three of the following parameters: triglyceride levels greater than 150 mg/dl, abdominal obesity (waist circumference greater or equal to 40 inches in men, greater or equal to 35 inches in women), HDL concentrations less than 40 mg/dl in men and 50 mg/dl in women, fasting glucose levels greater than 110 mg/dl, and blood pressure >130/>85 mmHg[14,15].

The progression of NAFLD to NASH is characterized by increased necro-inflammation, hepatocyte ballooning, hepatic steatosis, lipoapoptosis and progressive fibrosis. Interestingly, a high number of individuals suffering from hepatic steatosis do not develop NASH. It is estimated that 15-25% of cases of early stage NAFLD progress to NASH, and 15-20% of NASH cases further develop into cirrhosis[16]. Recently, along with NAFLD, NASH has rapidly increased around the globe, with NAFLD incidences between 12% and 46% that occur mostly in the middle-aged population[17]. Notably, NASH patients were mainly male (65%) with a significantly higher BMI and average alanine aminotransferase (ALT) of 50.9 U/L and increased IR compared to patients with simple steatosis on liver biopsy[17].

Moreover, NASH is an important contributor to mortality from cardiovascular disease independent of traditional risk factors[18], and progressive stages of NAFLD predict carotid intima-media thickness and carotid plaques[19]. Investigation of the underlying mechanisms has led to a concept in which a pro-inflammatory state, including decreased protective adipokines, increased levels of pro-inflammatory cytokines, enhanced oxidative stress, originating from the inflamed and expanding adipose tissue of obese patients, induce the release of atherogenic and pro-thrombotic factors from the liver[19].

1.2 Histopathology and pathogenesis of NAFLD/NASH

NAFLD potentially manifests with a variety of markers and symptoms including IR, increased hepatic uptake of fatty acids, peripheral lipolysis, release of pro-inflammatory cytokines, hormonal changes (including increased leptin levels) and mitochondrial dysfunction caused by hyperinsulinemia. Here NAFLD progresses from the accumulation of fat in the liver to severe inflammation (NASH), to cirrhosis and eventual death from cirrhosis or liver cancer (**Fig.1**)[20].

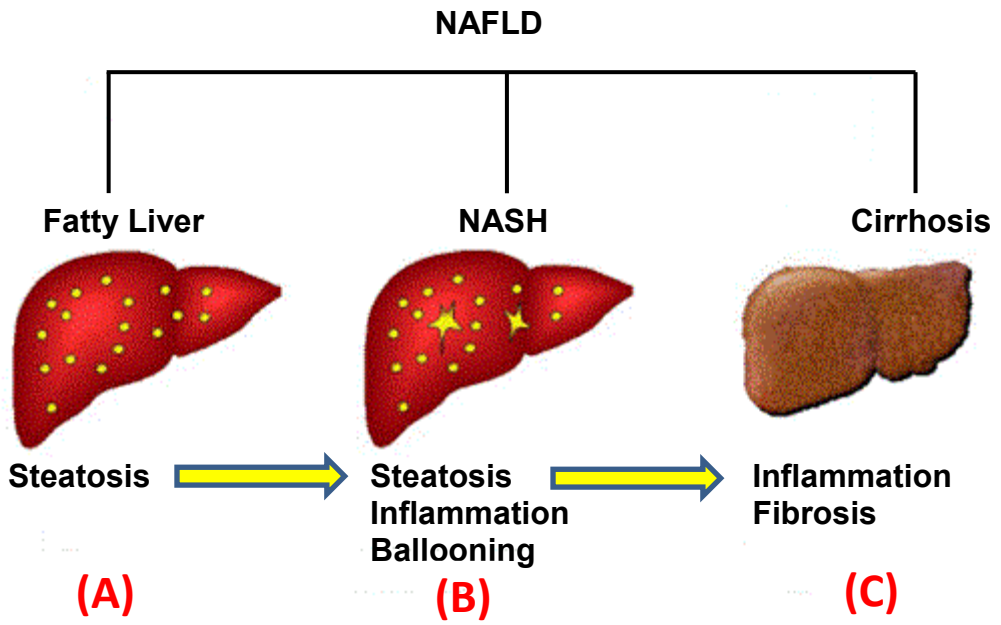

Fig.1 Schematic diagram of the progression of non-alcoholic fatty liver disease (NAFLD) (A) mere fatty liver, (B) non-alcoholic steatohepatitis (NASH), (C) cirrhosis (modified from Nutrientology.com)

For the development of suitable drugs to treat the condition, it is important to understand the pathogenesis of NAFLD/NASH. Although the pathophysiology of NAFLD/NASH has not yet been completely elucidated, the "two-hit"[21] and "multiple parallel hit"[22] hypotheses have been proposed. In the two-hit hypothesis, it was suggested that hepatic steatosis (representing the first hit) is able to condition the liver parenchyma to develop to a form of hepatic metabolic syndrome as second hit that then initiates a cascade of steatonecrosis, inflammation and fibrosis. Experts in this have criticized this model as an over-simplification of NASH pathogenesis and propose that multiple parallel hits are more likely to be responsible for disease progression[22]. The so called "multiple-hit hypothesis" describes NASH as a complex, two-step liver injury[23]. Insulin is an anabolic hormone that regulates gene expression, glucose metabolism, enzymatic functions and energy homeostasis[24]. IR, which is normally seen in obese individuals, appears to play a central role in both the first and second hits[25], because it alters nutrient distribution between tissues and nutrient metabolism[26]. Adipose tissue, liver and skeletal muscle are the most important insulin-target tissues[24,25]. In the adipose tissue, insulin controls free fatty acid esterification and triglyceride storage. When IR develops, free fatty acids are improperly shifted to non-adipose tissues, as the liver[27]. In the liver, insulin mainly regulates glucose

metabolism[24,25]. Peripheral IR leads to increased uptake of free fatty acids into the liver by decreased inhibition of lipolysis and increased *de novo* lipogenesis[28]. In addition, hyperinsulinemia mediates hepatic lipogenesis and facilitates profibrotic cytokine release[27,29]. IR and hyperinsulinemia also increase the secretion of triglycerides by the liver, resulting in raised serum levels of triglycerides[27,29]. Hepatic steatosis derives from an imbalance between triglyceride accumulation and elimination in the liver. Moreover, this initial step is then followed by a series of complex interactions among hepatocytes, Kupffer cells, adipocytes, inflammatory mediators and oxygen radicals.

Moreover, the steatohepatitis liver is more vulnerable to endoplasmic reticulum stress, mitochondrial dysfunction, hepatic apoptosis, oxidative damage, which incurs altered expression of adipokines, activation of inflammatory cytokines, accompanied by increased endotoxin levels originating from the intestinal bacterial flora, finally resulting in activation of fibrogenic pathways finally leading to fibrosis and cirrhosis (**Fig.2**)[3,22].

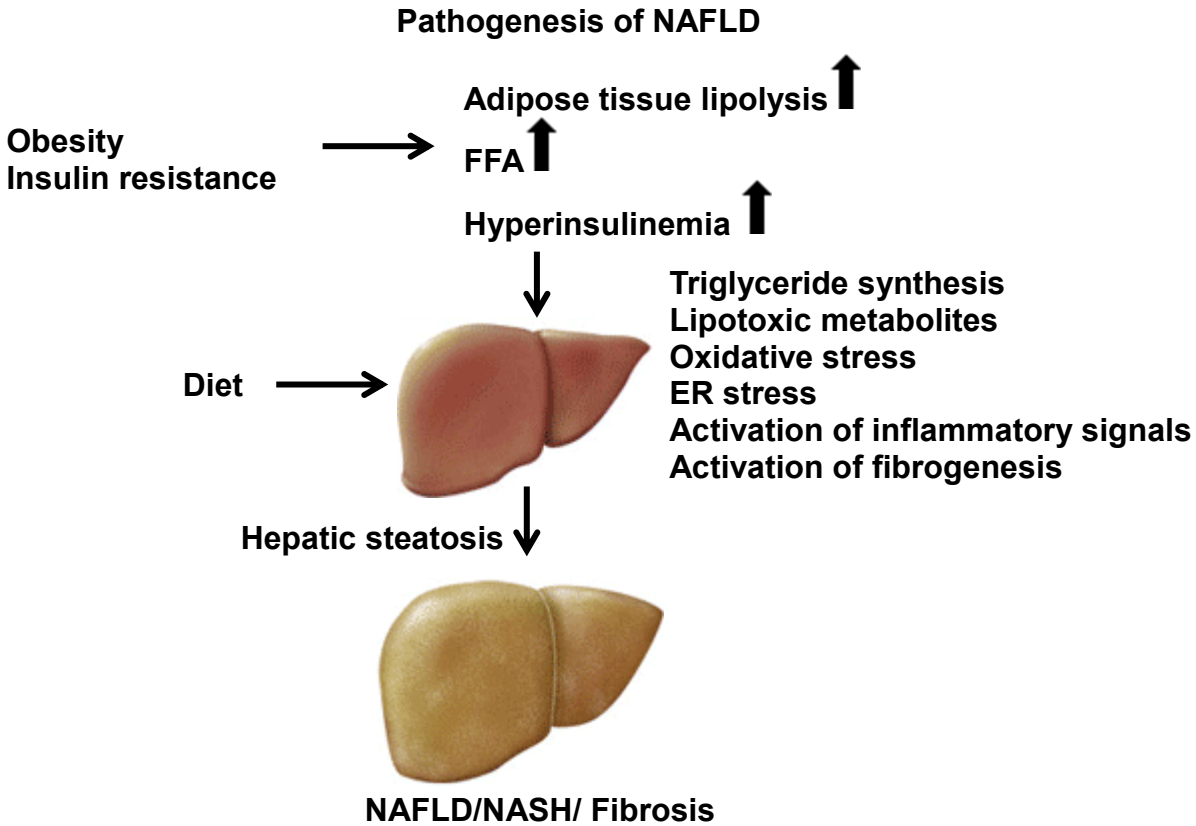

Fig.2 Pathomechanisms during the progression to hepatic steatosis and NAFLD/NASH/Fibrosis IR and an unfavorable utilization of fatty acids increase excessive accumulation of triglycerides in the hepatocytes enhances and promotes hepatic steatosis. The inability to process excess lipids in a metabolically nontoxic degradation process promotes inflammation and fibrosis due to oxidative stress, lipoapoptosis and cytokines released from pro-fibrogenic progenitor cells (summarized from[23-25,27,29]).

The increasing prevalence of NAFLD/NASH has led to a great demand for medical therapy, since introduction of central life style changes have hitherto mostly been futile. Thus the currently accepted therapeutic options with lifestyle changes such as reduction of weight with or without exercise are limited.

Due to ethical limitations, difficulties in therapeutic testing of drugs and the need to mainly address later stages of the disease (e.g., NASH, fibrosis or cirrhosis), human studies are difficult to conduct, and need best prior proof-of concept. Animal models establishing conditions of the early phases of NAFLD in humans (e.g., steatosis and steatohepatitis) but also the later stages such as severe lipoapoptotic inflammation and fibrosis have been used as tools to investigate mechanisms and pathophysiology underlying the development of NAFLD, and to model the spectrum of diseases for preclinical drug testing.

1.3 Methionine and choline deficient (MCD) diet models of NAFLD

Nutritional models are used to mimic the adverse effects of an unhealthy diet on the development of obesity and NASH. Changes in over-nutrition and dietary patterns both are related to progressive overweight and IR, which have been identified as important risk factors for the development of NAFLD. Some diets can also cause significant liver damage, steatosis, hepatocyte ballooning, lobular inflammation, and perivenular fibrosis similar to the histopathological forms of human NASH. In addition, certain high fat diets prominently mirror the metabolic syndrome, characterized by high levels of triglycerides and cholesterol and resulting in T2D similar to frequent features in human NAFLD/NASH[30]. The MCD diet is one of the most commonly used dietary models for the severe liver phenotype of NASH, and represents an essential nutrient-deficient model. The MCD diet contains a high quantity of fat and sucrose (10% fat, 40% sucrose) but is deficient in methionine and choline, which are essential for liver β-oxidation and the production of very-low-density lipoproteins (VLDL). The MCD diet results in hepatic accumulation of lipid and decreased VLDL synthesis[31]. Mice fed with the MCD diet rapidly develop hepatic inflammation within 3 days. Severe pericentral steatosis may develop within 1 to 2 weeks followed by necrosis and inflammation, subsequently evolving into pericellular and pericentral fibrosis that are driven by severe hepatocyte lipoapoptosis and oxidative stress[32]. Furthermore, oxidative stress[33], activation of Toll-like receptor (TLR) 4-dependent signaling pathways in the liver and

proinflammatory changes in cytokine as well as adipocytokines profiles, all of which contribute to the severe liver injury in this dietary model[34].

Mice fed with the MCD diet display increased serum ALT levels[35] and inflammatory responses through activation of liver macrophages. In this process the transcription factor nuclear factor kappa B (NF-kB), is a key modulator of inflammation but also hepatocyte survival. In addition to NF-kB activation, Interleukin 6 (IL-6), tumor necrosis factor α (TNFα) and tumor growth factor β (TGF-β) levels are elevated[36]. The MCD diet augments the expression of vascular cell adhesion molecule-1 (VCAM-1), intercellular adhesion-1 molecule (ICAM-1) and macrophage chemotactic protein-1 (MCP-1), resulting in increased activity, adhesion, migration, and accumulation of macrophages and neutrophils in the liver[37]. Although the MCD model induces more severe inflammation, mitochondrial damage, oxidative stress, apoptosis, and fibrogenesis compared to other nutritional models of NASH[38], MCD feeding has also clear limitations. This in contrast to human fatty liver disease, MCD diet-fed animals lose weight, exhibit low plasma triglyceride and cholesterol levels, and a reduced liver weight/body weight ratio[39]. Furthermore, IR, one of the main risk factors for the development of NAFLD as found in humans, is lacking in the MCD diet model[40]. Other discrepancies in the metabolic syndrome of the MCD diet are low levels of insulin, leptin and glucose, which are also opposite to the findings in human NASH[34,41]. In addition, the responsiveness of NASH in rodents fed the MCD diet may depend on the gender, species and strain of the animal[32]. The mouse strain C57/BL6 mimics some human lipid disorders and metabolic conditions when used in different experimental models[42]. Similar to humans, adult C57/BL6 mice have a strong genetic trend to develop hyperinsulinemia, obesity and glucose intolerance, independently of the diet[31]. Indeed, increases in transaminase levels in different mouse strains can be classified as follows: A/J > C57BL/6 > C3H/HeN = Balb/c = DBA/2J. Interestingly, long term feeding of a methionine deficient diet causes significantly more liver injury and even hepatocarcinogenesis in DBA/2J when compared to C57BL/6 mice[43-45]. An alternative study compares the effects of the MCD diet in female and male Long-Evans, Wistar and Sprague Dawley rats vs C57BL/6 mice. Here the Wistar strain and male sex exhibited the greatest degree of steatosis in rats. In C57BL/6 mice, male animals developed more necrosis and inflammation, and thus better mirrored the histological features of NASH than female mice[46].

1.4 Dipeptidyl peptidase-4 (DPP-4) inhibitors

Traditionally, most pharmacological developments arise from serendipitous observations. However, developing advanced pharmacotherapies need researchers to identify a pathogenically central molecular target that is prone to pharmacological manipulation. Studies on the pathogenesis of NAFLD have shown several potential targets for novel pharmacotherapies. Among those, two novel classes of drugs are of high interest: the DPP-4 inhibitors and glucagon-like peptide-1 (GLP-1) receptor agonists, but have been incompletely assessed for the treatment of NAFLD and NASH. On the other hand, they have a high safety, since they are already used for the treatment of T2D[47]. Therefore, the current thesis focused on the *in vivo* analysis of two major DPP-4 inhibitors Linagliptin and Sitagliptin, and also on the long-acting GLP-1R agonist Bydureon (BY).

DPP-4 is expressed in all organs, by capillary endothelial cells and activated lymphocytes and on apical surfaces of epithelia, including hepatocytes. In humans, DPP-4 is also present in the luminal gastrointestinal tract, biliary tract, exocrine pancreas, thymus, lymph node, kidney, uterus, prostate, placenta, parotid, adrenal, salivary, sweat and mammary glands, and larger vascular endothelia of all organs examined, including spleen, liver, brain and lungs[48,49]. The catalytic triad of DPP-4 is composed of residues S630, D708, and H740, which are located within the last 140 residues of the C-terminal region[50]. The enzyme specifically removes dipeptides from the N terminus of peptide substrates that contain on average 30 residues and have a Pro or Ala in the penultimate position. In addition, a slow release has been observed for dipeptides composed of X-Ser or X-Gly[51]. As an exopeptidase of the serine protease type, DPP-4 cleaves numerous substrates at the penultimate position and thereby mostly inactivates them. Among these are peptides (e.g. stromal cell-derived factor 1 alpha (SDF1α), eotaxin) and cytokines (MCP-1, interleukin 2 (IL-2)) as well as the incretin hormones[52]. The incretin hormones GLP-1 and glucose-dependent insulinotropic polypeptide (GIP) are major regulators of the postprandial insulin release[53]. The DPP-4 gene family includes cytoplasmic peptidases such as DPP-6, DPP-8, DPP-9 and DPP-10, which are expressed on the cell surface but show a lower enzymatic activity than DPP-4[54-56]. DPP-4 has been implicated in several essential biological processes, including immune responses, fibrosis, glycemic control, cell-

extracellular matrix (ECM) interactions, tumor growth, vascular physiology and neuronal functions[20].

Although DPP-4 activity may broadly regulate the physiology of numerous signaling systems impacting numerous organs and diseases, since it can cleave numerous substrates involved in hormone (neuroendocrine) turnover and inflammation (**Table 1**)[57]. Because DPP-4 activity controls immune cell activity and both subclinical and overt inflammation can accelerate the progression of diabetes and obesity, much data links regulation of chemokine biology to DPP-4 activity.

Table 1: Possible enzymatic substrates of DPP-4

Regulatory peptides	Brain natriuretic peptide, GIP, gastrin-releasing peptide (GRP), GLP-1, GLP-2, GRH (growth hormone-releasing hormone), pituitary adenylate-cyclase-activating polypeptide (PACAP)-(1–38), vasoactive intestinal peptide (VIP)
Chemokines	Eotaxin (CCL11), IP10 (CXCL10), I-TAC (CXCL11), monokine induced by gamma-interferon (CXCL9), stromal cell-derived factor-1 (SDF-1/ CXCL12), macrophage-derived chemokine (MDC, CCL22), RANTES (CCL5), monocyte chemotactic protein-2 (MCP-2), granulocyte chemotactic protein-2, Macrophage inflammatory protein-1α (MIP-1α/CCL3)
Neuropeptides	NPY(1–36), substance P, PYY(1–36), bradykinin, endomorphin-2
Others	Granulocyte macrophage-colony stimulating factor (GM-CSF,) G-CSF, erythropoietin, Interleukin-3, fibroblast growth factor-2, thrombopoietin

IP, interferon-γ-inducible protein; I-TAC, Interferon-inducible T cell a chemoattractant; RANTES, regulated on activation normal T cell expressed and secreted (Modified from[57]).

Several members of CXC and CC chemokine subfamilies share a conserved Xaa-Pro or Xaa-Ala sequence at their N-terminal which conforms to the substrate specificity of DPP-4[58]. Integrated *in vivo* experiments that study the relevance for DPP-4 as an important regulator of inflammation and chemotactic responses are therefore still lacking. Among the DPP-4 substrate chemokines, stromal cell-derived factor-1 (SDF-1) has been intensively studied. SDF-1, expressed as two different splice variants, SDF-1α (1–68) and SDF-1β (1–72), is a homing molecule for hematopoietic stem cells (HSCs), hematopoietic progenitor cells (HPCs), and endothelial progenitor cells

(EPCs)[57]. SDF-1 is widely expressed in numerous cell types, and its expression and secretion are often induced concomitant with cellular injury. Both SDF-1 isoforms are cleaved by soluble or cellular DPP-4, which inactivates their antiviral and chemotactic properties in cell-based assays *in vitro*[59]. Because SDF-1 activity enhances migration of hematopoietic and endothelial progenitor cells to sites of ischemic injury, DPP-4 inhibitors have been employed to enhance tissue healing, most commonly in the setting of myocardial or vascular ischemia. Importantly, DPP-4 inhibition reduces N-terminal degradation of SDF-1 and potentiates SDF-1 action *in vivo* by enabling enhanced activation of its receptor, CXCR4, with greater stem cell mobilization to sites of injury[60]. Some preclinical studies have shown that DPP-4 inhibition after acute myocardial infarction improves cardiac homing of stem cells and enhances heart function[61]. DPP-4 inhibitor therapy in patients with T2D was shown to increase circulating SDF-1α and EPC levels[62]. Therefore, apart from preserving GLP-1 activity, SDF-1α may contribute to one of pleiotropic effects of DPP-4 inhibition with important implications for cardiovascular (CV) protection and T2D.

DPP-4 may also be an important player in the pathogenesis of NAFLD[63,64]. A study involving 31 patients of NASH found significantly increased levels of serum DPP-4 compared with control subjects[63]. In addition, a strong association was observed between serum DPP-4 activity, the histopathological grade and degree of liver steatosis and hepatic DPP-4 expression in the liver[63]. As well as inducing pro-inflammatory immune responses[63], DPP-4 also regulates liver fibrogenesis by modulating the interaction between DPP-4 expressing hepatocytes, immune cells and ECM proteins[64,65]. Expression levels of liver DPP-4 increased in diabetic rats fed a high-fat diet[66], while serum levels of DPP-4 were elevated in rodent models of cirrhosis [67] and in patients with hepatitis C virus-related glucose intolerance[68].

GLP-1 induced anti-apoptotic activity in cholangiocytes[69] suggested that DPP-4 may play an indirect pro-inflammatory role in liver. Thus, a reasonable principle for using DPP-4 inhibitors is to slow the progression of liver inflammation and steatosis, either via their effect on increasing GLP-1 activity or via their potential direct or indirect anti-inflammatory activities in the liver and other tissues. DPP-4 inhibitors are already well accepted, well-tolerated and effective treatments for T2D[70] and have considerable therapeutic effects in chronic liver diseases[71]. DPP-4 inhibition in diet-induced diabetic glucokinase$^{+/-}$ mice reduced hepatic inflammation and suppressed expression of

sterol-regulatory binding protein (SREBP)-1c, stearoyl-CoA desaturase (SCD)-1 and fatty acid synthase (FAS), and up-regulated peroxisome proliferator-activated receptor-α (PPAR-α), thereby ameliorating hepatic steatosis[72]. Equally, DPP-4 inhibition improved hepatic steatosis and insulin sensitivity in diet-induced obese C57BL/6 mice, with suppressed hepatic expression of SREBP-1c, SCD-1 and FAS[73]. Several DPP-4 inhibitors, i.e., “gliptins”, including vildagliptin, Linagliptin , Sitagliptin, alogliptin and saxagliptin, are now available for clinical use[74]. DPP-4 inhibitors perform by increasing the *in vivo* half-lives of glucose-dependent insulinotropic peptide (GIP) and especially of GLP-1. Thus DPP-4 inhibitors could mainly alleviate NAFLD by increasing bioactive GLP-1[75], or via both GLP-1 and GIP[76]. Vildagliptin and Linagliptin improved hepatic steatosis, insulin sensitivity and adipose tissue inflammation in obese and diabetic sugar rats and in high fat diet-fed mice[73,77]. Clinical data suggested that Linagliptin displayed favourable pharmacokinetics, and the pharmacokinetic profile had a placebo-like safety and tolerability together with a long-lasting effect of DPP-4 inhibition compared with other DPP-4 inhibitors[78]. Linagliptin (10 and 30 mg/kg) significantly attenuated the NAS score and the mRNA levels of IFN-γ and TNFα in a high-fat diet model combined with streptozotocin injection in mice[79]. Sitagliptin reduced CD36 expression, ER stress, NF-κB activation, lipid peroxidation and CYP2E1 expression in MCD diet-induced hepatic steatosis, inflammation, and fibrosis in mice[80]. Sitagliptin also showed anti-inflammatory effects in pancreatic islets and adipose tissue that accompanied the insulinotropic effect in a high fat diet-induced obesity model[81]. In addition, Sitagliptin ameliorated hepatic inflammatory biomarkers in patients with T2D and NAFLD treated for 4 months[82]. Furthermore, a small human study demonstrated that Sitagliptin improved liver enzymes and hepatocyte ballooning in NASH patients with T2D[83]. However, the mechanisms underlying the contribution of DPP-4 to the pathogenesis of NASH-induced hepatic steatosis, inflammation and fibrosis, which leads to the grave clinical consequence of cirrhosis, and hepatocellular cancer, remain largely unresolved.

1.5 GLP-1

GLP-1 is a family member of the incretins, a group of gastrointestinal hormones secreted by endocrine L-cells in the distal ileum and proximal colon and is produced by tissue-specific post translational processing of the proglucagon gene[84]. Nutrients, including fatty acids, glucose and dietary fiber, are known to increase the gene

transcription of GLP-1 and can stimulate the release of this hormone[85]. Upon the ingestion of food, levels of both GLP-1 and GIP increase rapidly. It is now well accepted that nutrients, principally fats and sugars, liberate GLP-1 and GLP-1–releasing factors, including GIP, gastrin-releasing peptide (GRP) and selective neural regulators that, as well, stimulate GLP-1 secretion as a secondary effect[84-86]. Multiple kinds of GLP-1 are secreted *in vivo*, including GLP-1(1-36) and GLP-1(1-37), which are thought to be inactive, and GLP-1(7-36) and GLP-1(7-37), which are biologically active (**Fig.3**)[87,88].

One of the main physiological roles of GLP-1 is to act directly on the pancreatic β-cells to induce insulin in a glucose-dependent manner (**Fig.3**)[89]. GLP-1 also has other functions such as enhancing satiety, inhibiting glucagon release, delaying gastric emptying, and suppressing appetite[90]. The half-life time of bioactive GLP-1 in the circulation is less than 2 minutes due to rapid inactivation by the ubiquitous proteolytic enzyme DPP-4[87]. Thus in diabetic or healthy humans, subcutaneous or intravenous GLP-1 is metabolized rapidly (within 30 min) to inactive GLP-1 (9-36), which accounts for more than 75% of the immune detectable circulating GLP-1 in these individuals (**Fig.3**)[89].

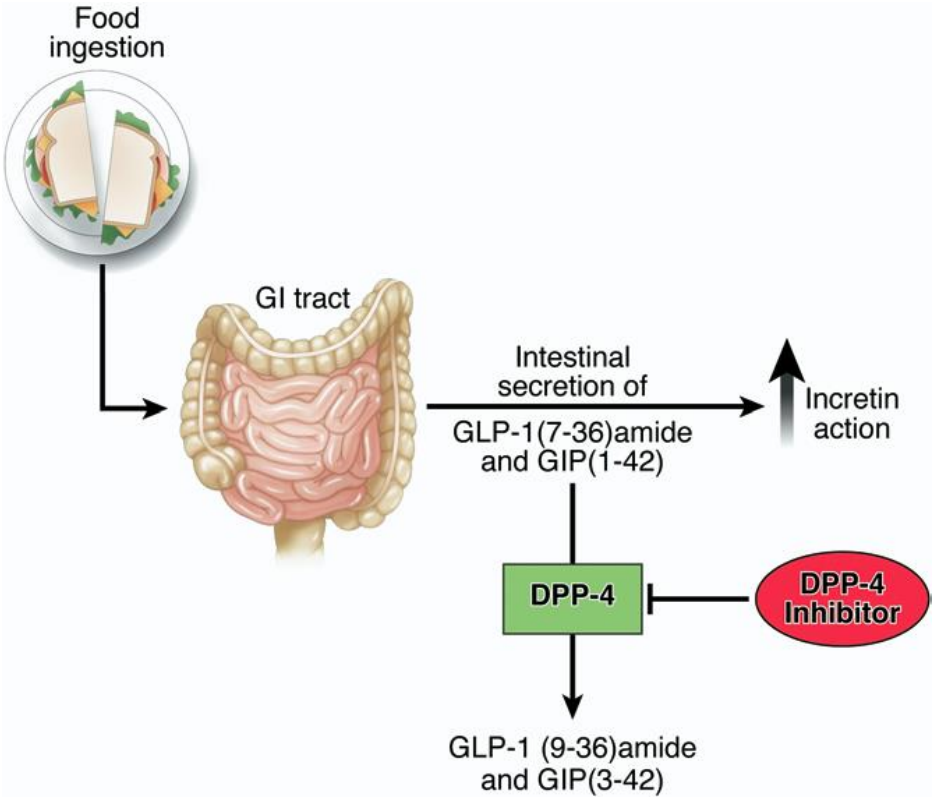

Fig.3 Bioactive GLP-1(7-36) amide and GIP (1-42) are released from the small intestine after meal ingestion and enhance glucose-stimulated insulin secretion (incretin action) DPP-4 rapidly converts GLP-1 and GIP to their inactive metabolites GLP-1 (9-36) and GIP (3-

42) *in vivo*. Inhibition of DPP-4 activity prevents GLP-1 and GIP degradation, thereby enhancing incretin action (adapted from[88]).

GLP-1 influences multiple target tissues throughout the body, and exerts its physiological effects through binding to its specific GLP-1 receptor (GLP-1R). The GLP-1R is a member of the class B family of seven-transmembrane–spanning, heterotrimeric G protein–coupled receptors, which also contain receptors for glucagon, GLP-2, and GIP[91]. In humans and rodents, a single structurally uniform GLP-1R has been identified and is expressed in a wide range of tissues, including α-, β-, and δ-cells of the pancreatic islets, lungs, heart, stomach, kidneys, pituitary, intestine, skin, ganglion neurons of the vagus nerve, and some regions of the CNS including the brainstem and hypothalamus[88]. Recently it has been demonstrated that both GLP-1R mRNA and protein are expressed in primary human hepatocytes and in cultured rodent hepatocytes[92]. The functions of GLP-1 have been extensively investigated over the last two decades because its acute intravenous infusion or subcutaneous administration reduces blood glucose and increases insulin secretion one of its most promising characteristics from a clinical perspective. Importantly, in human diabetes native GLP-1 cannot be used as a therapeutic agent because of its rapid degradation by DPP-4[87]. Therefore, the therapeutic potential of GLP-1 has been realized by using two pharmacologic approaches: First, inhibiting the action of DPP-4 via DPP-4 inhibitors and second by mimicking and focusing on GLP-1 via biologically stable GLP-1 receptor agonists[93,94].

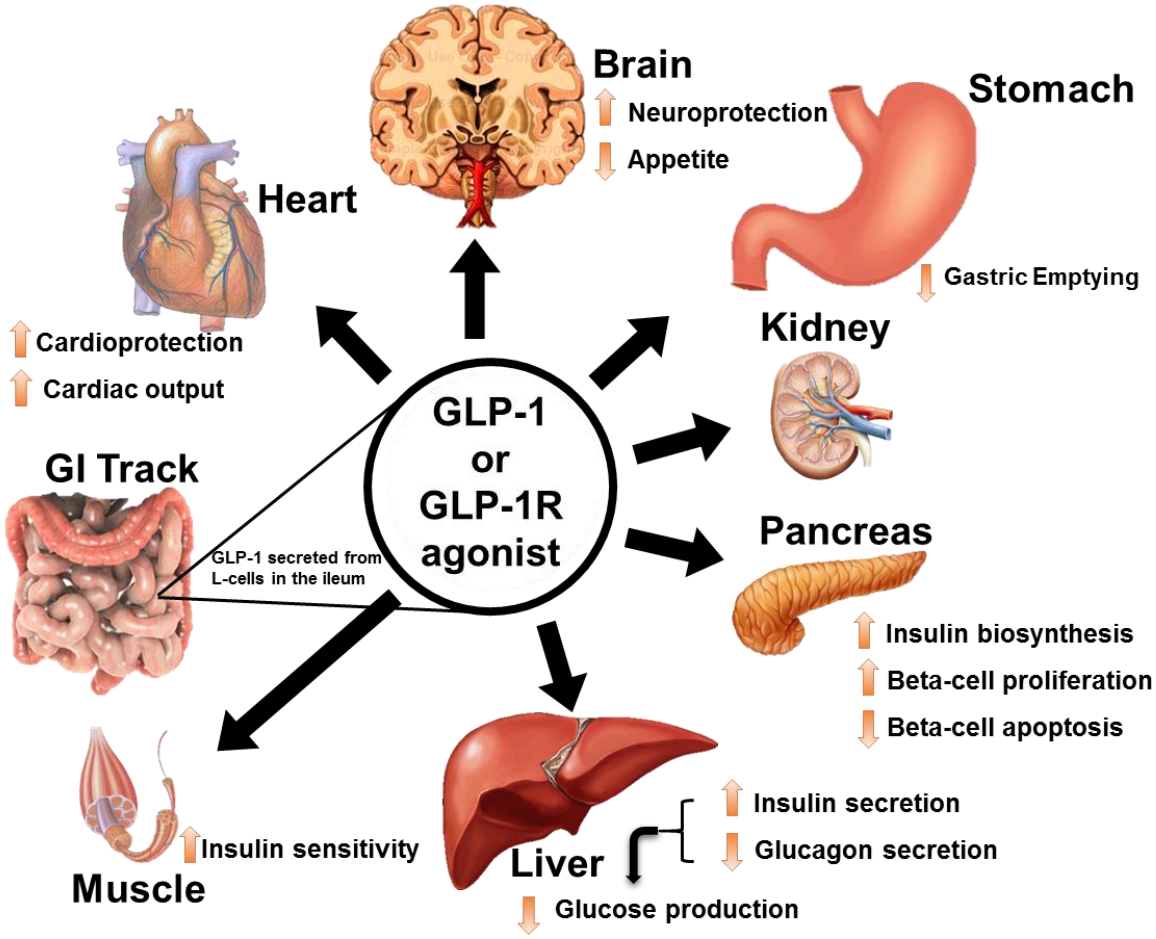

Fig. 4 Physiology of GLP-1 secretion and action on GLP-1 receptors in different organs and tissues The majority of the effects of GLP-1 are mediated by direct interaction with GLP-1Rs on specific tissues. GLP-1 is produced postprandially by intestinal L-cells. Through activation of insulin receptors on β-cells, GLP-1 (like GIP) stimulates insulin biosynthesis and secretion and inhibits glucagon secretion in the pancreas, which in turn reduces hepatic gluconeogenesis. GLP-1 also exerts protective effects on the heart and brain. Insulin sensitivity in the periphery is increased by improved insulin signaling and reduced gluconeogenesis (adapted from[95]).

GLP-1R agonists mediate their effect by acting directly on the GLP-1R. GLP-1R agonists produce several biological actions in the pancreas (**Fig. 4**)[88] including stimulation of glucose-dependent insulin secretion[96-98]. Exenatide (Byetta™) was the first GLP-1R agonist approved for glycemic control in diabetes. This 39-amino acid synthetic peptide is based on exendin-4 from the venom *Heloderma suspectum* (produced by the Gila monster), sharing 53% homology with human GLP-1[99]. Exendin-4 has many of the glucoregulatory properties of human GLP-1 and binds to the pancreatic GLP-1 receptor[100]. In addition, exendin-4 has a substantially longer plasma half-life than GLP-1 due to the second amino acid residue in the N-terminal region, which is the site of DPP-4-mediated inactivation. At this position alanine is replaced by

glycine in exendin-4[101]. The half-life time of exendin-4 after subcutaneous injection is about 2.4 hours, and it is therefore given twice daily starting at a dose of 5 µg upwards to 10 µg twice a day within 1 hour of a main meal. Liraglutide (Victoza™) bears only one amino acid substitution (Lys34Arg) with the addition of a C-16 acyl group (palmitoyl) attached to Lys26 through a glutamate linker and thus retains 97% sequence homology to human native GLP-1. These characteristics contribute to prolongation of the plasma half-life to 10-12 hours in humans, and treatment is recommended for once-daily administration[102]. The dose of liraglutide is initiated with 0.6 mg once daily, increasing to 1.2 mg after 1 week and in some patients up to 1.8 mg[103].

Both exenatide and liraglutide significantly improve glycemic control and cause a significant body weight loss in T2D patients[104,105]. GLP-1R agonists might thus also represent a novel treatment for NAFLD due to these actions and to their effect on genes and signaling pathways that are associated with hepatic lipid and glucose metabolism. Animal studies showed that exendin-4 reversed high-fat diet-induced hepatic lipid accumulation and inflammation in hepatocytes and C57BL/6J mice[106]. The exendin-4 analogue AC3174 significantly suppressed liver steatosis and immunostaining for collagen I, a marker of hepatic fibrosis, in *Lepob/Lepob* mice (that are deficient in leptin) and C57BL/6J mice on a high trans-fat diet[107]. Exendin-4 also reversed hepatic steatosis in obese ob/ob mice (that are deficient in the leptin receptor) through improving insulin sensitivity[75]. In the same study, GLP-1-treated mouse hepatocytes showed a significant increase in cAMP production along with increased expression of genes involved in fatty acid oxidization, and reduced the expression of SCD-1 and genes associated with fatty acid synthesis[75]. In addition to an improvement of lipid metabolisms, exendin-4 improved hepatic insulin sensitivity. Thus its administration increased the expression of sirtuin 1 (Sirt1) along with AMP-activated protein kinase (AMPK) in livers of high-fat-fed C57BL/6J mice, and also in the hepatic cell lines Huh7 cells and HepG2, suggesting involvement of GLP-1 signaling in both hepatocyte lipid and glucose metabolism. Another study showed that incubation of rat hepatocytes with exendin-4 up-regulated the expression of peroxisome proliferator-activated receptors-gamma (PPAR-γ), which exerted its insulin-sensitizing function by reducing c-Jun N-terminal kinase (JNK) phosphorylation and also increased phosphorylation of the Rac-alpha serine/threonine-protein kinase 1 (Akt1) and AMPK[108]. It was also shown that exendin-4 up-regulated the phosphorylation of Akt1

and protein kinase C zeta (PKC-ζ) in HepG2 and Huh7 cells[92]. Similarly, Liraglutide improved insulin sensitivity and reduced lipid accumulation in liver through multiple mechanisms including an increase of β-oxidation of lipid transport in C57BL/6J mice exposed to a high fat diet containing trans-fats and high-fructose corn syrup (ALIOS diet)[109]. Collectively, GLP-1R agonist mediate glucose metabolism and ameliorate insulin sensitivity in the liver. Another effect of GLP-1R agonist in the liver includes direct role in steatotic livers by inhibiting cell death through upregulation of genes associated with autophagy, reducing endoplasmic reticulum (ER) stress-related apoptosis in human hepatocytes followed by fatty acid treatment, as well as in mice fed a high-fat diet[110]. The only study that addressed inflammatory cells, showed that exendin-4 suppressed the influx of macrophages into both the vessel wall and liver, and thereby limited the progression of hepatic inflammation and atherosclerosis in *APOE*3-Leiden.CETP* (*E3L.CETP*) mice fed a Western-type diet[111].

Recently, GLP-1 receptors have been observed on human hepatocytes, and the number of GLP-1 receptors has been found to be decreased in liver biopsy specimens of NASH patients compared to normal controls[92]. Exenatide has been prospectively studied in 8 patients with T2D who were treated with subcutaneous drug for 28 weeks[112]. Paired liver biopsies showed that 3 patients had significantly improved liver histology, and four patients had a 1–2-point improvement in fibrosis. Treatment was associated with weight loss, improved fasting glucose, decreased hemoglobin A1c, and improved ALT levels[112]. Still this tiny study is prone to a type 2 error, including sampling variability of liver biopsy

A long-acting agonist of the GLP-1R (exenatide once-weekly; EQW; exendin-4, Bydureon™, BY) was synthesized by encapsulating exenatide into 0.06-mm-diameter microspheres of medical-grade poly-(*D*, *L*-lactide-coglycolide) which releases the drug over an extended period of time[113]. The efficacy of BY (2mg) was compared to that of once-daily Liraglutide (1.8mg) in T2D patients in a 26-week trial. Both treatments significantly improved glucose homeostasis and induced body weight reduction, although Liraglutide-treated patients experienced a greater reduction in HbA1c levels, fasting serum glucose and reduction in body weight as compared to BY[114]. In contrast, in another study that compared the effects of exenatide once-weekly to exenatide twice-daily, overall BY was more effective at improving glycemic control and also

induced less gastrointestinal side-effects although both compounds caused a similar degree of weight loss[115,116].

The above findings plus differences in injection frequency and tolerability can guide therapeutic decisions for treatment of patients with T2D. Thus, enhancement of GLP-1R agonism showed modest to considerable improvements *in vitro* and in animal models of NASH. Although these drugs have shown favourable safety profiles in patients with T2D, further more thorough mechanistic and hard outcome-oriented preclinical studies in NAFLD/NASH are warranted.

1.6 The role of macrophages

NAFLD /NASH is associated with chronic inflammation of the liver and adipose tissue via the infiltration of immune cells such as dendritic cells, T-lymphocytes and macrophages[117]. Compelling evidence indicates that hepatic macrophages, comprising liver-resident macrophages (Kupffer cells) and monocytes infiltrating the injured liver, as well as specific lymphocyte subsets, play a pivotal role in the initiation and perpetuation of the inflammatory response, with a major adverse impact on main steps of fatty liver progression to fibrosis in both patients with NASH and experimental animal models[118-120].

Tissue macrophages are phenotypically heterogeneous and can be characterized according to their activation/polarization as M1, or “classically activated” pro-inflammatory macrophages, and M2, or “alternatively activated” non-inflammatory macrophages (**Fig.5**)[121-123].

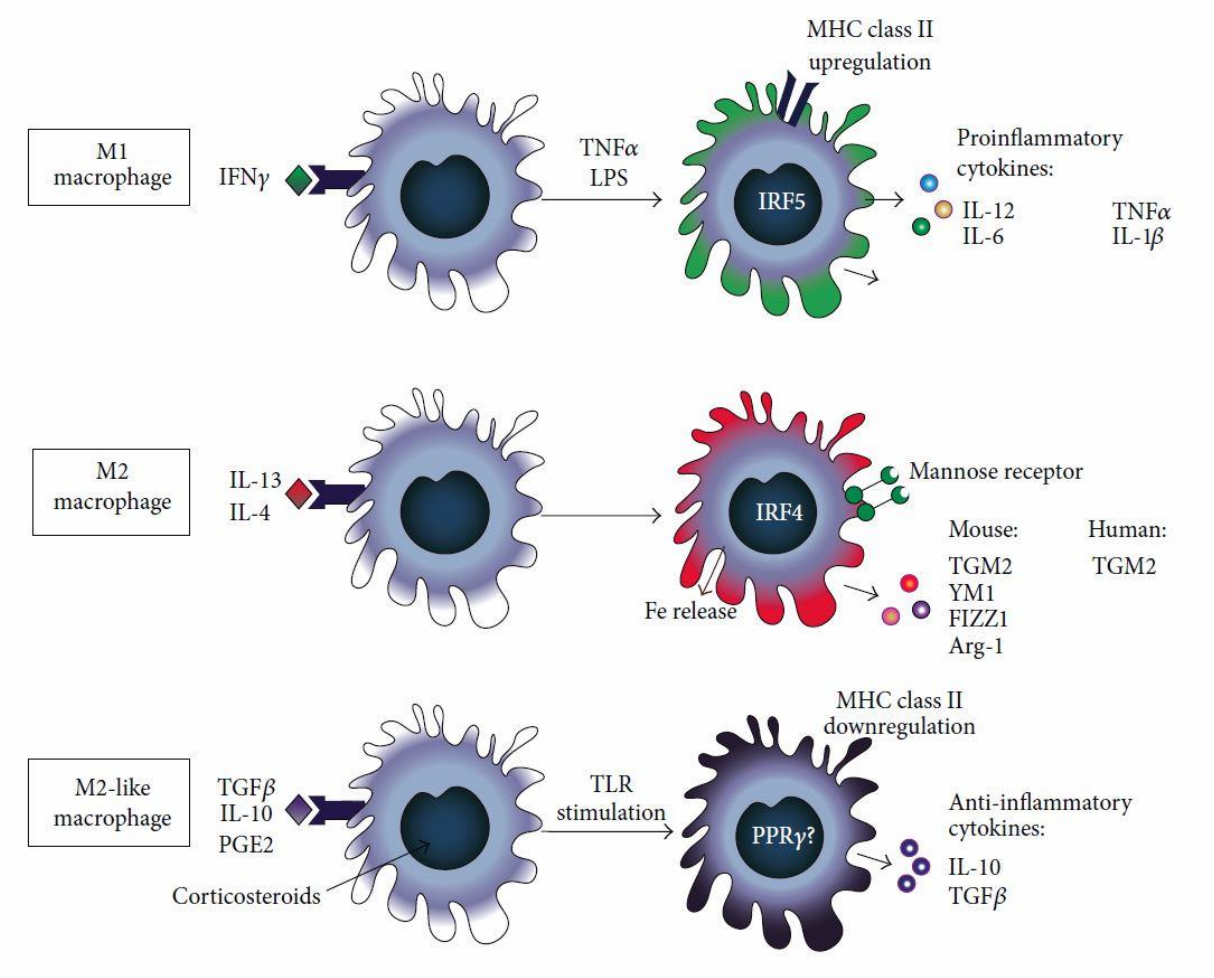

Fig.5 Schematic representation of the three macrophage phenotypes and their characteristics IFNγ, interferon gamma; TNFα, tumor necrosis factor α; LPS, lipopolysaccharide; MHC class II, major histocompatibility complex class II; IL, interleukin; NO, nitric oxide; IRF5, interferon regulatory factor 5; Fe, iron; TGM2, transglutaminase 2; YM1, chitinase-3-like protein-3; FIZZ1/Relmα, resistin-like molecule α; Arg-1, arginase-1; TGFβ, transforming growth factor beta; TLR, Toll-like receptor; PGE2, prostaglandin E2; PPARγ, peroxisome proliferator activated receptor gamma (adapted from[123]).

During NAFLD, Kupffer cells (KCs) are vulnerable to a variety of endogenous and exogenous signals that shift their phenotype towards a proinflammatory M1 state, especially danger signals released by steatotic hepatocytes and toxic lipids accumulated in KCs (**Fig. 6**). M1 macrophages secrete various pro-inflammatory cytokines, such as IL-6 and TNFα, which induce IR through the JNK and inhibitor of kappa B kinase IKKb pathways (regulated inhibitory serine phosphorylation of insulin receptor substrate (IRS) proteins)[124]. TNFα and chemokines such as RANTES/CCL5 and MCP-1 that are produced by M1-activated macrophages induce hepatic cholesterologenesis and increase triglyceride production, which results in a

deregulated homeostasis and lipid metabolism (**Fig. 6**)[125]. In contrast, M2 macrophages secrete anti-inflammatory cytokines, such as IL-10 and IL-1 receptor antagonist (IL-1Ra), Ym1 (chitinase 3), arginase, and macrophage galactose-type lectin 1 (MGL 1, **Fig. 5**)[122,126].

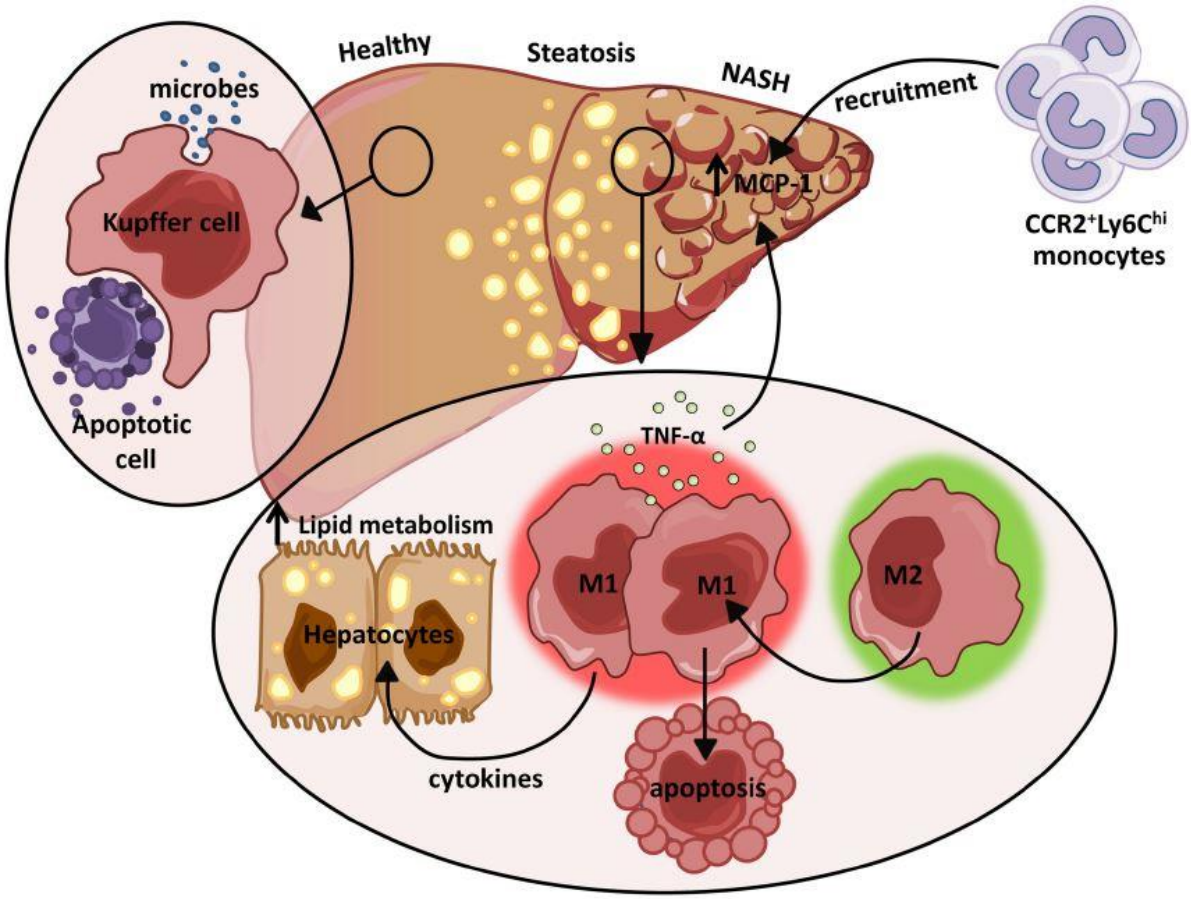

Fig. 6 The dual role of M1/M2 KCs in NAFLD KCs play a pivotal role in host defense where they routinely clear microbes and apoptotic bodies from the portal circulation. During diet-induced liver injury, tissue-resident macrophages exhibiting a classically activated M1 phenotype predominate and secrete cytokines that can alter hepatocyte lipid metabolism and induce MCP-1-dependent recruitment of monocytes into the liver. In turn, these infiltrating cells facilitate the development and progression of NAFLD. Restrained induction of M1 Kupffer cell apoptosis further perpetuates liver inflammation (adapted from[127]).

In mice, IL-4 treatment promotes an M2-like activation of adipose tissue macrophages, which in turn attenuates a high fat diet (HFD)-induced IR[128]. Similarly, IL-10 secreted from M2 macrophages enhances insulin signaling in skeletal muscle and liver and protect against obesity-induced IR[129]. Moreover, activated M2-polarized macrophages represent another pathway for the resolution of inflammatory responses in subjects with NAFLD. M2 KCs enhance caspase 3-dependent apoptosis of classically activated M1 macrophages and provide a protective mechanism against

NAFLD[130]. Thus, M1 macrophages play a critical role in the development of inflammation and IR whereas resident M2 macrophages are able to promote anti-inflammatory responses and tissue homeostasis.

Dysregulation of the hepatic M1/M2 phenotypic balance including general KC activation is emerging as a central mechanism governing NAFLD[131,132]. Recent studies have shown that M1-polarized macrophages release IL-1β that inhibits fatty acid oxidation by decreasing PPAR-alpha trans-activating activity and promoting triglyceride synthesis in hepatocytes following activation of diacylglycerol acyltransferase 2[133,134]. In addition, deficiency of PPAR δ in myeloid cells, which inhibits M2 and favors M1 macrophage polarization, results in enhanced steatosis via inhibition of fatty acid oxidation in hepatocytes[131]. These studies demonstrate the underlying relationship between the loss of alternative KC polarization and/or acquisition of the M1 phenotype, and the development of steatosis.

Activation of KCs also regulates the recruitment of blood–derived monocytes during NASH. Macrophage infiltration into the liver is primarily promoted by CCL2, a chemokine up-regulated in the liver and in the serum of patients with NASH, driving the recruitment of C–C chemokine receptor 2 (CCR2) expressing monocytes[135]. Thus inactivation of CCR2 (receptor for CCL2/MCP-1) reduced macrophage content and changes the inflammatory profile in adipose tissue, resulting in improvement of insulin sensitivity and reduction of hepatic steatosis in obese mice[136]. Specifically, pharmacological or genetic deficiency of CCL2 or CCR2 reduced macrophage infiltration in mice fed MCD or CDAA (choline-deficient L-amino-acid-defined)diets, in addition to preventing steatosis[137,138]. A recent study showed that M1 hepatic macrophages produced TNFα and increased intrahepatic expression of MCP-1, a major chemokine responsible for the recruitment of leukocytes to the liver during hepatic inflammation through the activation of CCR2 receptor mainly found on inflammatory cells such as Ly6C^{hi} monocytes[139]. It has also been reported that other molecules of the chemokine family play a possible role in the pathogenesis of NASH, including CCL5 (RANTES), which is primarily involved in the migration of T-cells, neutrophils, monocytes, and dendritic cells (DCs) through binding to its cognate transmembrane receptors, CCR1, CCR3, and CCR5[140]. The CCR5 receptor has also been identified on isolated hepatic stellate cells (HSCs), suggesting that these hepatic cells are both the target and source of RANTES/CCL5[141]. The level of CCR5 is

markedly up-regulated in diet-induced obese mice and obese patients[142,143] and the deficiency of CCR5 protects mice from hepatic fatty infiltration and IR, and allows a switch in the polarization of macrophages to the M2 phenotype[142]. Hepatocytes are major source of serum and hepatic RANTES/CCL5 in NASH and NAFLD, and this is mediated by the deposition of triglycerides in hepatocytes[144]. Chemokine receptors would represent an ideal target for the treatment of NASH. Inflammatory chemokines such as CCL5 or CCL2 are mainly expressed in conditions of inflammation, and inhibition of their action may be achieved without major off-target effects. Furthermore, chemokine receptors belong to the seven-transmembrane G-protein-coupled receptor superfamily that is targetable by antibodies or small molecules[145]. However, addressing such receptors may well generate unwanted effects due to the many inflammatory as well as anti-inflammatory immune cells expressing them.

In addition to their important role in the initiation of the inflammatory reaction associated with early steps of NAFLD, KCs and recruited monocytes can also contribute to liver fibrosis progression, both by perpetuating inflammatory cell recruitment and by triggering hepatic stellate cell (HSC) activation. Liver fibrosis as a common feature of NAFLD/NASH is characterized by hepatocyte damage and Kupffer cell activation leading to activation of HSC that produces excess ECM proteins, resulting from both their increased synthesis and decreased degradation[146]. Thus extensive evidence demonstrates a complex interplay between KCs and HSCs during hepatic fibrogenesis.

Notably, macrophages also play an important role in the resolution of liver fibrosis[147]. Although the mechanistic profile of these pro- and anti-fibrotic macrophages is still unclear, recent data have indicated that macrophages originating from resident KCs and $Ly6C^{+}$ ($Gr1^{+}$) monocytes promote the progression of liver fibrosis by releasing inflammatory mediators such as IL-1β and by activating HSC[133]. In addition, in hepatic fibrosis, $Ly6C^{hi}$ inflammatory monocyte-derived macrophages express higher levels of transforming growth factor beta 1 (TGFβ1) and other pro-fibrotic cytokines that activate HSC[148]. TGFβ1 does not only promote the fibrogenic activity of HSCs but also increases the expression of tissue inhibitors of metalloproteinases (TIMPs) by HSC and thus block the degradation of ECM[149]. Interestingly, the pro-fibrogenic effect of infiltrating monocytes in mouse models depends on the genetic background. Balb/c mice, in which an immunosuppressive immune cell naturally prevails, are relatively

protected from liver damage and ensuing fibrosis by the interference of monocyte infiltration compared to C57BL/6 mice, indicating that functional macrophage (and T cell) polarization might directly influence the outcome of chronic hepatic injury[150].

The role of especially macrophages in inflammation and fibrosis is complex. Thus often alternatively activated M2 macrophages are involved in dampening inflammation, would healing and fibrosis through the production of TGFβ1, a potent inducer of the HSC fibrotic phenotype[151,152]. On the other hand, M2-like KC may display anti-fibrogenic functions[153-155]. Indeed, mice carrying a specific deletion of either the M2 marker arginase-1 or the chemokine receptor CX3CR1 in macrophages showed that expression of M2 related genes was reduced, and those mice were prone to accelerated liver fibrosis[154,155]. Similarly, the chemokine CX3CL1 suppressed HSC fibrogenic functions by triggering M2 KC polarization[153]. These studies highlight the fact that modulating the KC phenotype is an interesting strategy to protect from NAFLD progression, although the need for a better characterization/classification of pro- and anti-fibrogenic macrophage populations is a prerequisite for such interventions.

1.7 Purpose of this thesis

The aim of this thesis was to investigate the therapeutic efficacy of the DPP-4 inhibitors Linagliptin and Sitagliptin and the long acting GLP-1 receptor agonist BY in

preclinical *in vivo* models of NASH. Since macrophages and in particular polarized macrophages are very likely to play a major role in the pathogenesis of NASH, it was also planned to study the effect of GLP-1 mimetics and DPP-4 inhibitors on macrophage polarization and to reveal possible mechanistic links between GLP-1/GLP-1R signaling, NASH, fibrosis, inflammation and macrophage polarization. Complementary to the above questions, this study aimed to investigate how therapeutic GLP-1/GLP-1R modulation in NASH changes the overall pathogenesis, general clinical parameters, the cellular and molecular micro-environment and the expression and regulation of genes linked to inflammation, cell death, steatosis and fibrosis. In summary, the here presented work was aimed at testing the therapeutic potential of clinically applicable GLP-1/GLP-1R modulators in mouse models of NASH and liver fibrosis and to understand the mechanisms and cellular pathways underlying their potential efficacy.

2. Materials and methods

2.1 Materials

2.1.1 Instrumentation

Name	Manufacturer
A&B applied biosystems step one plus real-time PCR system	Life technologies GmbH, Darmstadt, Germany
Balance Sartorius AX2202	PK Electronic Ettlingen, Germany
Balance Sartorius AX124	PK Electronic Ettlingen, Germany
Bio-Rad T100™ thermal cycler	Bio-Rad, München, Germany
Bio Rad Powerpac basic	Bio-Rad, München, Germany
Bio Rad Powerpac HC	Bio-Rad, München, Germany
Centrifuge HeraeusFresco21	Thermoscientific, Schwerte, Germany
Centrifuge 5804R	Eppendorf, Hamburg, Germany
Centrifuge VWR mini star	VWR International, Darmstadt, Germany
ChemiDoc™ XRS+ System	Bio Rad, München, Germany
Ergone Pipette 1000ul	Starlab GmbH, Hamburg, Germany
Ergone Pipette 200ul	Starlab GmbH, Hamburg, Germany
Ergone Pipette 20ul	Starlab GmbH, Hamburg, Germany
Ergone Pipette 10ul	Starlab GmbH, Hamburg, Germany
Ergone Pipette 2,5ul	Starlab GmbH, Hamburg, Germany
Eppendorf centrifuge 5804R	Eppendorf, Hamburg, Germany
Eppendorf centrifuge 5415R	Eppendorf, Hamburg, Germany
FACS Canto II	BD Biosciences, Heidelberg, Germany
Gentle MACS Dissociator 3013	MACS miltenybiotec
HeraeusMultifuge X3R centrifuge	Thermoscientific, Schwerte, Germany
HXP120C kublercodix	Carl Zeiss, München, Germany
Leica EG 1150c	Leica, Wetzlar, Germany
Leica TP1020	Leica, Wetzlar, Germany
Leica CM1950	Leica, Wetzlar, Germany
Microrome Leica RM2255	Leica, Wetzlar, Germany
Microrome Leica HI1210	Leica, Wetzlar, Germany
Microtome blade MX 35 premier 34°/80mm	Thermoscientific, Schwerte, Germany
MulticalPH meter pH 538	WTW, Weilheim, Germany
Rocking platform	VWR International, Darmstadt, Germany
Rotamax 120	Heidolph Instruments, Schwabach, Germany
TECAN hydrospeed	Tecan, Männedorf, Germany
TECAN infinite M 200Pro	Tecan, Männedorf, Germany
Zeiss microscope AX10	Carl Zeiss, München, Germany

2.1.2 Consumables

Name	Manufacturer
1000µl Tips	Starlab GmbH, Ahrensburg, Germany
200µl Tips	Starlab GmbH, Ahrensburg, Germany
0,1-20µl GradanteTips	Starlab GmbH, Ahrensburg, Germany
96 well plates flat bottomed	Greiner Bio-One, Frickenhausen, Germany
96-well fast thermal cycling	Life technologies GmbH, Darmstadt, Germany
MicroAmp optical adhesive film	Life technologies GmbH, Darmstadt, Germany
Cellstar tubes(15ml and 50ml)	Greiner Bio-One, Frickenhausen, Germany
Cell strainer (100µm)	BD Bioscience, Heidelberg, Germany
Cryo tubes	Greiner Bio-One, Frickenhausen, Germany
DAKO Pen	Dako Deutschland GmbH, Hamburg ,Germany
Disposal bags	Carl Roth, Karlsruhe, Germany
Disposal base molds	Simport, Beloeil, Canada
FACS tubes, polystyrene, 5 ml	BD Biosciences, Heidelberg, Germany
Filter paper	Whatman, Dassel, Germany
Gentle MACS C tubes	Miltenyi Biotec, Bergisch-Gladbach, Germany
Histosette tissue processing/embedding cassettes	Simport, Hague, The Netherlands
Inject-F (single use injection) 1ml	B.Braun, Melsungen, Germany
Knittel glass cover slips 24*50mm	Iss, Bradford, United Kingdom
Microscope coverslips	Life technologies GmbH, Darmstadt, Germany
PCR tubes 0.2 ml Flat cap	Greiner Bio-One, Frickenhausen, Germany
Polysine slides	Thermo scientific, Braunschweig, Germany
Superfrost ultra plus slides	Thermo scientific, Braunschweig, Germany
Safe-lock tubes 2.0 ml	Eppendorf, Hamburg, Germany
Safe-lock tubes 1.5 ml	Eppendorf, Hamburg, Germany
Serological pipette, sterile (5,10,25 ml)	Greiner Bio-One, Frickenhausen, Germany
Superfrostultraplus slides	Thermoscientific, Braunschweig, Germany

2.1.3 Reagents and kits

Name	Manufacturer
1-Propanol pure	Applichem, Darmstadt, Germany
2-Propanol pure	Applichem, Darmstadt, Germany
30% Acrylamide	Carl Roth GmbH, Karlsruhe, Germany
4-(Dimethylamino) benzaldehyde	Sigma Aldrich, Steinheim, Germany
70% Ethanol	Carl Roth GmbH, Karlsruhe, Germany
Ammonium Persulfate	Sigma Aldrich, Steinheim, Germany
Antibody diluent	Dako Deutschland GmbH, Hamburg ,Germany
Bovine serum albumin(BSA)	Sigma Aldrich, Steinheim, Germany
Bydureon	Lilly Deutschland GmbH, Bad Homburg Germany
cDNA SuperMix reverse transcription kit	Quanta, Gaithersburg, USA
Chloroform	Applichem, Darmstadt, Germany
Clarity™ Western ECL Substrate	Bio Rad, München, Germany
Collagenase from Clostridium histolyticum	Sigma Aldrich, Steinheim, Germany
Direct RED 80	Sigma Aldrich, Steinheim, Germany
DAB Peroxidase (HRP) Substrate Kit	Vector Laboratories, Inc., Burlingame, USA
DEPC treated water	Life technologies GmbH, Darmstadt, Germany
DNase I	Sigma Aldrich, Steinheim, Germany
Ethanol absolute	VWR chemicals, Fontenay-sous-bois, France
Ethylendiamintetraacetatic acid (EDTA)	Sigma Aldrich, Steinheim, Germany
Eosin	Carl Roth GmbH, Karlsruhe, Germany
FACS-Clean	BD Bioscience, Heidelberg, Germany
FACS- Flow	BD Bioscience, Heidelberg, Germany
FACS-Rinse	BD Bioscience, Heidelberg, Germany
Fetal calf serum(FCS)	Invitrogen, San Diego, USA
Formaldehyde 4%	Carl Roth GmbH, Karlsruhe, Germany
Glycerol minimum 99%	Sigma Aldrich, Steinheim, Germany
Glycine	Sigma Aldrich, Steinheim, Germany
Hematoxylin	Merck, Darmstadt, Germany
Horse serum	Vector Laboratories, Inc., Burlingame, USA
Hydrochloric acid 6N	VWR, Darmstadt, Germany
Hydrogen peroxide 30%	Carl Roth GmbH, Karlsruhe, Germany
Ketamin Hameln 50mg/ml	Hameln pharmaceuticals, Hameln, Germany
L-Hydroxyproline	Merck KGaA, Hessen, Germany
Linagliptin	Boerhringer Ingelheim Pharma, GmbH&Co. KG
Methanol Technical grade	Applichem, Darmstadt, Germany
Potassium dihydrogen phosphate	Carl Roth GmbH, Karlsruhe, Germany
Oil Red O	Sigma Aldrich, Steinheim, Germany

Perchloric acid 70%	Sigma Aldrich, Steinheim, Germany
Phosphatase inhibitor	Roche, Mannheim, Germany
Picric acid	Sigma Aldrich, Steinheim, Germany
Protease inhibitor	Roche, Mannheim, Germany
Potassium chloride	Carl Roth GmbH, Karlsruhe, Germany
Potassium phosphate monobasic	Sigma Aldrich, Steinheim, Germany
qScript cDNA SuperMix	VWR(Quantabio) Darmstadt, Germany
Rompun 2%	Bayer vital GmbH, Leverkusen, Germany
Roti-Histokitt II	Carl Roth, Karlsruhe, Germany
Sitagliptin	Sequoia, Oxford, United Kingdom
Skim milk powder	Sigma Aldrich, Steinheim, Germany
Sodium chloride	Carl Roth GmbH, Karlsruhe, Germany
Sodium phosphate dibasic	Carl Roth GmbH, Karlsruhe, Germany
Sodium citrate dihydrate	Fisher- scientific New Jersey, USA
Sodium dodecyl sulfate	Sigma Aldrich, Steinheim, Germany
Sudan III	Sigma Aldrich, Steinheim, Germany
SYBR Green PCR mix	Life technologies GmbH, Darmstadt, Germany
Taqman master mix	Life technologies GmbH, Darmstadt, Germany
Triton^{TM} X-100	Sigma Aldrich, Steinheim, Germany
Trizma base	Sigma Aldrich, Steinheim, Germany
Ribozol	Ampresco, Solon, USA
Tween 20	Merck KGaA, Darmstadt, Germany
VECTASTAIN ABC Systems	Vector Laboratories, Inc., Burlingame, USA
Xylene	Applichem, Darmstadt, Germany
β-mercapthoethanol	Sigma Aldrich, Steinheim, Germany

2.1.4 Antibodies

Name	**Manufacturer**
anti α-SMA (E184)	Abcam plc, Cambridge, United Kingdom
anti CD11b(M1/70)	Biolegend, Fell, Germany
anti CD11c(N418)	Biolegend, Fell, Germany
anti CD45(30-F11)	Biolegend, Fell, Germany
anti CD68(FA-11)	Biozol Diagnostica Vertrieb GmbH, Eching, Germany
anti- caspase-3 (9661)	Cell signaling technologies, Cambridge, United Kingdom
anti-collagen type III	Produced in house by Harvard University
anti-c-Jun(9165)	Cell signaling technologies, Cambridge, United Kingdom
anti-phospho-c-Jun(9261)	Cell signaling technologies, Cambridge, United Kingdom
anti-ERK1/2(216703)	Cell signaling technologies, Cambridge, United Kingdom

anti-phospho- ERK1/2(9101)	Cell signaling technologies, Cambridge, United Kingdom
anti F4/80(BM8)	Biolegend, Fell, Germany
anti-phospho-JNK(9251)	Cell signaling technologies, Cambridge, United Kingdom
anti Ly6c(HK1.4)	Biolegend, Fell, Germany
anti-α-tubulin(DM1A)	Sigma Aldrich, Steinheim, Germany
anti Ym1(01404)	Stem cell Technologies, Köln, Germany
Biotinylated goat anti rabbit IgG (H+L)(BA-1000)	Vector Laboratories, Inc., Burlingame, USA
Biotinylated goat anti rat IgG (H+L) (BA-9400)	Vector Laboratories, Inc., Burlingame, USA
Goat anti mouse IgG-HRP(sc-2005)	Santa Cruz Biotechnology Inc., Santa Cruz, USA
Goat anti rabbit IgG-HRP(sc-2004)	Santa Cruz Biotechnology Inc., Santa Cruz, USA

2.1.5 General buffers and solutions

Acidified water	Glacial acetic acid 5ml dd H_2O 1000 ml
Antigen unmasking citrate buffer	2,94 g sodium citrate trisodium salt dehydrate to 1l d H_2O adjusted to pH 6.0
Blocking solution	2.5% normal horse serum
Citric acetate buffer	5% citric acid (5 g) 7.24% sodium acetate (7.24 g) 3.4% sodium hydroxide (NaOH 3.4 g) 1.2% glacial acetic acid (1.2 ml) dissolved in 100 ml dH_2O, adjusted to pH 6.0
Chloramine T	32 ml citric acetate buffer pH 6.0 4 ml distilled water 4 ml n-propanol 564 mg chloramine T hydrate heated to 50°C to dissolve
Ehrlich's reagent	7.9 ml n-propanol 3.31 ml 70% perchloric acid 1.91 mg 4-Dimethylaminobenzaldehyde prepared freshly before the experiment.
FACS fixation buffer	0.1% formaldehyde in PBS
Phosphate buffered saline(PBS) 10X stock solution	137 mM sodium chloride (NaCl 80 g) 2.0 mM potassium chloride (KCl 2 g) 10 mM sodium phosphate dibasic (Na_2HPO_4 14.4 g) 1.8 mM monopotassium phosphate (KH_2PO_4 2.4 g) to 1 L dH_2O adjust pH to 7.4 with hydrochloric acid (HCl)
Tris buffered saline (TBS)	24,2 g trizma base (C4H11NO3)

10X stock solution	80 g sodium chloride (NaCl) to 1l Adjusted to pH 7.6 with HCl
PBST 1X	100 ml 10X PBS stock solution 900 ml d H_2O, 1 ml Tween 20
TBST 1X	100 ml 10X TBS stock solution 900 ml d H_2O, 1 ml Tween 20
Ammonium persulfate (APS) 10%(w/v)	10 g APS in 100 ml d H_2O
Blocking buffer	1X TBST with 5% w/v nonfat dry milk
Tris-Glycine 10X stock solution	121 g trisma base glycine 577 g dissolved in 4 L d H_2O
Running Buffer	100 ml 10X Tris-glycine buffer 10 ml 10% SDS 890 ml dH_2O
Primary antibody dilution buffer	1X TBST with 5% BSA or 5% nonfat dry milk
Stripping buffer	0.76 g Trizma base 2 g sodium dodecyl sulfate (SDS) 700 µl β-mercaptoethanol Bring to 100 ml with d H_2O Adjusted to pH 6.8 with HCl.
Sodium dodecyl sulfate10%	10 g SDS into 100ml d H_2O
Transfer Buffer	100 ml 10X Tris-Glycine buffer 200 ml methanol 700 ml dH_2O
0.1% Sirius Red solution	Sirius Red 0.5 g saturated picric acid 500 ml
Oil Red O stock solution	0.5 g Oil Red O Isopropanol 100 ml, warmed in a water bath at 56℃ for 1 h
Oil Red O working solution	Stock :dH2O= 6:4 mix well left for 10 min, filtered

2.1.6 Quantitative real time PCR (qPCR) primer for marker analysis

Target gene	**Forward primer (5'-3')**	**Taqman Probe**	**Reverse primer (5'-3')**
α-SMA	ACAGCCCTCGCACCCA	CAAGATCATTGCCCCTCCAGAACGC	GCCACCGATCCAGACAGAGT
Procollagen α1(I)	TCCGGCTCCTGCTCCTCTTA	TTCTTGGCCATGCGTCAGGAGGG	GTATGCAGCTGACTTCAGGGATGT
TGFß1	AGAGGTCACCCGCGTGCTAA	ACCGCAACAACGCCATCTATGAGAAAACCA	TCCCGAATGTCTGACGTATTGA
TIMP-1	TCCTCTTGTTGCTATCACTGATAGCTT	TTCTGCAACTCGGACCTGGTCATAAGG	CGCTGGTATAAGGTGGTCTCGTT

Smad2	CCCATTCCTGTTCTGGTTCA	AGCAGTACAGCAGAATGACGTCGTGC	AGCCAGCAGTGCAACTTTTT
Smad3	GGGCCTACTGTCCAATGTCA	CCGGAATGCAGCCGTGGAAC	CCCAATGTGTCGCCTTGTA
MMP2	CCGAGGACTATGACCGGGATAA	TCTGCCCCGAGACCGCTATGTCCA	CTTGTTGCCCAGGAAAGTGAAG
MMP3	GATGAACGATGGACAGAGGATG	TGGTACCAACCTATTCCTGGTTGCTGC	AGGGAGTGGCCAAGTTCATG
MMP8	CAGGGAGAAGCAGACATCAACA	TGCTTTCGTCTCAAGAGACCATGGTGA	GATTCCATTGGGTCCATCAAA
MMP9	CAGGATAAACTGTATGGCTTCTGC	CTACCCGAGTGGACGCGACCGT	GCCGAGTTGCCCCCA
MMP13	GGAAGACCCTCTTCTTCTCT	TCTGGTTAACATCATCATAACTCCACACGT	TCATAGACAGCATCTACTTTGTT
CCL3	ACCTGGGTCCAAGAATAC	ACTGACCTGGAACTGAATGCCT	CAGCAAACAGCTTATAGGAG
TNFα	CTCAGCCTCTTCTCATTC	CACCACGCTCTTCTGTCTACTGA	GCCATAGAACTGATGAGA
CCR7	CCTGGTTGAGTAGTCTTC	ACTGTCATCTCTTGCTTGCTTGC	CTGTGGGAGCATTTAGAG
IL10	CCTCAGGATGCGGCTGAG	CGCTGTCATCGATTTCTCCCCTGTG	GCTCCACTGCCTTGCTCTTATT
CD36	CTCGTTTCAACTCTCACA	ACCATCCACCAGTTGCTCCA	GCACTTCAAATCATTTGTAAAC
CCL5	GAGGGTTTCTTGATTCTGA	CCTGTCATTGCTTGCTCTAGTCCTA	GCTGATTTCTTGGGTTTG
Arg1 (SRBY)	GGTCCAGAAGAATGGAAGAGTCAG		CAGATATGCAGGGAGTCACC
CD68 (SRBY)	CTTCCCACAGGCAGCACAG		AATGATGAGAGGCAGCAAGAG
GAPDH	AGGTCGGTGTGAACGGATTTG		GGGGTCGTTGATGGCAACA
SREBP-1c (SRBY)	ACGGAGCCATGGATTGCACA		AAGGGTGCAGGTGTCACCTT
ACC (SRBY)	ATGGGCGGAATGGTCTCTTTC		TGGGGACCTTGTCTTCAT CAT
FAS (SRBY)	TGCTCCCAGCTGCAGGC		GCCCGGTAGCTCTGGGTGTA
LPL (SRBY)	CCACAGCAGCAAGACCTTC		AGGGCGGCCACAAGTTTG

2.1.7 MCD and MCS diets

Product	MCD Diet (E15653-94)		MCS Diet (E15654-04)	
	genetically modified (gm)	%kcal	gm	%kcal
Protein	17	16	17	16
Carbohydrate	66	63	65	62
Fat	10	21	10	21
		100		100
Ingredient(gm)				
L-Alanine	3.5	14	3.5	14
L-Arginine	12.1	48.4	12.1	48.4
L-Asparagine-H2O	6	24	6	24
L-Aspartate	3.5	14	3.5	14
L-Cystine	3.5	14	3.5	14
L-Glutamine	40	160	40	160
Glycine	23.3	93.2	23.3	93.2
L-Histidine-HCl-H2O	4.5	18	4.5	18
L-Isoleucine	8.2	32.8	8.2	32.8
L-Leucine	11.1	44.4	11.1	44.4
L-Lysine-HCl	18	72	18	72
L-Phenylalanine	7.5	30	7.5	30
L-Proline	3.5	14	3.5	14
L-Serine	3.5	14	3.5	14
L-Threonine	8.2	32.8	8.2	32.8

L-Tryptophan	1.8	7.2	1.8	7.2
L-Tyrosine	5	20	5	20
L-Valine	8.2	32.8	8.2	32.8
Total L-Amino Acids	171.4	685.6	171.4	685.6
Sucrose	455.3	1821.2	452.3	1809.2
Corn Starch	150	600	150	600
Maltodextrin10	50	200	50	200
Cellulose	30	0	30	0
Corn Oil, Stripped	100	900	100	900
Mineral Mix S10001	35	0	35	0
Sodium Bicarbonate	7.5	0	7.5	0
Vitamin Mix V10001	10	40	10	40
L-Methionine	**0**	**0**	**3**	**12**
Choline Bitrartrate	**0**	**0**	**2**	**0**
Total	1009.2	4246.8	1011.2	4246.8

2.2 Methods

2.2.1 Animals and diet

Male C57BL/6J mice were purchased from Janvier (Saint Berthevin Cedex, France). Mice were either fed a lipogenic diet deficient in methionine and choline (MCD diet) or received the MCD diet supplemented with methionine and choline (MCS control diet, Ssniff GmbH, Germany). In the steatohepatitis induction group mice were fed the MCD diet and in the control group the MCS diet for 4 or 8 weeks. In Linagliptin and Sitagliptin treatment studies, 8-week old male C57BL/6 mice were first fed the MCS or MCD diet for 4 weeks and then gavaged daily either with vehicle, Linagliptin 5 mg/kg or Sitagliptin 50 mg/kg of body weight for 6 weeks[156,157]. Group n values were as follows: MCS diet (N=10), MCD diet-fed mice with vehicle treatment (MCD+VH, N=10), MCD diet-fed mice with Linagliptin treatment (MCD+Linagliptin, N=10) and MCD diet-fed mice with Sitagliptin treatment (MCD+ Sitagliptin, N=10). To test the therapeutic effects of BY, animals that had received the MCD diet for 4 weeks were administered 0.4 mg/kg BY via subcutaneous injection in the human equivalence dose (HED, mg/kg)=animal dose(mg/kg) multiplied by the animal Km factor /human Km factor, which is x12.3 for mice[158]). Another group received a high By-dose (2 mg/kg, BY-H group), and mice receiving PBS only served as controls.

Mdr2 (abcb4)$^{-/-}$ female mice were on a FVB background and were imported from our lab in Boston (ref. Popov 2005, 2008), FVB normal controls were obtained from Jackson Laboratories (Bar Harbor, Maine, USA). Mdr2$^{-/-}$ mice spontaneously develop progressive secondary biliary fibrosis due to absence of the hepatocyte phospholipid flippase and show advanced fibrosis already at 8 weeks of age to further progress beyond age 12 weeks, with lesions closely resembling that of human primary sclerosing cholangitis and congenital biliary cirrhosis[159]. All mice were bred and kept at the Central Animal Facility of the University of Mainz (TARC). After 8 weeks, Mdr2$^{-/-}$ mice were treated with gavage therapy using 0.5 mg/kg, 5 mg/kg and 10 mg/kg of Linagliptin for 4 weeks (group size: N=7).

Mice were euthanized with vaporized isoflurane, exsanguinated via cardiac puncture, and serum was collected and frozen immediately. Dissected tissues were weighed and flash-frozen in liquid nitrogen. All experiments were approved by the ethical committee of the Landesuntersuchungsamt Rheinland-Pfalz under the reference number 23 177-07/G 12-1-007.

2.2.2 Routine blood and dot blot analysis

Aspartate aminotransferase (AST), ALT, alkaline phosphatase (ALP) and serum triglyceride levels were determined in the Clinical Chemistry and Laboratory Medicine Department at the Mainz Medical Center. Individual features, including degree of steatosis, inflammation and ballooning were scored on the basis of the NAFLD activity score[160].

For dot blot analysis, 50 µg of serum protein was spotted on PVDF membranes (Bio-Rad), blocked with TBS-T (Tris-buffered saline, 0.05% Tween 20) containing 5% nonfat dry milk for 1 hour and incubated with the IL-6 antibody (1:500 in 5% skimmed milk/TBS-T, Abcam, Clone number ab6672) overnight at 4℃. Subsequently, a horseradish peroxidase-linked anti-rabbit IgG secondary antibody (1:10000, Vector labs Clone number PI-1000) was added for 45 minutes at room temperature and the blots were washed twice in TBS-T. Signals were revealed using the ECL chemiluminescence kit (Thermos scientific) and documented on a Chemilux ECL Imager (Intas). Dot intensities were determined with the GelPro analyzer software Version 6.0 (Media Cybernetics).

2.2.3 Hydroxyproline (Hyp) assay

Briefly, two snap-frozen liver pieces from the left and right liver lobe (150–160 mg each) were hydrolyzed at 110°C for 16 hours. 5 µl hydroxyproline standards (Merck) and hydrolysate samples and blanks were added into a 96 well plates. 50 µl citrate-acetate buffer (Fisher-scientific) and 100 µl chloramine T (Sigma) solutions were separately added to the hydrolyzed samples and hydroxyproline standards. After a 30 min incubation on an orbital shaker at room temperature the samples were incubated in a solution containing of 4-dimethylaminobenzaldehyde (Sigma), dissolved in 70% perchloric acid (Sigma) and 1-isopropanol (Applichem) for 30 minutes at 65°C. The absorbance of the solution was measured at 550 nm wavelength and the levels of Hyp per milligram of liver tissue were colorimetrically quantified and calculated using the standard curve of a serial dilution of L-Hyp (Merck). Total hepatic Hyp content was calculated by multiplying the above determined liver weights with the relative hepatic Hyp concentration as described[159,161].

2.2.4 Histopathological staining

Fresh mouse livers were either fixed with formalin for paraffin sectioning or immediately embedded in O.C.T. compound (Sakura) for frozen sectioning. Liver staining was performed on 4 µm paraffin sections or 7 µm cryo-sections. For the histopathological evaluation, formalin-fixed liver tissue samples were deparaffinized and hydrated serial liver tissue sections were stained with hematoxylin and eosin (H&E), Liver fibrosis was quantified with Sirius Red. Direct Red 80 was provided by Sigma-Aldrich. Alternatively, cryo-sections for lipid accumulation (7 µm thick) were stained with Oil red O (Sigma) or Sudan III (Sigma).

2.2.4.1 H&E staining

Paraffin sections were deparaffinized in xylene I and II and III (5 minutes, hydrated in isopropylacohol 100% I and II (3 minutes), followed by isopropylacohol 95% I and II (3 minutes) isopropylacohol 70% (3 minutes) and rinsed in distilled water (5 minutes). After deparaffinization, the tissue was stained with the blue nuclear stain hematoxylin for 3 min (filtered before each use to remove oxidized particles) and washed for 10 min in running tap water. After immersing once in distilled water, slides were stained with the red cytoplasmic stain eosin for 15 seconds and once again passed through the graded isopropylacohol solutions (70%, 95%, 95%, 100% and 100%) and finally immersed twice in xylene for 5 min. Slides were mounted with resinous medium in the fume hood and visualized in a Zeiss Axio Imager AX10 Microscope with the appropriate filters. Representative images were taken with an AxioCamMRc 5 camera. A minimum of 10 random high-power fields was analyzed for each section. Quantitative analysis was performed using the Image J software (National Institute of Health, Bethesda, Maryland, USA).

2.2.4.2 Sirius red staining

The tissues were deparaffinized and rinsed twice for 5 min in distilled water. Excess moisture was removed from the slides and these were then incubated in 0.1% Sirius red in saturated picric acid solution for 30 min. Excess stain was removed by rinsing twice in 0.05% acetic acid for 5 min. The slides were rinsed in distilled water and dehydrated by dipping several times in 70% isopropylacohol and twice in 95% and 100% isopropylacohol followed by two 5 min immersion in xylene. The slides were mounted with resinous medium and visualized in a Zeiss Axio Imager AX10 Microscope with the

appropriate filters. Representative images were taken with an AxioCamMRc 5 camera. A minimum of 10 random high-power fields were analyzed for each section. Quantitative analysis was performed using the Image J software (National Institute of Health, Bethesda, Maryland, USA).

2.2.4.3 Oil red O and Sudan III staining

Tissues were air dried for 5 min and dehydrated in 60% isopropylacohol by dipping them 10 times and then stained in 0.3% Oil red O or Sudan III solution for 30 min. Excess stain was washed off in 60% isopropylacohol for several seconds. Next the slides were rinsed in deionized water, counter stained for 30s with Mayer's hematoxylin and put under running tap water for 5 min. The slides were mounted with resinous medium and visualized in a Zeiss Axio Imager AX10 Microscope with the appropriate filters. Representative images were taken with an AxioCamMRc 5 camera. A minimum of 10 random high-power fields were analyzed for each section. Quantitative analysis of lipid content was performed using the Image J software (National Institute of Health, Bethesda, Maryland, USA).

2.2.5 Immunofluorescence staining

For frozen sections biopsies were embedded in O.C.T. compound (Sakura) and fixed in 4% formaldehyde. Anti-CD68 (1:100, AbDSerotec, FA-11) and anti-collagen type III (1:800, produced in house) primary antibodies were diluted in 1X PBS plus 1% bovine serum albumin (BSA) / 0.3% Triton™ X-100 buffer and incubated overnight at 4 °C. After washing three times in PBS, the sections were incubated for 2 hours at room temperature with an Alexa Fluor 488-conjugated anti-rabbit immunoglobulin secondary antibody (1:500 diluted in PBS, Life technologies, A-11008) and counterstained with DAPI. For each staining a minimum of 10 randomly selected fields were analyzed and positive cells were scored in each individual field. Quantitative analysis was performed using the Image J software (National Institute of Health, Bethesda, Maryland, USA).

2.2.6 Immunohistochemical staining

For immunohistochemical stains were performed on formalin fixed. Sections were rehydrated and antigens retrieved using heated in 0.01 M sodium citrate buffer (pH 6.0) for 30 min. Endogenous peroxidase was quenched using 3% H_2O_2 in deionized water. After washed, sections were block with 5% goat serum or 2.5% horse serum. Anti-

CD68 (1:100, Biozol, FA-11), anti-F4/80 (1:50 eBioscience, BM8), anti-Ym1 (1:500, Stemcell, 01404), anti-cleaved Caspase 3 (1:300, cell signaling technology, 9661) and anti-α-SMA (1:500, Abcam, E184) antibodies were diluted in antibody diluent (Dako) and incubated overnight at 4°C. After washing three times in TBS, a biotinylated secondary antibody (1:500, Vector Labs, BA-1000) was added for 30 minutes at room temperature followed by three washes in TBS. Sections were revealed using the Vectastain ABC kit (Vector Laboratories) and the DAB substrate kit (Vector Laboratories) and counterstained with hematoxylin. Tissues were visualized using a Zeiss Axio Imager AX10 Microscope with the appropriate filters. Representative images were taken with an AxioCamMRc 5 camera. A series of images covering >90% of the total tissue sections were generated at uniform settings of magnification, light, and exposure time. Quantitative analysis was performed using the Image J software.

2.2.7 QPCR analysis

Total RNA was extracted using Trizol (Invitrogen) and cDNA synthesis was performed with the iScript TMcDNA Synthesis kit (Quantum Bio). TaqMan probes and primers were designed using the Primer Express software (Perkin Elmer, Foster City, CA). All sequences are summarized in table 2.1.6. QPCR reactions were running on an A&B step one plus real time PCR thermocycler (Applied Biosystems). RNA levels were normalized against the transcription levels of Gapdh using the relative standard curve method (Sequence Detection Systems software version 2.2.2, Applied Biosystems).

2.2.8 Flow cytometry

Immune cells were isolated from liver biopsies by incubation in digestion buffer (0.4% collagenase IV (Sigma), 154 mM NaCl, 5.6 mM KCl, 5.5 mM glucose, 20.1 mM HEPES, 25 mM $NaHCO_3$, 2 mM $CaCl_2$, 2 mM $MgCl_2$, 1.6 nM DNaseI (Applichem) pH7.4) for 30 min at 37°C, homogenized using a gentleMACS dissociator (Miltenyl Biotec) and incubated for 30 min at 37 °C. Subsequently, homogenates were passed through a 100 µm cell strainer (BD Bioscience) and centrifuged at 21 x g for 4 min. Supernatants containing the immune cells were centrifuged at 300 x g for 10 min. Cell pellets were resuspended in PEB buffer (PBS pH 7.2, 0.5% BSA / 2 mM EDTA) and red blood cells were lysed in lysis buffer (Miltenyl Biotec), followed by centrifugation at 300 g for 10 min and the each 10^6 cells were blocked with an anti-Fc receptor antibody (1:100, BD

Bioscience, 2.4G2). For detecting specific immune cell populations, anti-CD45 (1:100, 30-F11), anti-CD11b (1:100, M1/70), anti-CD11c (1:100, N418), anti-Ly6C (1:100, HK1.4) and anti-F4/80 (1:100, BM8) antibodies were used (all from Biolegend). After antibody staining the cells were fixed with 1% formaldehyde buffer. Data were acquired on a FACS Canto II (BD Bioscience) and analyzed using the FlowJo 7.6 software (TreeStar).

2.2.9 Western blotting

Tissues were disrupted using a tissue Lyser (QIAGEN) in RIPA buffer containing both a protease inhibitor (Roche 05892791001) and a phosphatase inhibitor (Roche 04906845001). Next, 30–40 mg liver lysates were centrifuged at 20 x g for 15 min and the protein concentration was measured with the BCA protein assay kit (Thermo scientific). For separation, 40 µg protein per well was fractionated on a 10% SDS-PAGE, transferred to PVDF membranes (Millipore) and the transferred proteins were detected using anti-α-SMA (1:1000, Abcam, E184), anti-Ym1 (1:1000, Stemcell, 01404), anti-ERK1/2 (1:500, R&D, 216703), anti-phospho-ERK1/2 (1:500, Cell Signaling Technology, 9101), anti-c-Jun (1:500, Cell Signaling Technology, 9165), anti-phospho-c-Jun (1:500, Cell Signaling Technology, 9261) and anti-phospho-SAPK/JNK (1:1000, Cell Signaling Technology, 9251) primary antibodies. As a loading control membranes were rehybridized with anti-α-tubulin antibody (1:10000, Sigma-Aldrich, DM1A). Bound antibodies were visualized using the chemiluminescence substrate kit (Bio Rad). Protein patterns were documented on a XRS+ System (Bio Rad).

2.2.10 Statistical analysis

All data points are expressed as mean values ±SEM (standard error of mean). Analysis of variance (ANOVA) with Bonferroni corrections was used for multiple group comparisons. When two groups were compared, unpaired Student's t-tests were used for data analysis. Differences were considered to be statistically significant at $p<0.05$. All statistical data was produced using GraphPad Prism 5.0 0 (GraphPad software).

3. Results

3.1 MCD diet-induced NASH in C56BL/6J mice

3.1.1 Body weight, liver weight and clinical observations

Administration of the MCD diet to C57BL/6J mice for 4 weeks and 8 weeks resulted in features of severe NASH compared to MCS diet feeding. However, the MCD diet caused a marked and progressive decrease in mouse body weight and liver weight at 4 and 8 weeks when compared with the MCS diet group. Importantly, mice fed the MCD diet lost weight due to a vastly reduced caloric intake. Since most humans with NASH are obese and insulin resistant, this represents an important difference between the MCD dietary mouse model and human NASH[162]. Serum ALT, AST and LDH levels were highly increased in MCD diet-fed mice (**Table 2**).

Table 2. Central parameters of mice fed the control (MCS) or MCD diet

	MCS (4 weeks)	MCD (4 weeks)	MCS (8 weeks)	MCD (8 weeks)
Body weight (g)	26.99±1.5	17.54±2.65 ***	31.24±2.83	16.81±2.73***
Liver weight (g)	1.11±0.29	0.53±0.09***	1.47±0.36	0.60±0.1***
Food intake/day (g)	4.08±0.07	2.90±0.20**	4.38±0.24	3.31±0.27**
AST (U/l)	25.22±4.42	410.8±61.14***	16.00±1.0	222.9±30.61***
ALT (U/l)	150.0±38.62	526.22±80.74***	140.5±19.73	466.4±63.32***
LDH (U/l)	189.0±48.71	450.0±57.07***	304.0±51.76	605.71±117.7***

Mice were administered MCD or MCS diets. At the beginning of the protocol, every other week and at the time of killing body weight was recorded. Liver weight was recorded at the time of killing. Data are expressed as means ± SEM. N=10 mice per group. *p < 0.05, **p < 0.01, and ***p < 0.001 versus MCS treated mice at the same time point.

3.1.2 Expression of fibrosis and inflammation related mRNA transcript levels

The mRNA expression levels of genes related to pro-inflammatory cytokines and fibrogenesis were measured by qPCR analysis of liver tissue. The mRNA levels of TGFβ1, alpha-smooth muscle actin (α-SMA), procollagen α1 (I) (COL1α1) and TIMP-1 were all significantly increased in mice fed the MCD diet for 4 and 8 weeks. In addition, there was an up-regulation of genes putatively involved in fibrolysis (but potentially also in unfavorable matrix remodeling), namely matrix metalloproteinase (MMP) 3 and MMP13 mRNA. After feeding the MCD diet, the M1 (proinflammatory) macrophage chemokine (C-C motif) ligand 3 (CCL3) and the fatty acid transporter CD36 mRNA levels were significantly increased after 4 weeks and 8 weeks (**Fig. 7**).

A

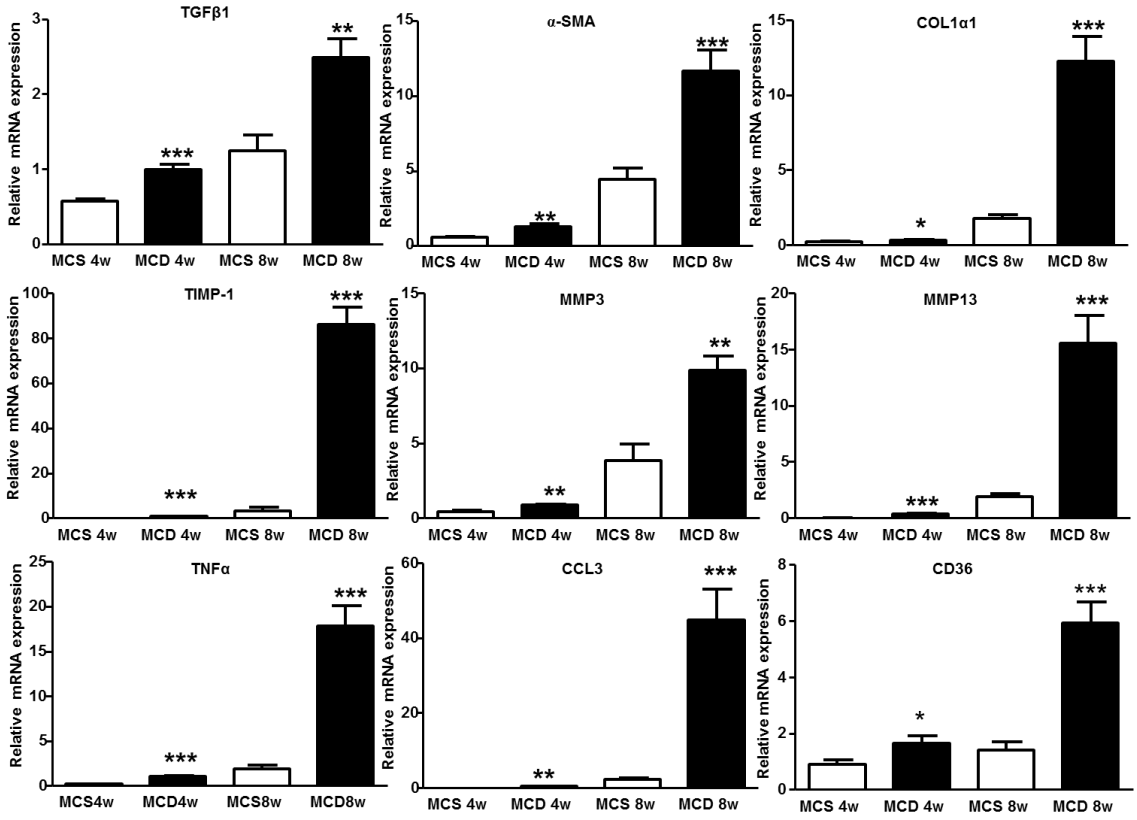

Fig.7 MCD diet feeding for 4 and 8 weeks strongly induces hepatic mRNA levels of fibrosis and inflammation related genes (**A**) qPCR analysis of the expression of mRNAs encoding TGFβ1, α-SMA, COL1α1, TIMP-1, MMP3, MMP13, TNFα, CCL3 and CD36. Data are means ±SEMs (N=10 per group). *p< 0.05, **p < 0.01, and ***p< 0.001 versus MCS treated mice at the same time point.

3.1.3 Hepatic collagen accumulation

MCD diet-fed mice demonstrated a steady increase of relative hepatic collagen accumulation (µg Hyp per 100 mg of tissue, as quantified biochemically), being 2-fold above the average levels of their MCS diet controls at 4 weeks, and 2.5-fold at 8 weeks (**Fig. 8A**). The total Hyp concentration was not significantly different in MCD diet-fed mice due to the loss of the liver weight when compared with MCS diet-fed mice.

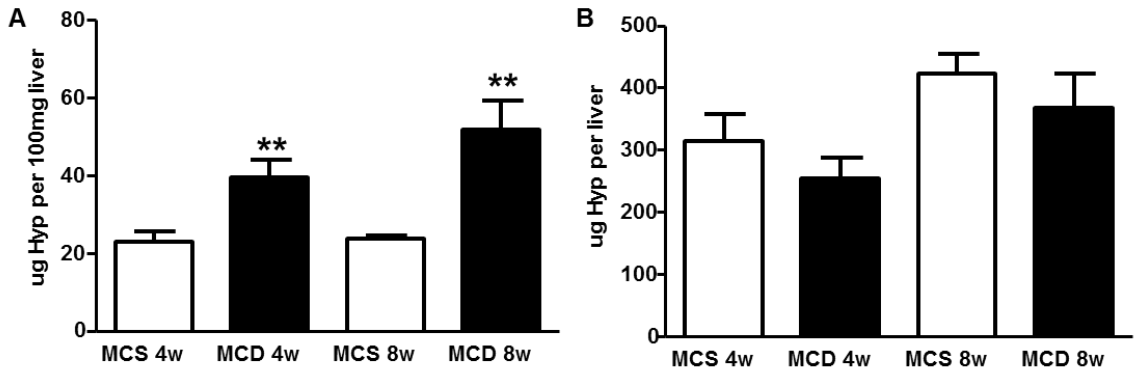

Fig. 8 MCD diet induces severe liver fibrosis (**A**) Quantification of relative hepatic collagen accumulation by biochemical determination of hydroxyproline (Hyp). (**B**) Quantification of Hyp per total liver. **p< 0.001 versus MCS treated mice at the same time point.

3.1.4 Histopathology of liver biopsies

Liver sections from the MCS group stained with H&E showed normal hepatic cells and regular histoarchitecture (**Fig. 9A**). By contrast, sections from mice fed the MCD diet showed massive hepatocyte ballooning and steatosis with mild inflammatory cell infiltration (**Fig. 9A**). These results confirm the successful establishment of the animal model. Fat diffusely accumulated in hepatic tissue in the MCD diet group, when stained with Sudan III, and massive yellow lipid droplets appeared in liver sections from MCD mice, while no obvious fat droplets were present in the liver sections from MCS mice (**Fig. 9B**). The MCD diet-induced hepatic steatosis presented mainly with a predominant macro-vesicular pattern, associated with severe inflammation and fibrosis.

Although steatosis and inflammation appear early during the course of experimental steatohepatitis, fibrosis is a late event that has a deep impact on prognosis, causing hepatocellular dysfunction and the emergence of portal hypertension. In normal livers, collagen is only present in the portal areas and in the walls of major blood vessels (**Fig. 9C**). If fibrosis is severe, collagen fibers appear in other areas and fibrous expansion of portal areas, with marked portal-to-portal as well as portal-to-central bridging, and is commonly observed. Liver fibrosis was analyzed using Sirius Red staining, which highlights collagen fibers in red color and severity of fibrosis was also scored using the clinical Ishak pathology score[163]. Fibrosis in the liver appeared after 4 weeks of the MCD diet, surrounding the centrilobular vein and creating a fine network of fibers around groups of hepatocytes.

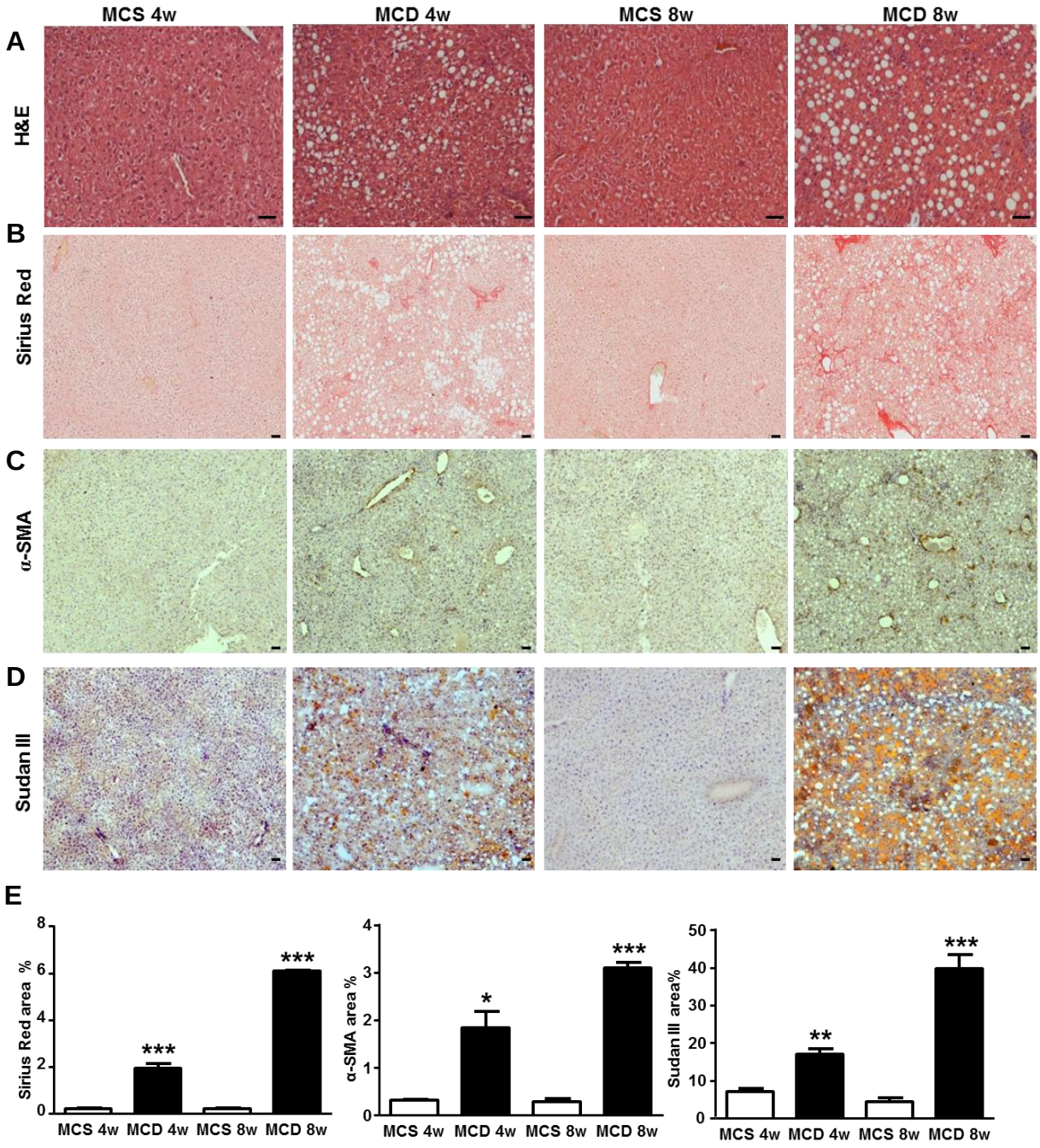

Fig. 9 The MCD diet induces severe steatosis and fibrosis (**A**) Liver sections were stained with hematoxylin and eosin. (**B**) Sudan III staining of liver sections. (**C**) Sirius Red staining for collagen. (**D**) α-SMA staining for myofibroblast activation. (**E**) The percentage of the total area of liver sections occupied by lipid droplets, Sirius red and α-SMA staining was quantified using an image analysis system (scale bars indicates 50 μm). Data are means ±SEMs (N=10 per group). *p < 0.05, **p < 0.01, and ***p < 0.001 versus MCS treated mice at the same time point.

The collagen ratio in the liver parenchyma was calculated to give a quantitative measure of fibrosis. This analysis showed that the collagen occupied area in the MCD group was 1.95% at 4 weeks and 6.09% at 8 weeks compared to 0.22%, 0.23% in the

MCS group at 4 and 8 weeks, respectively (**Fig.9E**). MCD-fed mice also showed a dramatic induction of the myofibroblast activation marker α-SMA (**Fig.9D, E**). The α-SMA positive areas in the MCD group were 1.84% at 4 weeks and 3.11% at 8 weeks, compared to 0.28%, 2.31% in the MCS group at 4 and 8 weeks, respectively. Mice receiving the MCD diet presented a more advanced form of liver disease, with values of fibrosis, ballooning and NAS score, which is a composite score of the degree of steatosis, inflammation and hepatocyte ballooning (severe oxidative damage; see **Table 3**), higher than mice that were fed the MCS control diet. In fact, only mice exposed to the MCD diet for 8 weeks had a NAS of 5.36 and a F3 fibrosis score, which is equivalent to advance, precirrhotic fibrosis (**Table 3**).

Table 3. Histological characteristics of the liver biopsies

Period	Diet	NAS score				Ishak score
		Steatosis	Inflammation	Ballooning	Sum	
4 weeks	MCS	0.07 ± 0.16	1.37 ± 0.41	0.24 ± 0.41	0.68 ± 0.92	0.26 ± 0.09
	MCD	0.88 ± 0.47***	1.44 ± 0.86**	1.25 ± 0.55***	3.56 ± 1.46***	2.03 ± 0.21**
8 weeks	MCS	0.50 ± 0.63	0.00 ± 0.00	0.36 ± 0.46	0.86 ± 0.95	0.75 ± 0.51
	MCD	1.06 ± 0.17*	2.84 ± 0.28***	1.53 ± 0.42***	5.36 ± 0.63***	2.66 ± 0.37***

Mice were administered MCD or MCS diets. NAFLD activity score (NAS) and Ishak scores were assessed by histopathology of H&E and Sirius red stained livers. Values represent means ± SEM. N=10 mice per group. *p < 0.05, **p < 0.01, and ***p < 0.001 versus MCS treated mice that were analyzed at the same time points.

3.2 Effect of Linagliptin and Sitagliptin on MCD diet-induced NASH

3.2.1 Body weight, liver weight and clinical observations

The phenotype of loss in body and liver weights observed in MCD diet fed mice did not change after either Linagliptin or Sitagliptin treatment when compared with the vehicle treated MCD group (**Fig.10A-B**). In MCS mice the average serum ALT level was 21.78 ± 1.35 U/L, compared with mice consuming a MCD diet showing an average ALT serum level of 251.3 ± 29.22 U/L (p<0.0001). However, Linagliptin and Sitagliptin treatment of MCD fed mice significantly reduced serum levels of ALT, AST, lactate dehydrogenase (LDH) and serum triglyceride when compared to vehicle-treated MCD

littermates (**Fig.10C-F**). Conversely, Linagliptin and Sitagliptin treatment significantly increased active GLP-1 levels compared to vehicle treatment (**Fig.10G**).

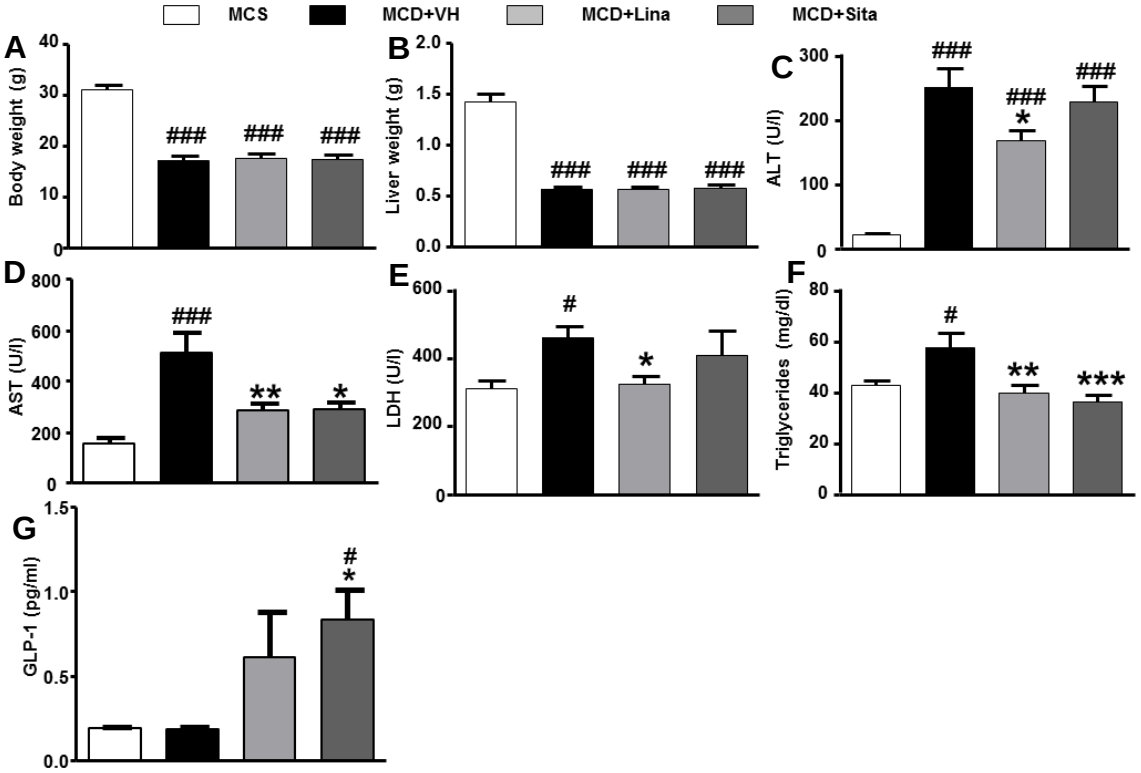

Fig.10 Mice were administered the MCD diet with vehicle or treated with Linagliptin and Sitagliptin for 6 weeks At the beginning of the protocol, every week and at the time of sacrifice liver and body weight were recorded. (**A-B**) No effect of Linagliptin or Sitagliptin treatment on body or liver weight. (**C-F**) Significantly lowered ALT, AST, LDH and triglyceride levels in Sitagliptin or Linagliptin treated mice with steatohepatitis. (**G**) Linagliptin and Sitagliptin treatment significantly increased active GLP-1 levels compared to vehicle treatment. Data are expressed as means ± SEM. N=10 mice per group. MCD with vehicle (VH) versus MCD with Linagliptin and MCD with Sitagliptin: *p < 0.05, **p < 0.01, and ***p < 0.001; MCS versus MCD with VH, MCD with Linagliptin, and MCD with Sitagliptin: #p < 0.05, ##p < 0.01, and ###p < 0.001.

3.2.2 Linagliptin and Sitagliptin attenuate MCD diet-induced hepatic steatosis

Strikingly, the pronounced hepatic steatosis observed in untreated MCD animals (as indicated by H&E and Sudan III stained areas) was significantly reduced upon Linagliptin and Sitagliptin treatment. The beneficial therapeutic effect of Linagliptin and Sitagliptin was also evidenced by a significantly improved histological steatosis, reduced NAFLD activity (NAS) scores and less stained steatotic areas (**Fig.11A, B**).

To further delineate the mechanisms responsible for the steatosis phenotype in MCD mice, gene expression of the key lipogenic transcription factor, sterol regulatory element-binding protein (SREBP)-1c, and its target genes, were assessed by real-time

PCR. Messenger RNAs encoding SREBP-1c, fatty acid synthase (FAS) and acetyl-Co a carboxylase (ACC) were up-regulated more than 3-fold in MCD diet-fed mice. However, all these genes were down-regulated upon Linagliptin and Sitagliptin treatment when compared to vehicle-treated controls (**Fig.11C**). Furthermore, Linagliptin and Sitagliptin treatment significantly lowered the mRNA expression of lipoprotein lipase (LPL), a key enzyme for lipolysis and free fatty acid generation in the liver (**Fig.11C**). These results demonstrated that treatment with Linagliptin and Sitagliptin attenuated liver injury and hepatic steatosis in MCD mice in a process that is likely to be attributable to the reduction of triglyceride accumulation and the decreased expression of genes involved in the stimulation of fatty acid synthesis and free fatty acid generation.

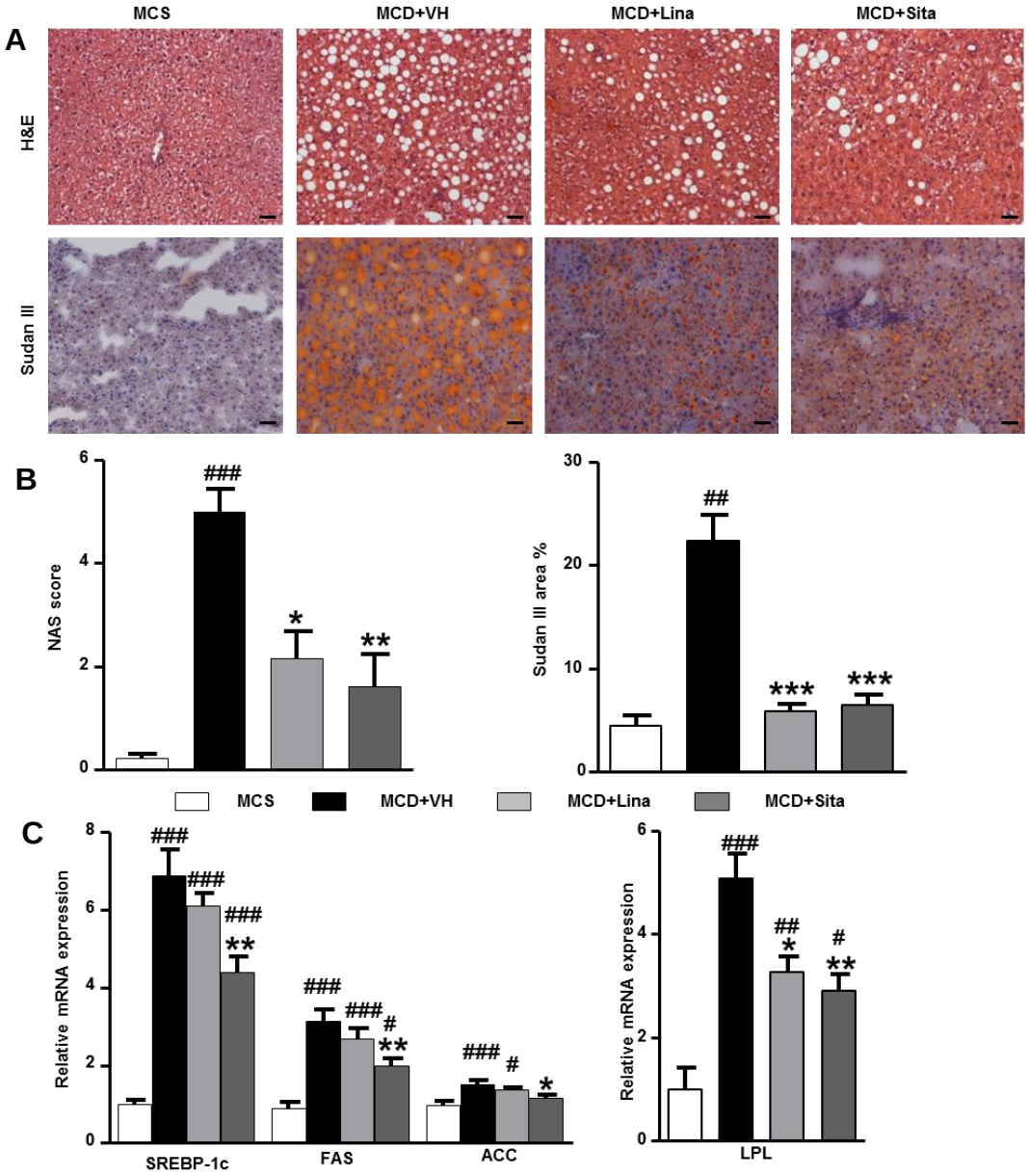

Fig.11 Effects of Linagliptin and Sitagliptin on MCD diet-induced liver steatosis
(**A-B**) Gliptins significantly attenuated hepatic steatosis, as assessed by H&E- and Sudan III-stained liver sections. NAS scoring and morphometry for lipid accumulation were performed on representative liver sections per mouse (20 × magnifications). (**C**) Sitagliptin and Linagliptin significantly suppressed transcript levels of genes central to fatty acid synthesis (SREBP-1c, FAS, ACC, and LPL). Data are expressed as means ± SEM. N=10 mice per group. MCD with VH versus MCD with Linagliptin and MCD with Sitagliptin: *p < 0.05, **p < 0.01, and ***p < 0.001; MCS versus MCD with VH, MCD with Linagliptin, and MCD with Sitagliptin: $^{\#}$p < 0.05, $^{\#\#}$p < 0.01, and $^{\#\#\#}$p < 0.001.

3.2.3 Linagliptin and Sitagliptin modify hepatocyte apoptosis and alter liver macrophage subsets

In order to characterize the mechanisms underlying the beneficial action of Linagliptin and Sitagliptin in experimental NASH and liver fibrosis, the activation of KC

(resident hepatic macrophages) and the expression of pro-inflammatory genes were analyzed. Following MCD treatment, the expression of CD68 and F4/80, which are both macrophage-specific markers, was significantly increased in MCD mice compared to the MCS control group as determined by immunohistochemistry and qPCR (**Fig. 12A-D**).

Macrophages are grossly categorized into “classically activated” M1-type macrophages that express inducible Nitric oxide synthases (iNOS) and favor a Type 1 T helper (Th1) cell environment, and “alternatively activated” M2-type macrophages that express arginase 1 and preferentially interact with Th2 cells[164]. Treatment with Linagliptin and Sitagliptin caused a significant decrease of $CD68^+$ and $F4/80^+$ macrophages in the liver and induced an upregulation of $Ym1^+$ alternatively activated M2 macrophages when compared with the vehicle treated MCD group (**Fig.12A,B**). Linagliptin and Sitagliptin also significantly attenuated the expression of the central apoptosis marker cleaved caspase-3, when compared to the vehicle-treated MCD group (**Fig.12A, B**).

Moreover, TNFα and IL-1β mRNA which is mainly expressed by KC/macrophages was highly up-regulated in MCD mice and decreased significantly upon treatment with both gliptins (**Fig.12C**). In the liver of MCD diet fed mice there was a substantial induction of macrophage-specific genes (CD68: 6.99 fold, M1 marker iNOS: 2.3 fold). Interestingly, both DPP-4 inhibitors suppressed CD68 and iNOS expression when compared to vehicle-treated MCD mice (**Fig.12C**). On the other hand, gliptin-treated MCD diet fed mice showed an upregulation of transcripts for arginase 1 (Arg1) (competing for the same substrate as iNOS) and for the anti-inflammatory cytokine IL-10 (**Fig.12D**). Together, these results show that DPP-4 inhibition attenuated liver steatosis, inflammation and apoptosis, all of which can be considered key features of NASH.

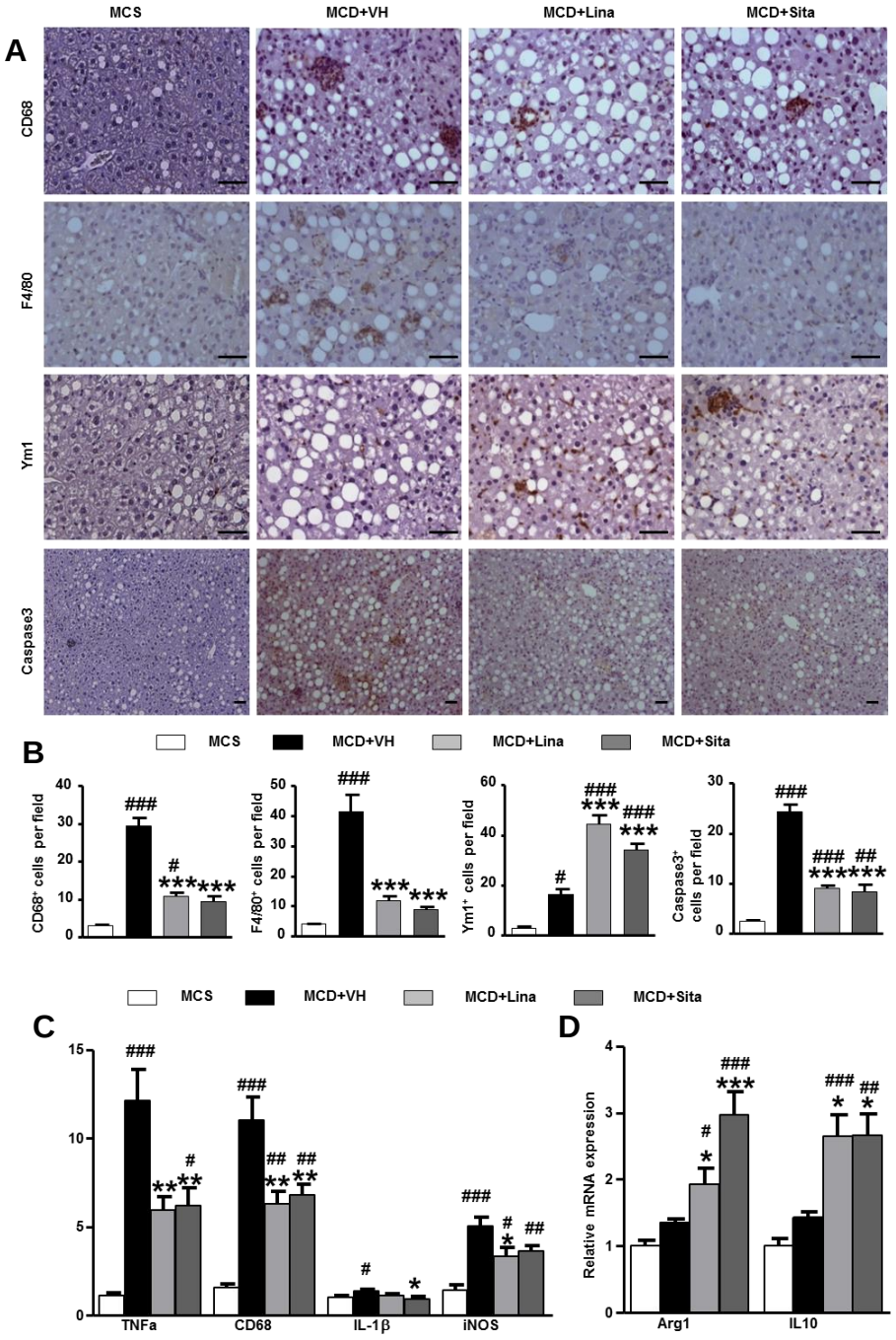

Fig.12 Gliptin treatment improves hepatic inflammation and apoptosis in mice on the MCD diet Mice were treated with gliptins from week 5-8. (**A-B**) Morphometric quantification from representative liver sections demonstrating the attenuation of pro-inflammatory innate immune activation and apoptosis in MCD diet-fed mice treated with Linagliptin or Sitagliptin, as assessed by CD68, F4/80, Ym1 (40x magnification) and cleaved caspase 3 staining (20x magnification). (**C**) Significant reduction of transcripts related to (macrophage) inflammation (CD68, TNFα, IL-1β, iNOS), and (**D**) upregulation of anti-inflammatory genes (Arg1, IL-10) in livers of MCD diet-fed mice treated with Linagliptin or Sitagliptin. Data are expressed as means ± SEM. N=10 mice per group. MCD with vehicle versus MCD with Linagliptin and MCD with Sitagliptin: *p < 0.05, **p < 0.01, and ***p < 0.001; MCS versus MCD with VH, MCD with Linagliptin, and MCD with Sitagliptin: $^{\#}$p < 0.05, $^{\#\#}$p < 0.01, and $^{\#\#\#}$p < 0.001.

3.2.4 Effect of Linagliptin and Sitagliptin on hepatic dendritic cells

To further determine the production of mediators of hepatic inflammation and immune cell infiltration, $CD45^+$ immune cells were isolated from livers and subjected to flow cytometry. Characterization of total intrahepatic leukocytes revealed no differences between gliptin-treated and vehicle-treated groups (**Fig.13A, B**).

$CD11c^+$ DCs have been associated with resolution of liver injury[165,166] and share a number of cell surface markers with macrophages[167]. Interestingly, the analysis of $CD11c^+$ DCs showed no differences between gliptin-treated and control mice (**Fig.13C**). To next characterize $CD11c^+$ cellular subsets, CD11c and the macrophage marker F4/80 were combined, leading to three distinct subsets: $CD11c^+F4/80^-$, $CD11c^-F4/80^+$ and $CD11c^+F4/80^+$ cells (**Fig.13A**). In the MCD group the inflammatory DC subset ($CD11c^+F4/80^+$)[168] was highly increased (3.5 fold) upon MCD exposure but reduced by 50% upon DPP-4 inhibitor therapy (**Fig.13C**). This was mainly due to a reduction of total $F4/80^+$ cells (**Fig.13B**), since these differences were less pronounced when the ratio between $CD11c^+F4/80^-$ and $CD11c^-F4/80^+$ cells were calculated.

3.2.5 Effect of Linagliptin and Sitagliptin on hepatic monocytes

Monocytes are circulating precursors for both tissue macrophages and DCs. Infiltrating monocytes that are positive for the myeloid marker CD11b were significantly reduced by Linagliptin>Sitagliptin treatment (**Fig.14B**). Monocyte subsets were further characterized by the differential expression of the inflammatory monocyte marker Ly6C. In MCD mice the $CD11b^+Ly6C^{hi}$ subset was highly increased (up to 7.8 fold) when compared to MCS fed mice. Linagliptin and Sitagliptin treatment reduced the number of $CD11b^+Ly6C^{hi}$ cells per liver to 43% ($p<0.05$) and 57% ($p=0.13$) respectively, indicating a major suppressive effect on the pro-inflammatory monocyte/macrophage population (**Fig.14B**). Differences were even more pronounced when the ratio of $CD11b^+Ly6C^{hi}$, $CD11b^+Ly6C^{lo}$ versus $CD45^+$ cells was calculated (**Fig.14D**). Hepatic expression of MCP-1 (CCL2, mainly expressed by $Ly6C^{hi}$ monocytes) and CD11b mRNA mirrored these findings (**Fig.14B-C**). In summary, gliptin treatment significantly reduced the number of inflammatory monocytes/macrophages but had no significant impact on hepatic DC populations.

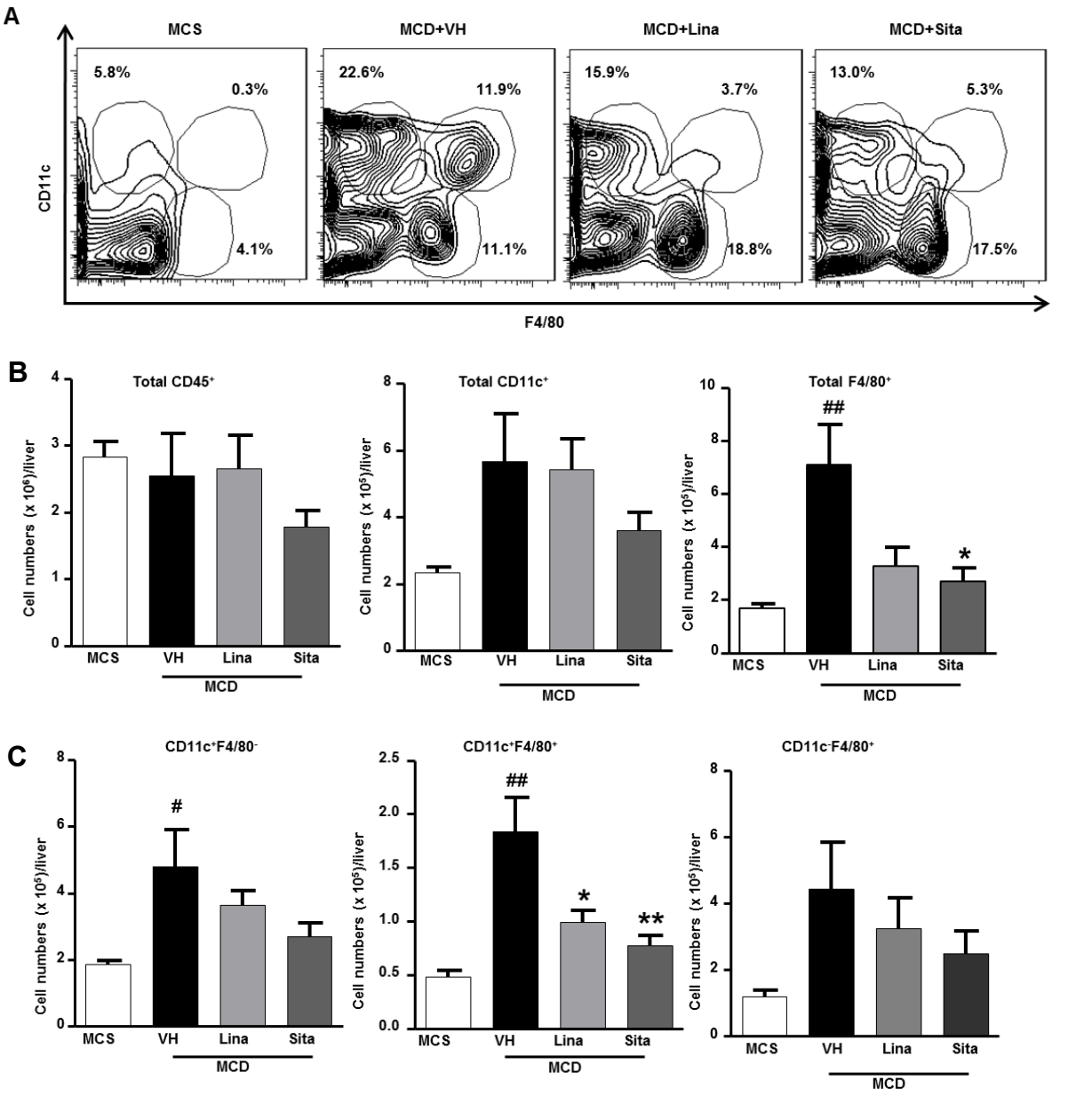

Fig.13 Flow cytometry analysis of immune cells isolated from the liver (**A**) Representative FACs plots and cell numbers show lowered total hepatic $CD11c^{+}F4/80^{-}$, $CD11c^{+}F4/80^{+}$ and $CD11c^{-}F4/80^{+}$ cells from $CD45^{+}$ gated liver mononuclear cells under Linagliptin or Sitagliptin treatment. (**B**) Significantly decreased $CD11c^{+}F4/80^{+}$ and total $F4/80^{+}$ cells per liver,(**C**) less marked decrease of the percentage of $CD11c^{+}F4/80^{-}$ and $CD11c^{-}F4/80^{+}$ cells per liver in gliptin-treated MCD mice. Data are expressed as means ± SEM. N=5 mice per group. MCD with vehicle versus MCD with Linagliptin and MCD with Sitagliptin: *$p < 0.05$, **$p < 0.01$, and ***$p < 0.001$; MCS versus MCD with vehicle, MCD with Linagliptin, and MCD with Sitagliptin: $^{\#}p < 0.05$, $^{\#\#}p < 0.01$, and $^{\#\#\#}p < 0.001$.

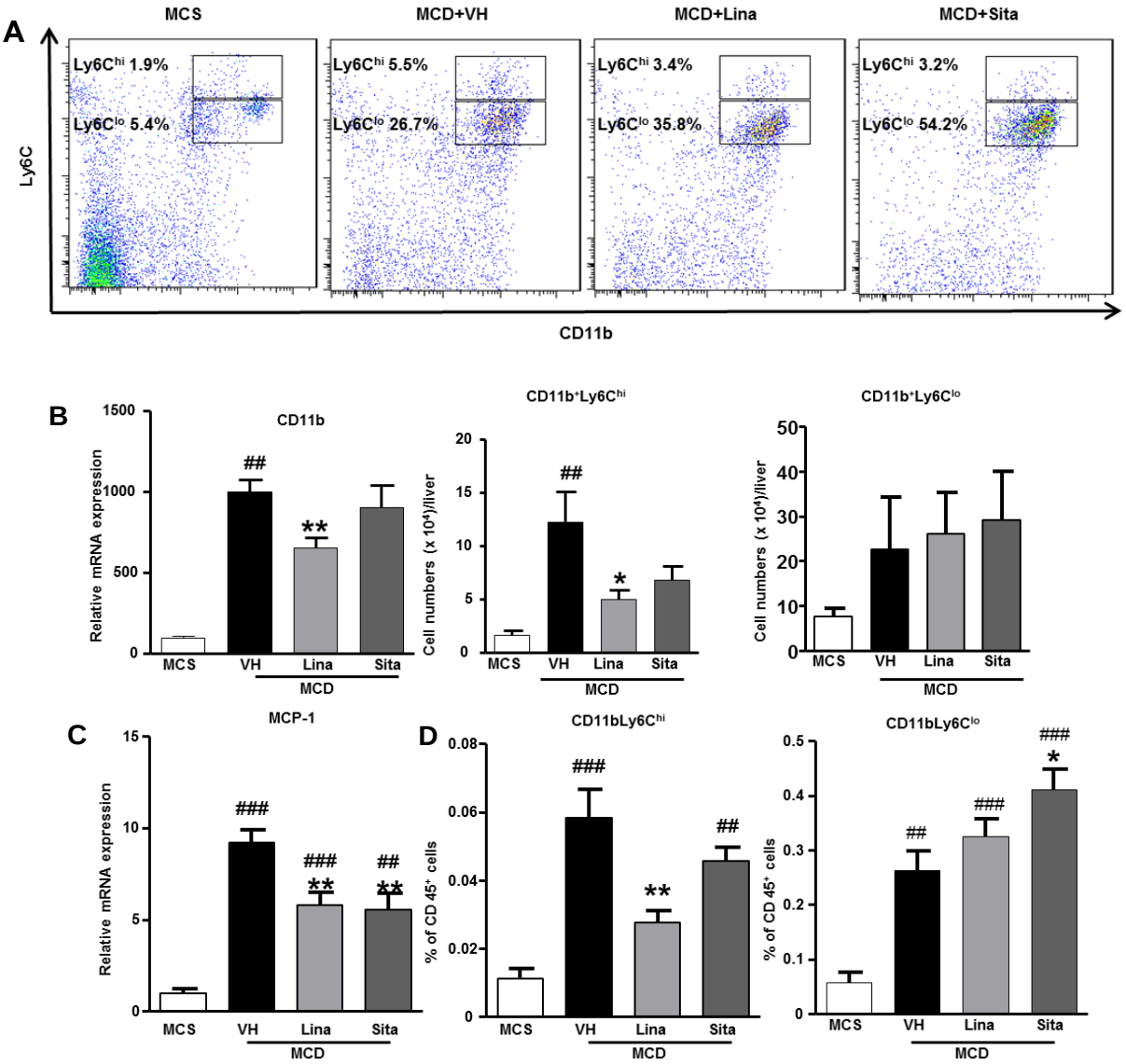

Fig.14 Flow cytometry analysis of immune cells isolated from the liver (**A**) CD45$^+$ cells were gated for CD11b$^+$Ly6C$^+$; numbers indicate the percentage of total isolated leukocytes. (**B**) Linagliptin or Sitagliptin treatment reduced pro-inflammatory CD11b$^+$Ly6C^{hi} monocyte/macrophage numbers but did not affect CD11b$^+$Ly6C^{lo} restorative monocyte/macrophages. (**C**) Decreased CD11b transcript levels upon Linagliptin treatment of MCD mice. (**D**) Linagliptin or Sitagliptin treatment reduced relative pro-inflammatory CD11b$^+$Ly6C^{hi} monocyte/macrophage numbers and also increased relative CD11b$^+$Ly6C^{lo} restorative monocyte/macrophages. N=5 mice per group. MCD with VH versus MCD with Linagliptin and MCD with Sitagliptin: *p < 0.05, **p < 0.01, and ***p < 0.001; MCS versus MCD with VH, MCD with Linagliptin, and MCD with Sitagliptin: $^{\#}$p < 0.05, $^{\#\#}$p < 0.01, and $^{\#\#\#}$p < 0.001.

3.2.6 Linagliptin and Sitagliptin attenuate MCD diet-induced liver fibrosis

MCD animals developed advanced hepatic fibrosis with a 2.5 fold increased relative Hyp content. Sitagliptin significantly ameliorated collagen deposition, as assessed by Hyp quantification (**Fig.8 and 15A**). The expression of genes involved in ECM deposition and fibrosis remodeling was increased in MCD diet-fed mice. However,

treatment with Linagliptin induced a pronounced decrease in mRNA expression of α-SMA, COL1α1, TIMP-1 and TGFβ1. In contrast, although Sitagliptin treatment decreased α-SMA, COL1α1 and TGFβ1 levels similar to Linagliptin, it decreased TIMP-1 mRNA levels to a lesser degree (**Fig.15B**). Genes associated with fibrolysis or ECM remodeling (MMP2, MMP3, MMP8, MMP9 and MMP13) were also significantly decreased by Sitagliptin and Linagliptin treatment when compared to MCD mice that were treated with vehicle alone (**Fig.15C**).

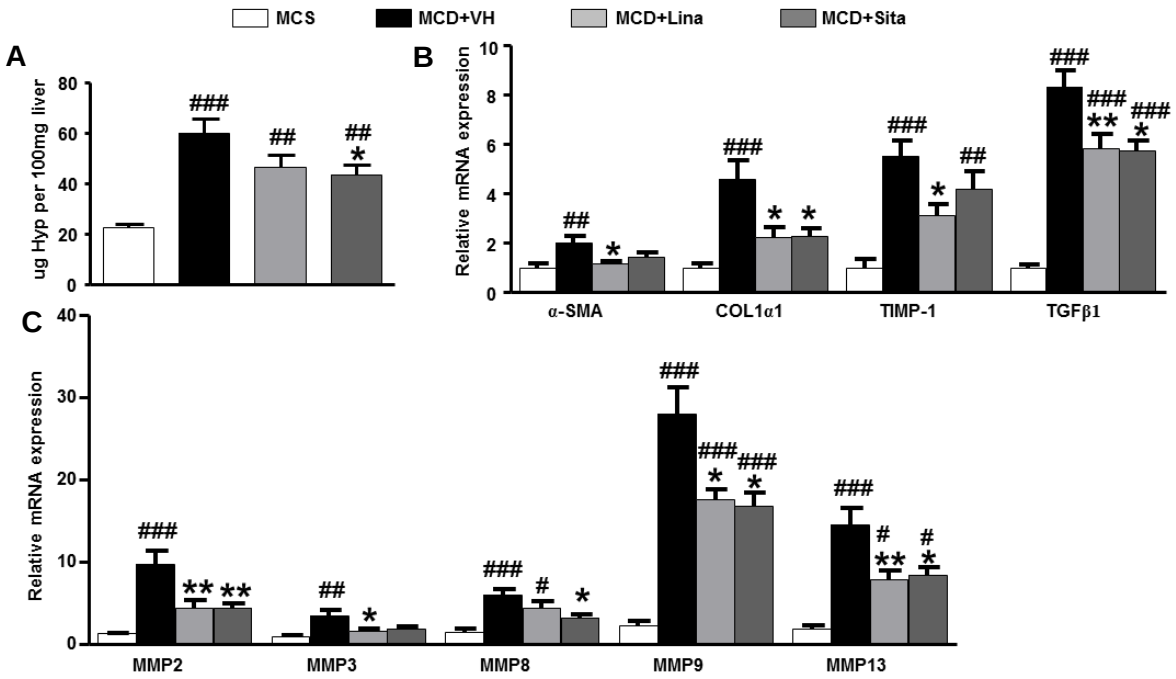

Fig.15 Administration of Linagliptin or Sitagliptin improves hepatic fibrosis in MCD diet-fed mice (**A**) Sitagliptin treatment significantly decreased relative hepatic collagen content in MCD mice, whereas Linagliptin showed only a trend. Both gliptins significantly reduced profibrotic transcripts for α-SMA, COL1α1, TIMP-1 and TGFβ1 (**B**), but also (**C**) putatively transcripts for MMP2, MMP3, MMP8, MMP9 and MMP13 that are involved in ECM remodeling or degradation. Data are expressed as means ± SEM. N=10 mice per group. MCD with vehicle versus MCD with Linagliptin and MCD with Sitagliptin: *p < 0.05, **p < 0.01, and ***p < 0.001; MCS versus MCD with vehicle, MCD with Linagliptin, and MCD with Sitagliptin: $^{\#}$p < 0.05, $^{\#\#}$p < 0.01, and $^{\#\#\#}$p < 0.001.

3.2.7 Histological analysis of MCD diet-induced liver fibrosis

Sirius red morphometry showed a marked reduction of collagen stained areas in the liver of gliptin-treated animals (~60%). Moreover, morphometry for α-SMA and procollagen/collagen type III (COL3) equally confirmed a highly significant reduction of activated HSC and myofibroblasts (>28%) and fibrillar collagen (>69%) in MCD mice with DPP-4 inhibition (**Fig.16A,B**). Taken together, these results show that gliptin therapy significantly ameliorated MCD diet-induced hepatic fibrosis.

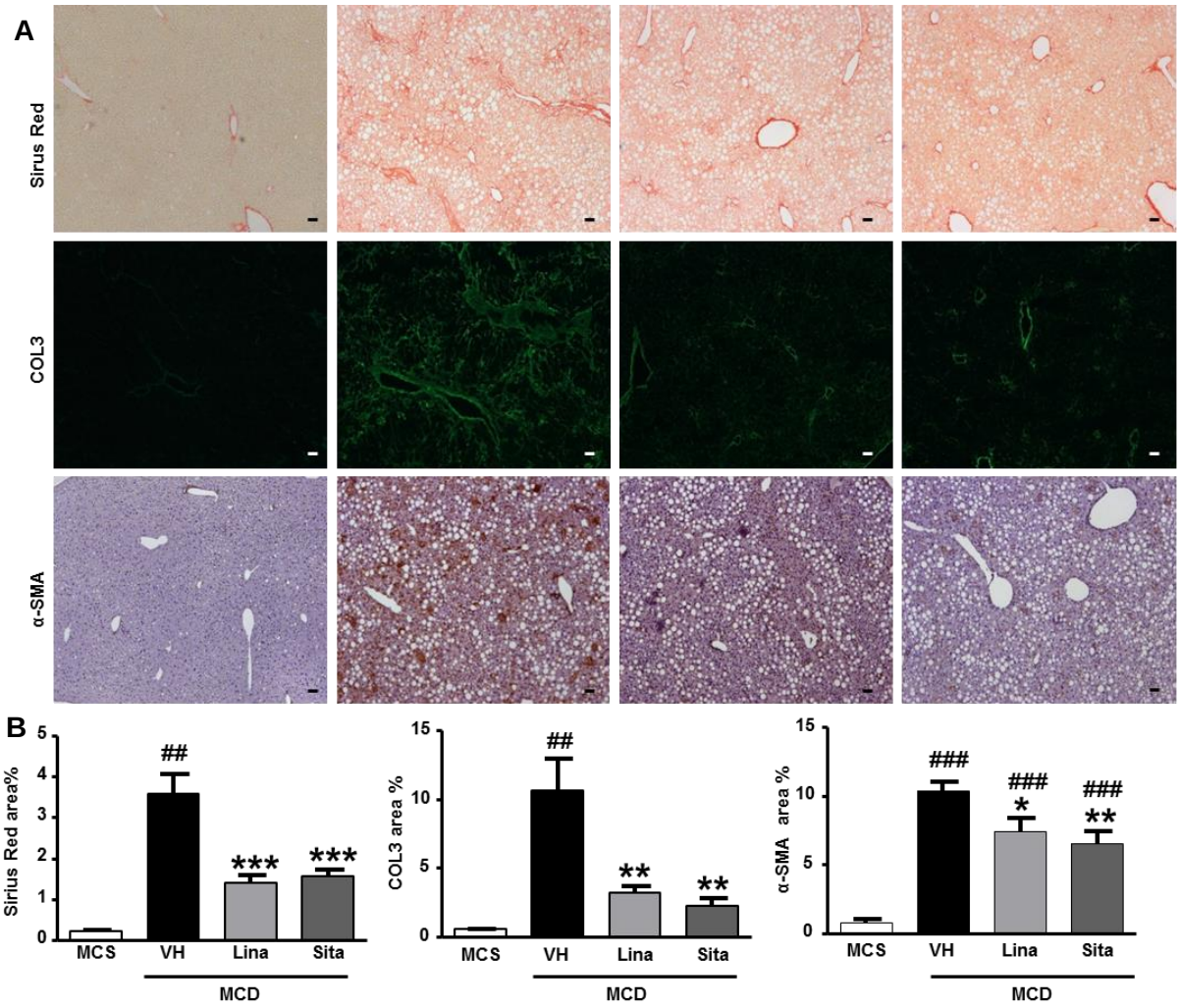

Fig.16 Administration of Linagliptin or Sitagliptin improves hepatic fibrosis in MCD diet-fed mice (**A-B**) Representative liver sections showing that Linagliptin or Sitagliptin significantly reduced deposition of collagen (as assessed by Sirius red staining), α-SMA expression and COL3 deposition (10 x magnifications) in MCD diet-fed mice. N=10 mice per group. MCD with vehicle versus MCD with Linagliptin and MCD with Sitagliptin: *p < 0.05, **p < 0.01, and ***p < 0.001; MCS versus MCD with vehicle, MCD with Linagliptin, and MCD with Sitagliptin: $^{\#}$p < 0.05, $^{\#\#}$p < 0.01, and $^{\#\#\#}$p < 0.001.

3.2.8 Linagliptin improves liver weight and liver serum parameters in Mdr2$^{-/-}$ mice

To study if and to what extent DPP-4-inhibition may have a direct effect on fibrosis in the absence of other pathological NASH related conditions such as steatosis and hepatocyte lipoapoptosis, Mdr2$^{-/-}$ mice that are a model for progressive spontaneous biliary fibrosis, were examined. In these experiments Mdr2$^{-/-}$ mice received different doses of Linagliptin (0.5 mg/kg, 5 mg/kg and 10 mg/kg) for 4 weeks. Linagliptin treatment did not change body weights (**Fig.17A**), but significantly decreased liver

weights (**Fig.17A**). Linagliptin treatment also decreased ALT and alkaline phosphatase (AP) levels (**Fig.17B)**.

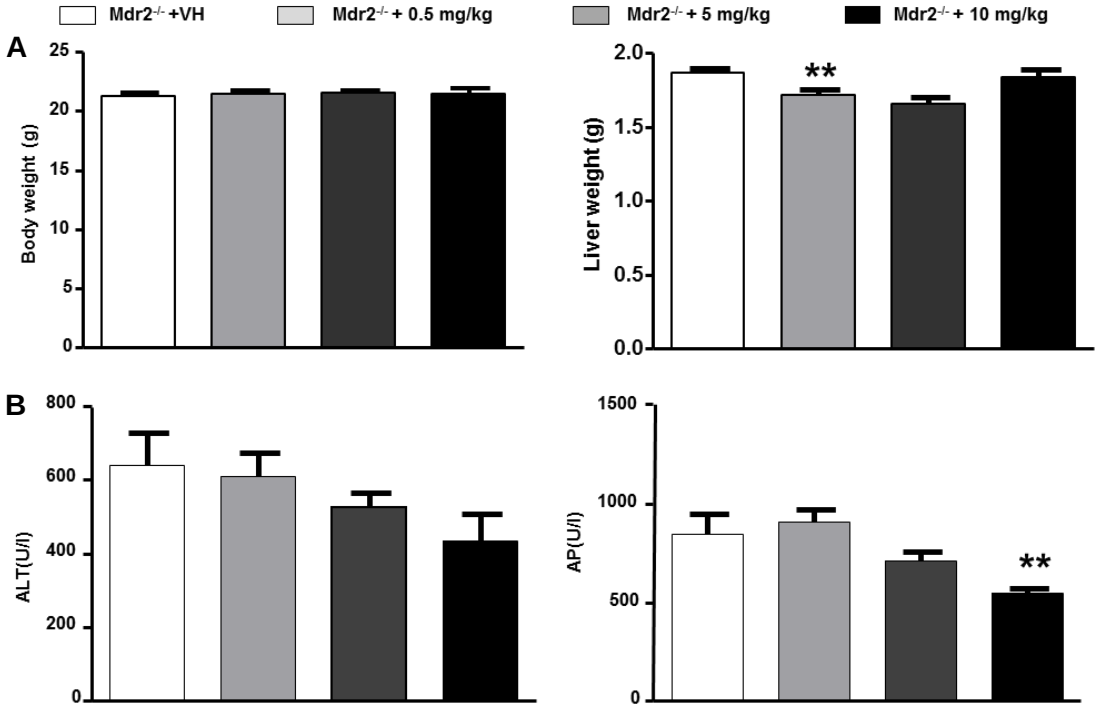

Fig.17 Four weeks of Linagliptin treatment ameliorates biliary fibrosis in Mdr2$^{-/-}$ mice At the beginning of the protocol, every week and at the time of sacrifice body and liver weight was recorded (**A**) Only a small reduction on body and liver weight was found upon Linagliptin treatment. (**B**) Application of escalating doses of Linagliptin showed a dose-dependent reduction on serum ALT and AP levels. Data are expressed as mean ± SEM, *p< 0.05, **p= 0.01 versus compared to Mdr2$^{-/-}$ mice that received vehicle only.

3.2.9 Linagliptin treatment does not significantly attenuate fibrosis related parameters in Mdr2$^{-/-}$ mice

There was no effect of Linagliptin treatment on hepatic collagen accumulation as quantified by hepatic Hyp (**Fig.18A**). Also, collagen deposition as documented by Sirius red staining and morphometric analysis was not significantly altered upon Linagliptin treatment, but showed a trend towards reduction suggesting a mild anti-fibrotic effect (**Fig.18B**).

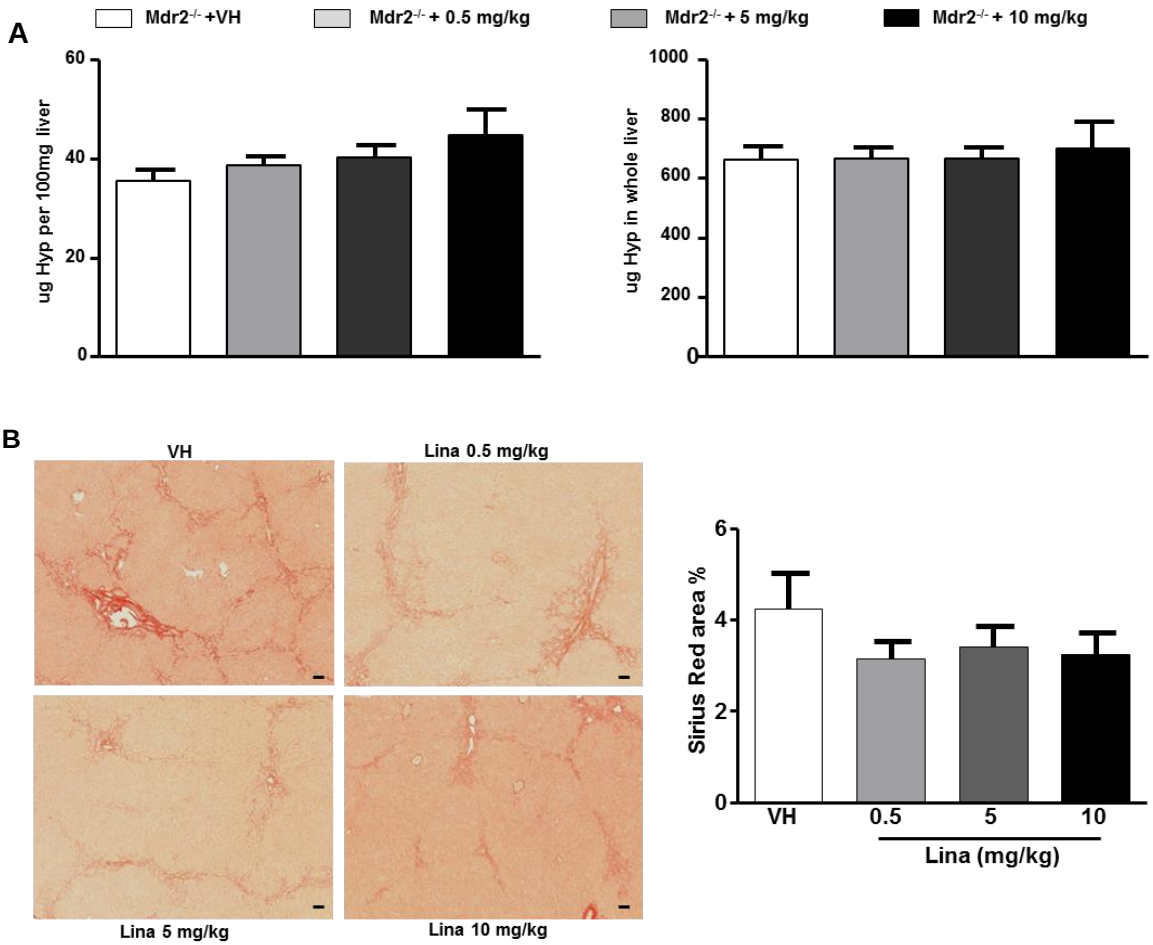

Fig.18 Four weeks of Linagliptin mildly treatment ameliorates biliary fibrosis in Mdr2$^{-/-}$ mice (**A**) No effect of Linagliptin treatment on relative hepatic Hyp (µg per 100 mg liver) and total liver collagen content. (**B**) Representative liver sections after Sirius red collagen staining showing that Linagliptin treatment mildly (but not significantly) reduced collagen deposition. Data are expressed as means ± SEM. N=7 mice per group. *p < 0.05 and **p < 0.01 versus Mdr2$^{-/-}$ mice that received the vehicle only.

TNFα and IL-1β are expressed predominantly by KCs and were highly up-regulated in Mdr2$^{-/-}$ mice and decreased significantly upon treatment with Linagliptin. There was also a substantial induction of macrophage specific genes (CCL3 and CCL5) in untreated Mdr2$^{-/-}$ mice, which were decreased in the Linagliptin- but not the vehicle-treated group (**Fig.19A**).

α-SMA, COL1α1, TGFβ1 and MMP3 mRNA levels were determined in the livers of the Mdr2$^{-/-}$ mice. Interestingly, treatment with Linagliptin for 4 weeks significantly decreased hepatic α-SMA, COL1α1, TGFβ1 and MMP3 transcripts at a dose of 5 or 10 mg/kg/d when compared to the vehicle treated group (**Fig.19B**). Expression of transcripts of the pro-fibrogenic TIMP-1 and the fibrolysis-related MMP8 genes showed a weak (but not statistically significant) dose response in correlation with

the amount of Linagliptin used, with a significant reduction of MMP3 transcripts at the highest Linagliptin dose (**Fig.19C**). In summary, Linagliptin modestly attenuated biliary fibrosis in Mdr2$^{-/-}$ mice, with significant and also dose-dependent effects on some pro-fibrotic parameters (COL1α1, TGFβ1 and MMP3) of the liver, being compatible with a primary effect on inflammatory (myeloid) cells.

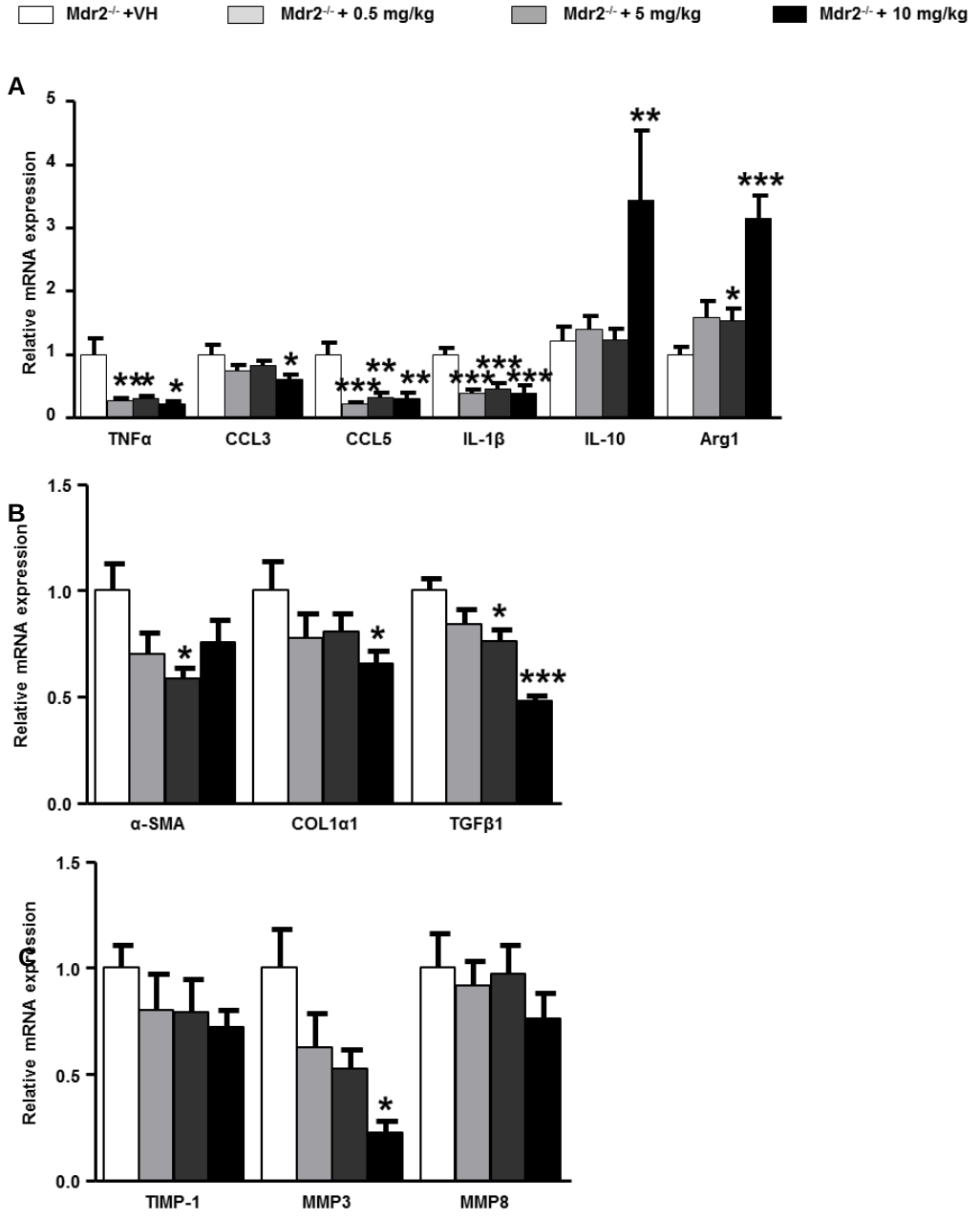

Fig.19 Four weeks of Linagliptin treatment reduce transcripts related to fibrosis and inflammation in Mdr2$^{-/-}$ mice (**A**) Linagliptin treatment significantly reduced the expression of transcripts related to (innate) inflammation (TNFα, CCL3, CCL5 and IL-1β) and up-regulated anti-inflammatory genes (IL-10, Arg1) in livers of Mdr2$^{-/-}$ mice. (**B**) Linagliptin treatment significantly reduces the expression of pro-fibrogenic α-SMA, COL1α1 and TGFβ1, but also of TIMP-1, MMP3 and MMP8. Data are expressed as means ± SEM. N=7 mice per group. *$p < 0.05$ and **$p < 0.01$ versus Mdr2$^{-/-}$ mice that received the vehicle only.

3.3 GLP-1 receptor agonist Bydureon improves MCD diet-induced NASH

3.3.1 BY attenuates metabolic and serum parameters in MCD diet-fed mice

Treatment of mice with the long-acting GLP-1 agonist Bydureon (BY) at 0.4 (BY-L) and 2 (BY-H) mg/kg did not lower the body weight, but BY-H treatment significantly reduced liver weight (**Table 4**). BY-treated MCD diet fed mice had a comparable food intake to their PBS-treated counterparts. In MCD mice serum ALT levels were lowered by 18.1% and 18.5%, resp., with the BY-L or the BY-H treatment compared to the PBS controls (**Fig.20A**). There were no differences in plasma AST, and AP in BY animals when compared to the PBS group. BY treatment also lowered triglyceride serum levels by 29.2% and 21.7% in the BY-L and BY-H groups, resp. (**Table 4**). The lack of significant alterations in liver enzymes upon BY treatment also suggests that BY may not be associated with unwanted therapeutic side effects in the MCD mice. Notably, expression of the pro-inflammatory cytokine IL-6 was significantly reduced by 37.1% in BY-L- and by 50.6% in BY-H-treated animals (**Fig.20B**). These data demonstrate that BY improves MCD diet-induced inflammation in NASH.

Table 4. Central parameters of MCD fed mice without/with BY treatment

	MCD+PBS	MCD+BY-L	MCD+BY-H
Body weight (g)	18.74±1.22	18.07±1.3	18.87±1.4
Liver weight (g)	0.64±0.02	0.64±0.01	0.52±0.02 **
Food intake (g)	11.48±2.73	11.50±2.84	11.48±2.24
AST (U/l)	468.6±38.62	466.4±34.64	429.5±64.32
AP (U/l)	114.7±4.71	113.6±4.35	114.8±14.94
Triglyceride (U/l)	53.00±5.54	37.50±4.40	41.50±6.61

Mice were administered the MCD diet for 4 weeks and treated with BY twice weekly for another 4 weeks. At the beginning, every other week and at the time of sacrifice body weight was recorded. Liver weight was recorded at the time of sacrifice. Data are expressed as means ± SEM. N=10 mice per group. *p < 0.05, **p < 0.01, and ***p < 0.001 versus PBS-treated mice at the same time point.

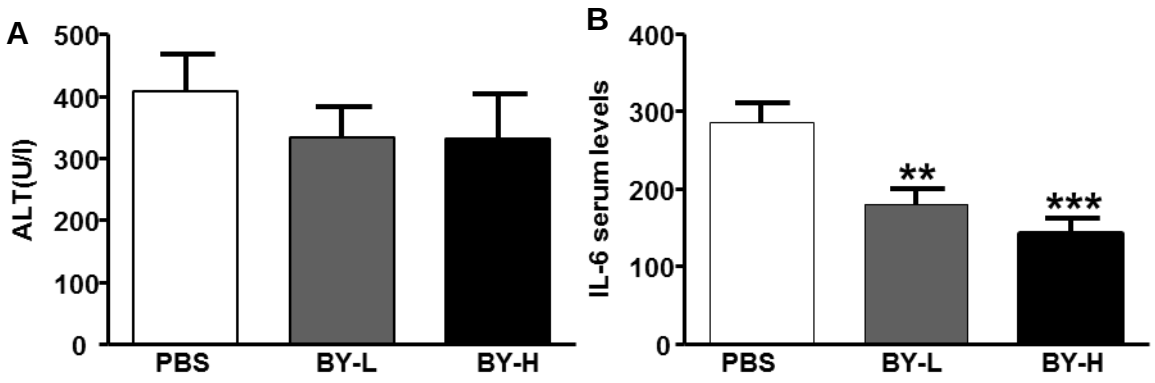

Fig.20 BY administration reduces MCD diet-induced hepatic liver inflammation (**A**) BY treatment insignificantly lowered serum ALT and (**B**) significantly serum IL-6 levels in MCD diet-fed mice. Data are expressed as means ± SEM. N=10 mice per group. *p < 0.05, **p < 0.01, and ***p < 0.001 versus PBS-treated mice in the same time point.

3.3.2 BY reduces the fat content in epididymal tissue in MCD diet-fed mice

After 4 weeks of BY treatment, MCD diet-fed mice had significantly lower (80.3 % reduction in the BY-L group and 96.1% reduction in BY-H group) epididymal fat tissue weight compared with PBS treated MCD diet-fed mice (**Fig.21A).** The epididymal fat tissue in BY-H group has very limited tissue left, so the next experiment was only measured the BY-L group and PBS group.

To determine whether BY treatment affected the size of adipocytes, sections of epididymal adipose tissue were prepared, stained with H&E. The size (diameter) of adipocytes was significantly reduced by 56.8% in the BY-L group when compared with PBS treated MCD diet-fed mice (**Fig.21B**). Sections were also stained for the macrophage marker CD68 and the anti-inflammatory M2 marker Ym1. These experiments demonstrated that the number of $CD68^+$ cells was significantly decreased (**Fig.21C**) and that $Ym1^+$ cells significantly increased (4.06 fold) in the BY-L group (**Fig.21D**). The number of $Ym1^+$ cells in the CD 68^+ population also increased significantly (**Fig.21E**).

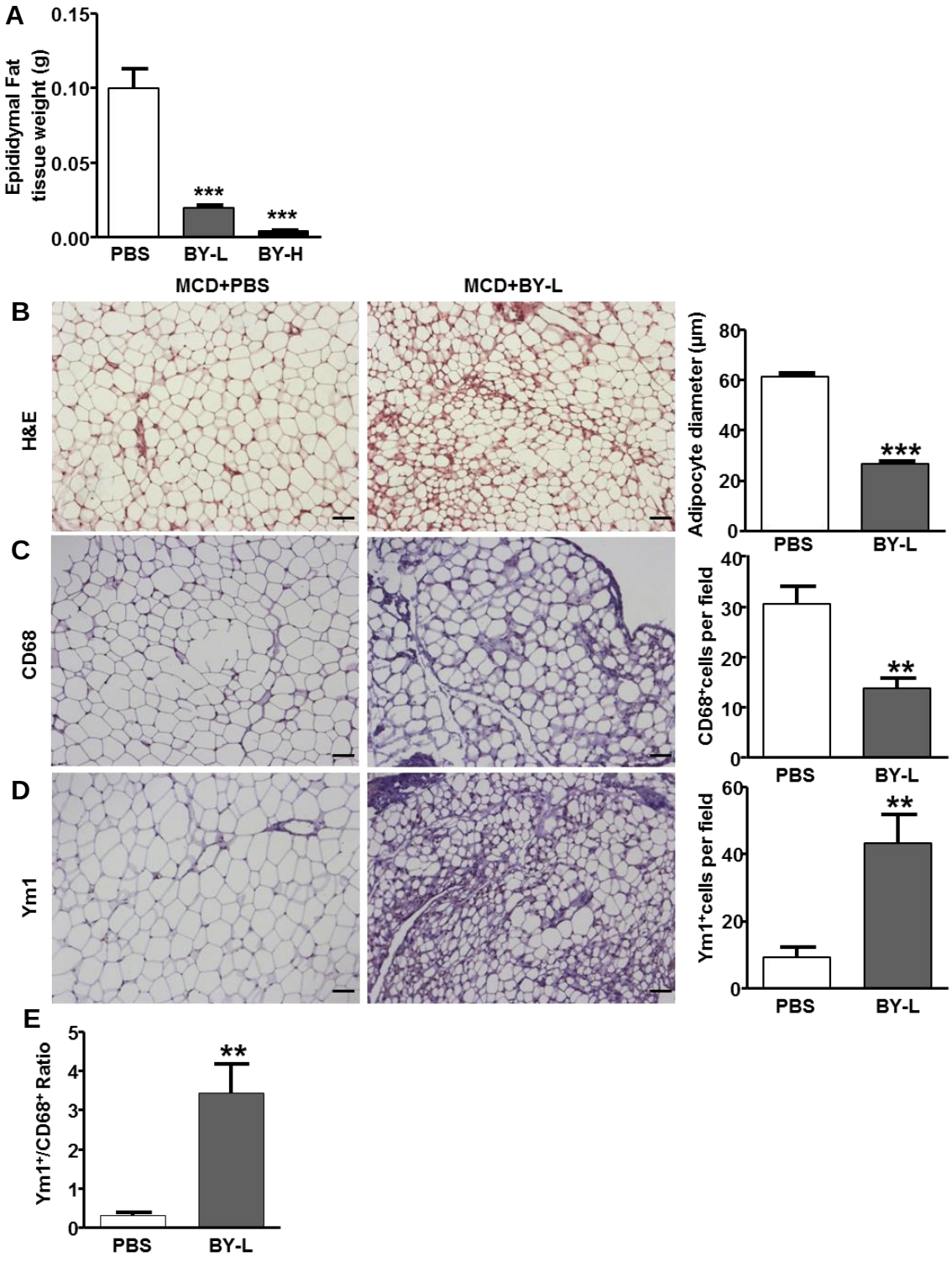

Fig.21 BY suppresses epididymal adipose tissue weight and inflammation and increases anti-inflammatory M2 macrophages (**A**) Epididymal adipose tissue weight was significantly lowered upon BY treatment. (**B**) Representative H&E-stained epididymal adipose tissue sections showed that BY significantly reduced adipocyte diameters. (**C**) The general macrophage marker $CD68^+$ was down-regulated upon BY treatment; however the anti-inflammatory M2-type macrophage marker Ym1 was up-regulated (**D**). (**E**) The $Ym1^+$ to $CD68^+$ cell ratio showed a highly significant increase in BY-L-treated mice. Scale bars indicate 50 µm; ***p< 0.001 versus PBS-treated mice determined at the same time point.

3.3.3 BY reduces lipid accumulation in the liver of MCD diet-fed mice

To first evaluate structural changes in liver sections, H&E-stained tissue samples were examined (**Fig.22A**). As expected, in all liver samples from PBS-treated MCD diet-fed mice, I observed severe degeneration associated with massive fat deposits and steatohepatitis accompanied by inflammatory cell infiltration (**Fig.22A**). In contrast, mice treated with BY showed a significant reduction of fatty deposits, and inflammation (**Fig.22A**). The NAS-score of mice of the MCD diet was 5.2 and improved highly significantly to 2.1 and 2.3, resp., upon BY-L and BY-H treatment (**Fig.22B**).

To examine the effect of BY on lipid accumulation, liver sections in MCD diet-fed mice were subjected to Oil Red O staining. Here Oil Red O positive areas in the BY-L and BY-H-treated MCD mice group were significantly lower than in PBS-treated controls (**Fig.22C**).

To better understand the mechanism underlying the progression of MCD diet-induced hepatic steatosis, mRNA levels of the central transcriptional factor SREBP-1c which regulates lipid metabolism and of its target genes FAS and ACC were determined. Hepatic mRNA expression of SREBP-1c was reduced by 37.4% in the BY-L group and by 46.0% in the BY-H group. Furthermore, transcript levels of FAS and ACC were decreased by 52.0% and 46.2%, and by 23.8% and 21.5% in the BY-L and BY-H groups, resp., when compared to PBS-treated mice (**Fig. 22B**). Levels of LPL, which is involved in fatty uptake, were also significantly lower upon BY-L and BY-H treatment (79.3% and 80.8% reduction, resp.) (**Fig.22A**). Taken together, these results indicate that BY treatment attenuates the development of hepatic steatosis by directly and indirectly modulating key enzymes that are involved in lipid metabolism.

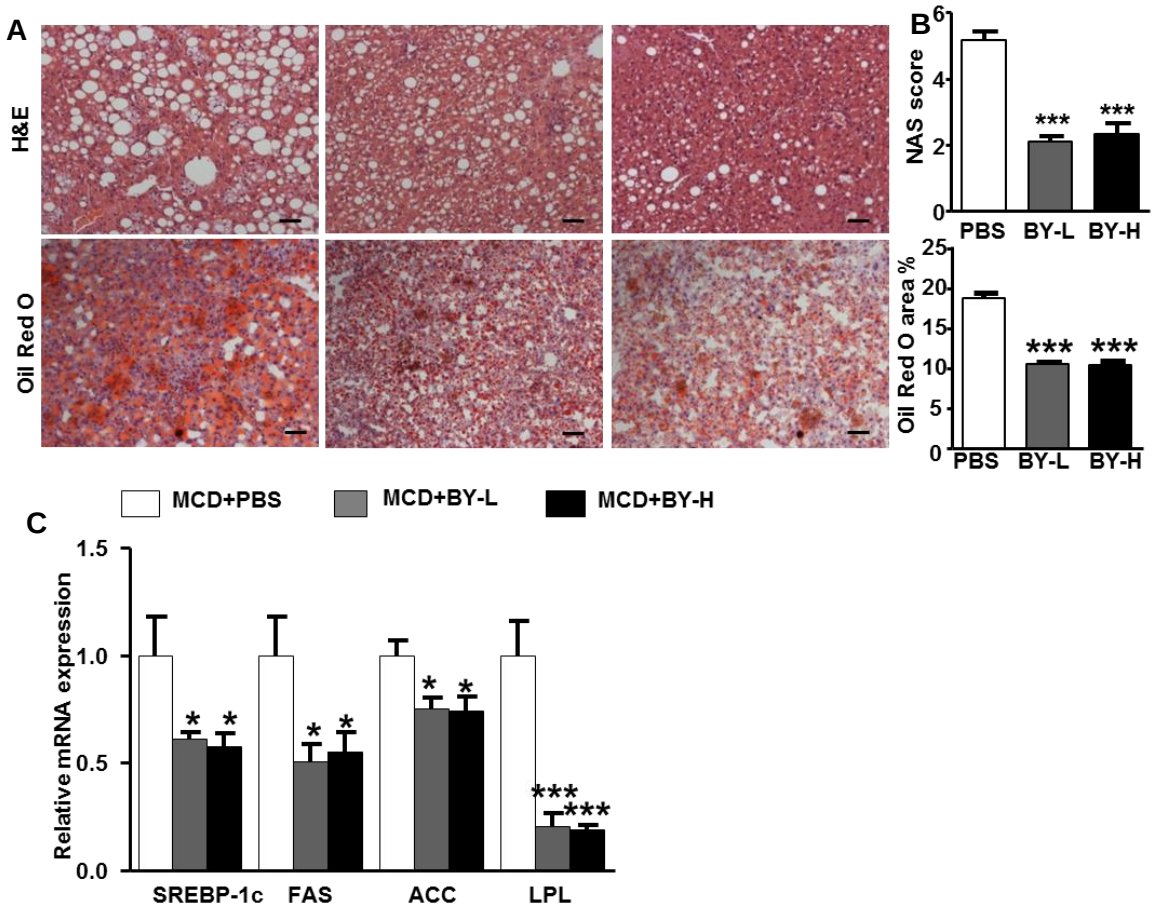

Fig.22 BY treatment improves MCD-induced hepatic steatosis (**A-B**) BY significantly attenuated hepatic steatosis, as assessed on H&E and Oil red O stained liver sections. NAS score and morphometry for lipid accumulation were performed on representative liver sections per mouse (20 x magnification). In each group 50 individual areas were scored in five mice per group. Scale bars indicate 50 µm. (**C**) BY significantly suppressed transcript levels of genes central to fatty acid synthesis (SREBP-1c, FAS, ACC, LPL). Transcription levels are represented relative to transcript levels of Gapdh. *p< 0.05; **p< 0.01 and ***p< 0.001 versus PBS-treated mice analyzed at the same time point.

3.3.4 Histological analysis reveals that BY attenuates inflammation in MCD diet-fed mice

To clarify the effect of BY with regard to central features of NASH, such as inflammation and apoptosis, the livers of MCD mice which exhibited severe steatohepatitis without treatment were examined. Hepatic macrophage infiltration was evaluated by Immunohistochemical staining which were used the Kupffer cell/macrophage markers CD68 and F4/80. The analysis of $CD68^+$ cells showed a 71.9% decrease upon BY-L and an 81.4% decrease upon BY-H treatment. $F4/80^+$ macrophages were reduced by 67.9% and 76.36%, resp. (**Fig.23A,B**). Furthermore, the M2 macrophage marker Ym1 was up-regulated 2.33 fold in BY-L and 2.15 fold in

BY-H-treated mice when compared to the untreated MCD control group (**Fig.23C**). To quantify the degree of hepatocyte apoptosis, livers were stained for caspase 3. These studies demonstrated a marked suppression of hepatocyte apoptosis by 73.1% in BY-L and by 79.0% in BY-H-treated animals (**Fig.23D**). Therefore, treatment with BY attenuates liver injury through inhibition of pro-inflammatory and apoptotic pathways.

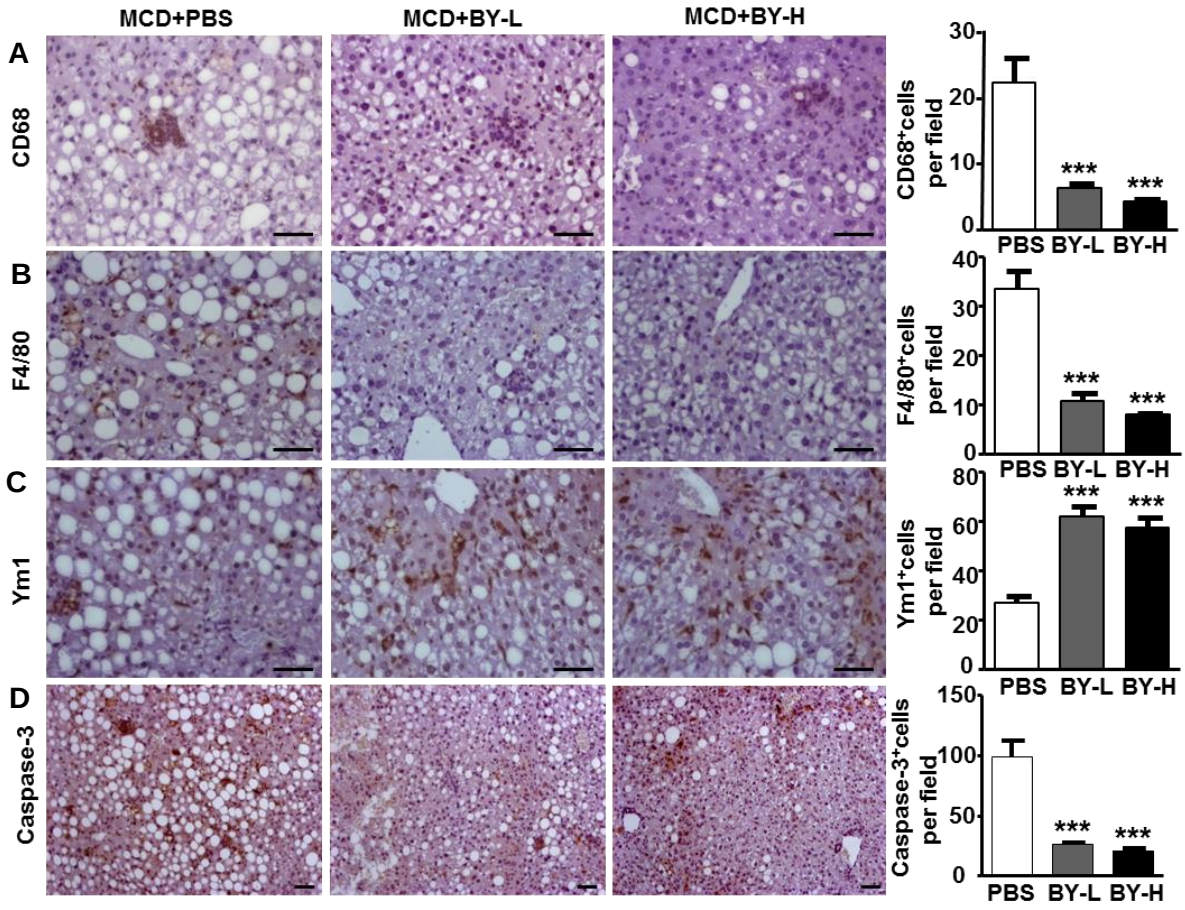

Fig.23 BY treatment improves MCD diet-induced hepatic steatosis, inflammation and apoptosis (**A-D**) Representative liver sections and morphometrical quantification demonstrating the attenuation of innate pro-inflammatory immune activation parameters and apoptosis in MCD diet-fed mice treated with BY. CD68, F4/80, Ym1 (40x magnification) and caspase-3 expression (20x magnification) were assessed. The bar diagrams show mean values±SEM of CD68, F4/80, Ym1 and caspase-3 expression levels representing 50 individual areas scored in five mice per group. Scale bars indicate 50 μm and ***p< 0.001 versus PBS-treated mice at the same time point.

3.3.5 BY reduces the transcription of inflammation-related genes in MCD mice

Upon treatment with BY transcript levels of pro-inflammatory TNFα, IL-1β, CCL3 and CCR7 were significantly reduced (**Fig.24A**). Arg1, a marker of anti-inflammatory M2 macrophages, increased 6.59 fold in BY-L and 5.19 fold in BY-H-treated MCD mice.

Similarly, the anti-inflammatory (M2 macrophage) markers IL-10, Ym1 and Mrc-1 were significantly up-regulated after BY treatment (**Fig.24B**).

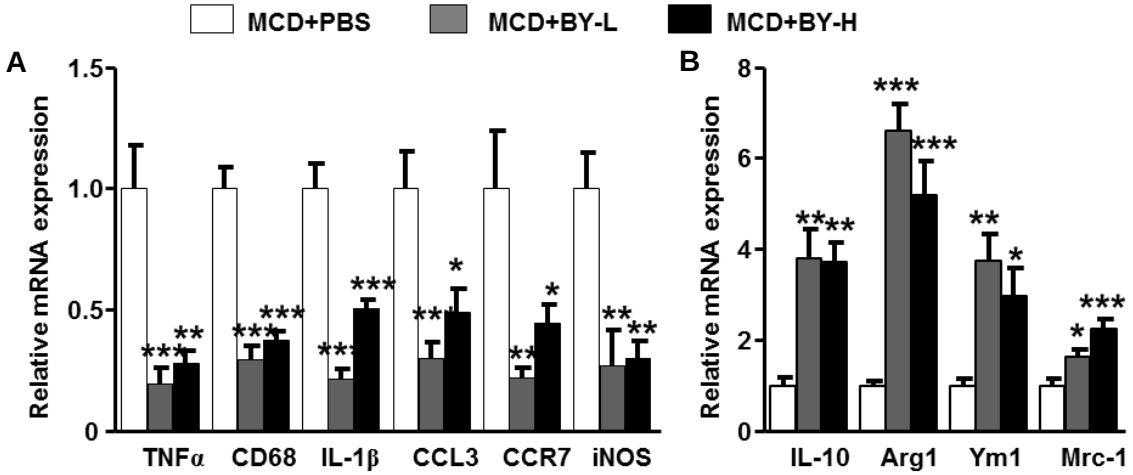

Fig.24 BY administration reduces MCD diet-induced hepatic liver inflammation markers (**A**) Significant reduction of transcripts related to (macrophage) inflammation (TNFα, CD68, IL-1β, CCL3 and CCR7) and (**B**) upregulation of anti- inflammatory genes (Arg1) in livers of MCD diet-fed mice treated with BY. Bars indicate mRNA levels ±SEM in livers of experimental mice (N=10 per group). Transcript levels are represented relative to Gapdh transcript levels. *p< 0.05; **p< 0.01 and ***p< 0.001 versus PBS-treated mice at the same time point.

The MAPK/ERK pathway regulates a variety of physiological processes, such as cell growth, differentiation and survival. Liver expression of ERK protein in mice that were exposed to the MCD diet were highly increased and significantly reduced by BY-treatment, as were levels of phosphorylated-ERK1/2 (p-ERK) levels (**Fig.25A,B**). There was a dose-dependent inverse correlation between ERK/p-ERK expression and Ym1 protein expression upon BY treatment (**Fig.25A,B**), in line with the previous results of a dose-dependent increase of Arg1 transcripts in MCD diet-fed mice treated with BY (**Fig.24B**). M2 macrophage activation and the suppression of mRNA transcription of key inflammatory factors may therefore be at least in part regulated through BY-driven modulation of ERK 1/2 signaling.

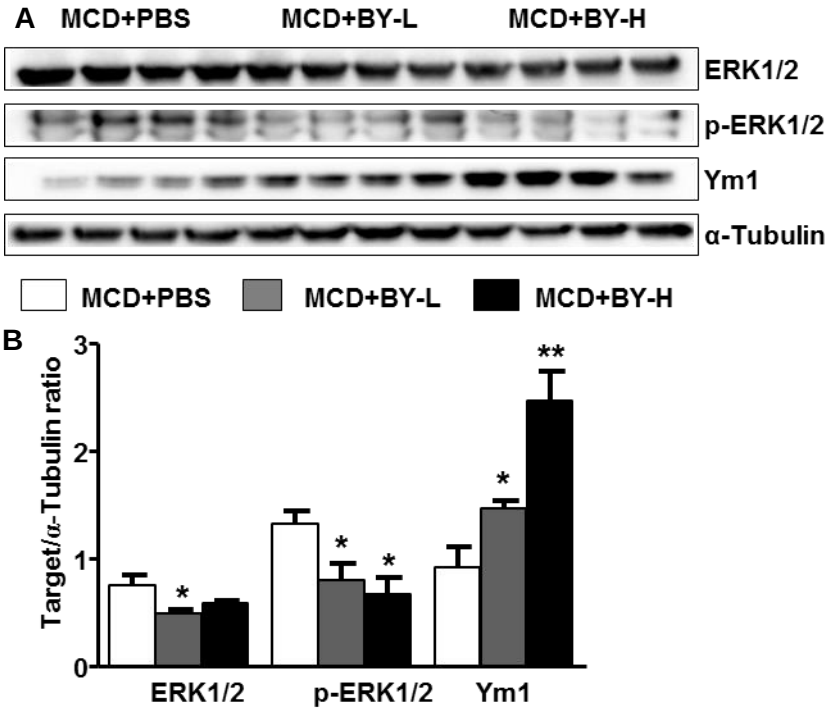

Fig.25 BY treatment enhances ERK 1/2 signaling and increases Ym1 protein expression (**A-B**) Western blot analysis and densitometric quantification of protein levels showed that BY-L or BY-H-treated mice had lower expression of ERK1/2, p-ERK1/2 but increased expression of Ym1 protein. In each case livers from 4 individual animals were analyzed and α-tubulin expression was used as a loading control. *p< 0.05, **p< 0.01 and ***p< 0.001 versus PBS-treated mice at the same time point.

3.3.6 Effects of BY on hepatic dendritic cells and macrophages

To further determine the influence of MCD and BY treatment with regard to immune cells and in particular DCs and macrophages, flow cytometry was performed. No differences in total $CD45^+$ leucocytes were observed between livers of mice fed the MCD diet receiving BY or the PBS control (**Fig.26A**). Similarly, $CD11c^+$ hepatic DCs were not different between BY- and PBS-treated animals. However, the total percentage of $F4/80^+$ cells within the $CD45^+$ population was significantly decreased after BY-L treatment (**Fig.26B**). Moreover, when the CD11c marker was combined with the F4/80 macrophage marker, three different populations that showed a different abundance between BY- and PBS-treated MCD mice could be identified. Thus $CD11c^+F4/80^+$ macrophages/DCs were significantly decreased after BY-L treatment while $CD11c^-F4/80^+$ macrophage/DC subsets and $CD11c^+F4/80^-$ DCs were reduced, though not yet reaching significance (**Fig.26C**). The above results indicate that BY treatment modulated different macrophage/DC subsets but did not significantly change the number of total hepatic DCs.

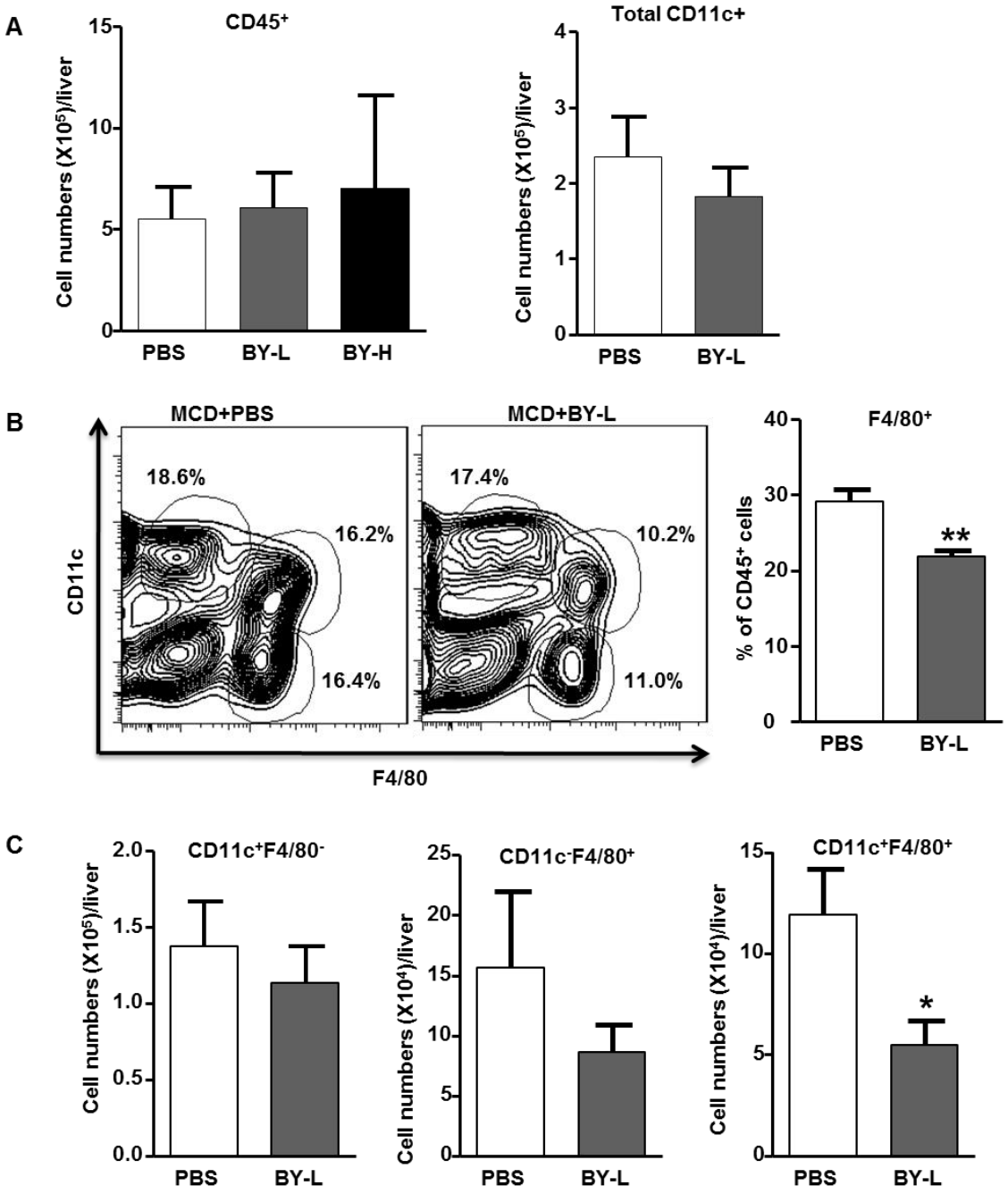

Fig.26 Flow cytometry analysis of macrophage/DC subsets isolated from the liver (**A**) There were no differences in $CD45^+$ and $CD11c^+$ cells per total liver between the groups after BY treatment. (**B**) Representative FACS plots and cell numbers show lowered total hepatic $CD11c^+F4/80^-$, $CD11c^+F4/80^+$ and $CD11c^-F4/80^+$ cells from $CD45^+$ gated liver mononuclear cells upon BY treatment. Total $F4/80^+$ of $CD45^+$ cells were reduced after BY treatment. (**C**) BY treatment significantly decreased $CD11c^+F4/80^+$ cells per liver. A less marked decrease of the percentage of $CD11c^+F4/80^-$ and $CD11c^-F4/80^+$ cells per liver was found. Data are expressed as means ± SEM. N=5 mice per group. *$p < 0.05$, **$p < 0.01$, and ***$p < 0.001$ versus PBS-treated mice at the same time point.

3.3.7 Effects of BY on hepatic monocyte and macrophage subsets

Since the above data suggested a differential regulation of monocyte/macrophage subsets upon BY treatment, the expression of the Ly6C marker that can differentiate inflammatory versus restorative monocyte/macrophage populations in the liver was assessed[148]. Flow cytometric analysis revealed that BY treatment significantly decreased pro-inflammatory hepatic $CD11b^{+}Ly6C^{hi}$ cells (**Fig.27A,B**). Conversely, BY treatment promoted an increase of hepatic $CD11b^{+}Ly6C^{lo}$ cells (**Fig.27A,B**), which have anti-inflammatory effect as so-called "restorative" macrophages. Differences were even more pronounced when the ratio of $CD11b^{+}Ly6C^{lo}$ or $CD11b^{+}Ly6C^{hi}$ versus $CD45^{+}$ cells was calculated (**Fig.27C**).

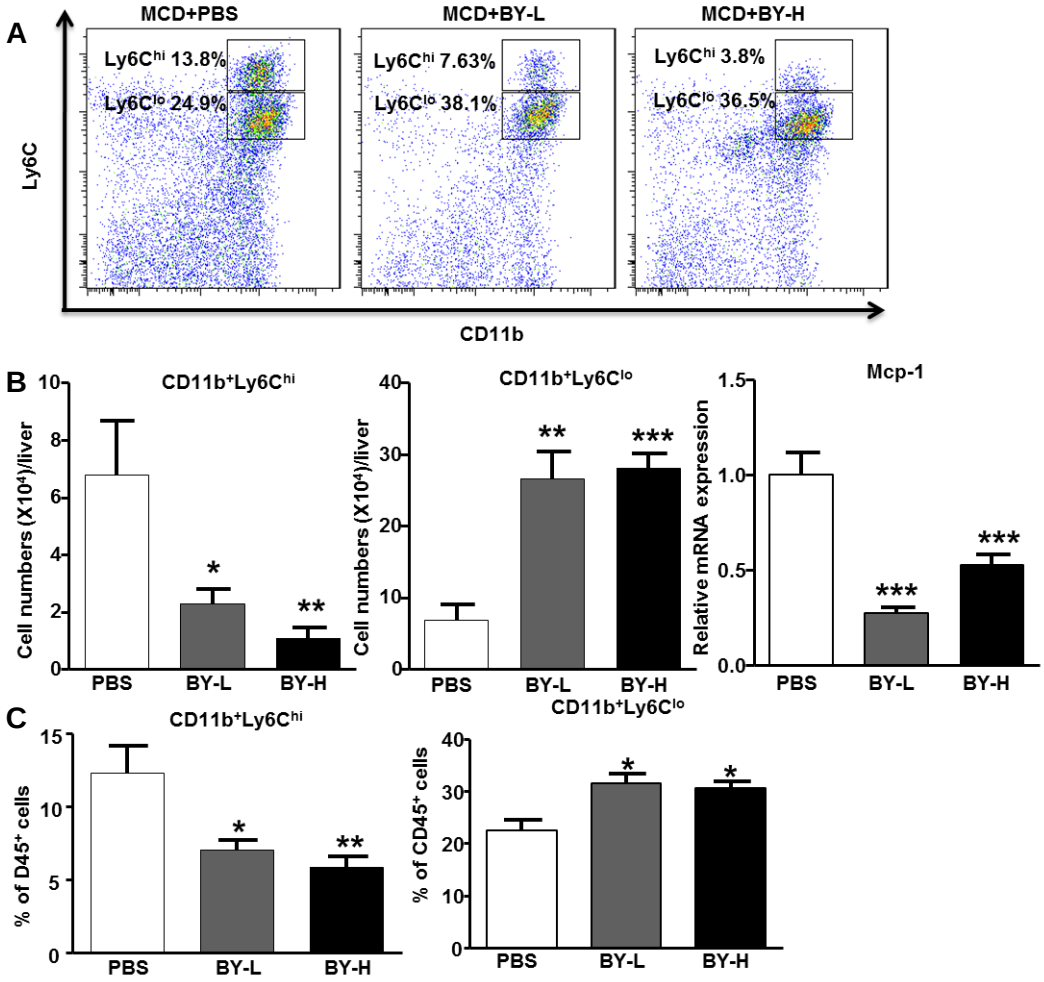

Figure 27: BY treatment reduces inflammatory and increases restorative monocyte/macrophage numbers (**A**) Representative FACS plots showing $CD45^{+}$ cells that were gated for the $CD11b^{+}$ and $Ly6C^{+}$ markers. Numbers indicate the percentages of $CD11b^{+}Ly6C^{hi}$ and $CD11b^{+}Ly6C^{lo}$ monocytes/macrophages within the $CD45^{+}$ population. (**B**) BY treatment reduced pro-inflammatory $CD11b^{+}Ly6C^{hi}$ and increased $CD11b^{+}Ly6C^{lo}$ restorative monocyte/macrophage numbers. (**C**) Bar diagrams showing the ratios between

$CD11b^{+}Ly6C^{hi}$ and $CD11b^{+}Ly6C^{lo}$ cells. Data are expressed as means ± SEM. N=5 mice per group. *p < 0.05, **p < 0.01, and ***p < 0.001 versus PBS-treated mice at the same time point.

3.3.8 BY ameliorates hepatic fibrosis in MCD diet-fed mice

After 4 weeks of BY treatment the liver to body weight of MCD mice was not significantly different in BY-treated vs PBS-treated control mice (**Fig.28A**). However, the hepatic Hyp content was reduced by 41.8% in the BY-L group and by 41.4% in the BY-H group when compared to the PBS-treated MCD controls (**Fig.28B**).

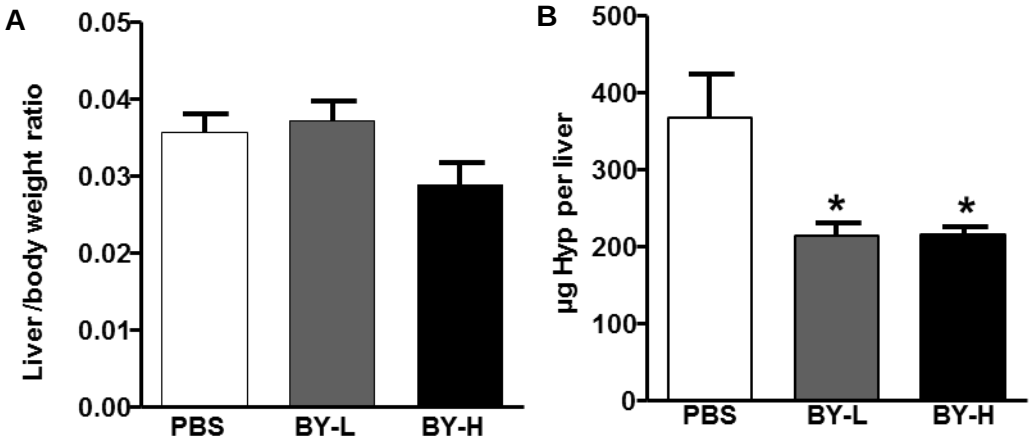

Fig.28 BY treatment improves hepatic fibrosis in MCD diet-fed mice (**A**) There was no difference in the liver to body weight ratios between all groups. (**B**) BY treatment significantly decreased Hyp and thus hepatic collagen content in MCD diet-fed mice. N=10 per group.*p< 0.05 versus PBS-treated mice at the same time point.

3.3.9 BY attenuated the liver pathology of MCD diet-fed mice

The MCD diet leads to activation HSCs, which directly contribute to liver fibrosis (**Fig.3D**). To study the potential of BY for reducing liver fibrosis, liver sections from BY- and PBS-treated MCD mice were analyzed morphometrically after Sirius red staining. 8 weeks of the MCD diet lead to severe fibrosis throughout the liver parenchyma (**Fig.9 and Fig.29A**). Notably, in BY-L- and BY-H-treated mice fibrosis was reduced by 70.0% and by 61.0% respectively (**Fig.29A**).

Next, liver sections were stained with anti-α-SMA antibody to detect activated hepatic stellate cells. BY treatment reduced α-SMA-stained cells by 80.7% in the BY-L group and by 81.8% in BY-H group (**Fig. 29B**). Finally, the protein expression of collagen/procollagen type III (Col3) that is a major member of the fibrillar collagens was analyzed morphometrically, revealing a significant reduction by 67.9%

in the BY-L- and by 43.7% in BY-H-group when compared with the controls (**Fig. 29C**).

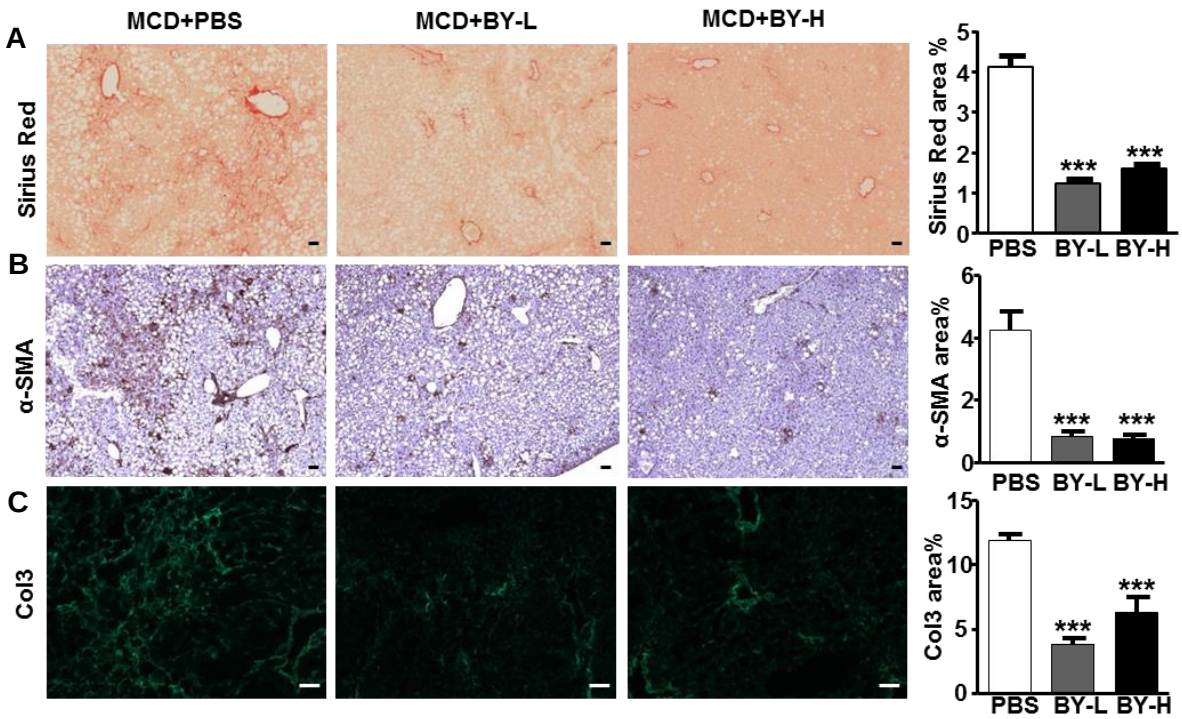

Fig.29 Effect of BY on MCD diet-induced liver fibrosis (**A-C**) Representative liver sections and morphometrical quantification demonstrating that BY significantly reduced collagen deposition (as assessed by Sirius red staining), α-SMA expression and Col3 deposition (10 x magnifications) in MCD diet-fed mice. N=10 per group. In each group 100 individual areas were analyzed. Scale bars indicate 50 μm and ***p< 0.001 versus PBS treated mice at the same time point.

3.3.10 BY suppresses liver fibrosis related transcripts in MCD diet-fed mice

To further study the dynamics of hepatic fibrosis, the expression of TGFβ1, a master regulator of fibrogenesis, and its target genes COL1α1 and TIMP-1 were assessed in the livers by quantitative real-time PCR. Feeding of the MCD diet for 8 weeks increased hepatic transcripts for TGFβ1, COL1α1 and TIMP-1 2.0, 7.0 and 26.0 fold, respectively, compared with the MCS control diet (**Fig.7**). BY-L treatment of MCD mice down-regulated hepatic mRNA expression of TGFβ1, COL1α1 and TIMP-1 by 53.3%, 92.3% and 69.6%, respectively, compared with the PBS treated MCD diet-fed mice. Similarly, treatment with BY-H, TGFβ1, COL1α1 and TIMP-1 transcripts was down-regulated by 57.7%, 90.8% and 70.3%, respectively. Moreover, hepatic transcripts for α-SMA were reduced by 64.5% in the BY-L group and by 72.4% in the BY-H group compared with PBS-treated control mice. Accordingly, BY-L and BY-H treatment reduced hepatic

mRNA levels for pro-fibrogenic MMP2, but also for ECM-remodeling MMP3, MMP8, MMP9 and MMP13 significantly by >40% (**Fig.30B**).

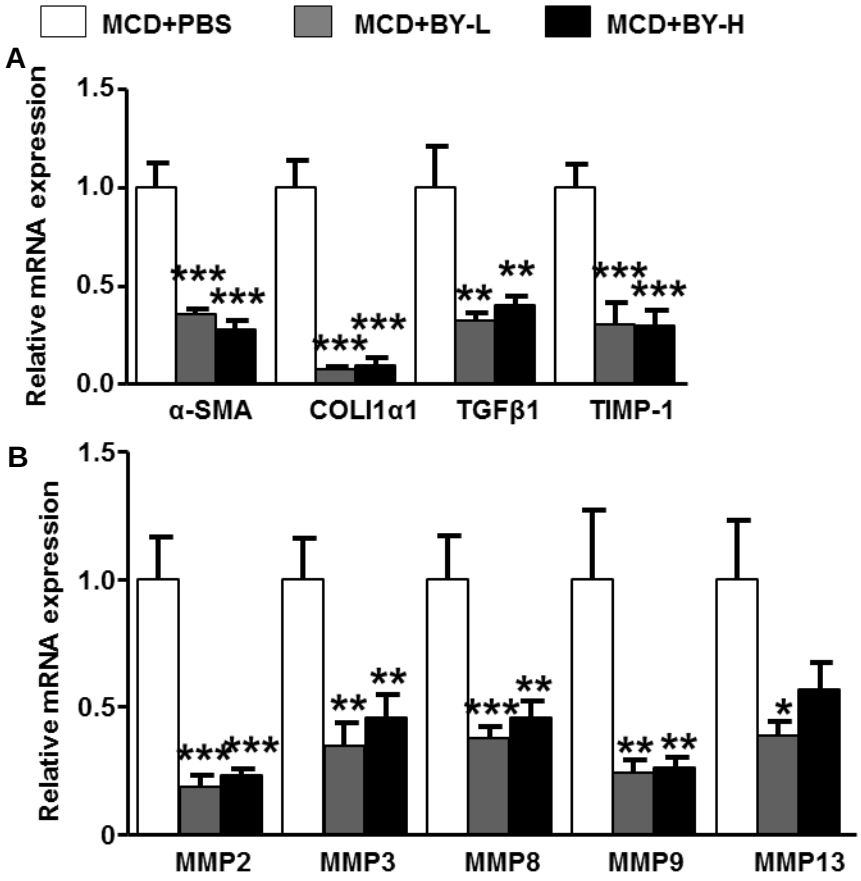

Fig.30 BY treatment reduces the levels of fibrogenic and MMP transcripts in livers of MCD diet-fed mice (**A**) BY significantly reduced the mRNA levels of the pro-fibrotic genes α-SMA, COL1α1, TGFβ1 and TIMP-1. (**B**) Relative mRNA transcript levels of the matrix metalloproteinase family genes MMP2, 3, 8, 9, 13 were also reduced upon BY treatment. Data are shown as mean mRNA levels ± SEM and are represented relative to mRNA transcription of Gapdh. N=10 per group. *p< 0.05, **p< 0.01 and ***p< 0.001 versus PBS treated mice at the same time point.

3.3.11 BY reduces JNK activation in MCD diet-fed mice

JNK signaling is implicated in hepatic wound healing responses to chronic injury[169]. To elucidate if JNK signaling might be influenced by BY treatment, hepatic protein levels of JNK and its target c-Jun or phosphorylated c-Jun (p-Jun) were assessed in MCD mice that were treated with BY or PBS. Western blot analysis of fibrotic liver tissues that were treated with PBS revealed activation of the JNK pathway as demonstrated by phosphorylated JNK (p-JNK) and p-Jun (**Fig.31A,B**). BY treatment strongly reduced p-JNK, total c-Jun and especially p-c-Jun (**Fig.31A,B**). Notably, confocal immunofluorescence microscopy demonstrated colocalization of p-JNK and

α-SMA in patients with hepatitis C suggesting that p-JNK is predominantly expressed in activated HSC in fibrotic areas with high α-SMA expression[169]. Since activation of JNK signaling was correlated with α-SMA protein levels (**Fig. 31A, B**), these findings suggest that α-SMA expression might be directly or indirectly linked to JNK activation and that JNK signaling is in turn down-regulated upon BY treatment.

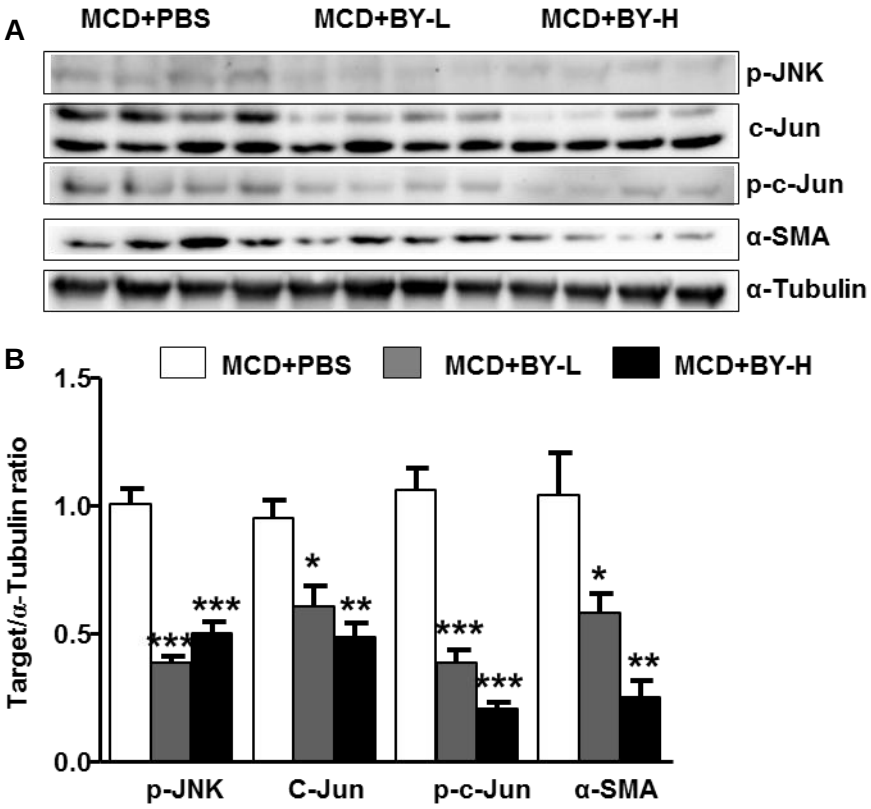

Fig.31 BY treatment reduces α-SMA protein expression and induces down-regulation of the JNK signaling pathway (**A-B**) Western blot analysis and quantification showed a down-regulation of phospho-JNK, total c-Jun, phospho-c-Jun and α-SMA protein levels after BY treatment. In each case livers from 4 individual animals were analyzed and α-tubulin expression was used as a loading control. *p< 0.05, **p< 0.01 and ***p< 0.001 versus PBS treated mice at the same time point.

3.3.12 The anti-fibrotic potential of BY in Mdr2$^{-/-}$ mice

To analyze the anti-fibrotic potential of BY in a pure model of liver fibrosis that has no relation to NASH, Mdr2$^{-/-}$ mice that are deficient in the hepatocyte phospholipid flippase and spontaneously develop secondary biliary fibrosis between age 4 to 12 weeks were used[161]. Since direct GLP-1 receptor agonism was associated with reduced hepatic fat accumulation in MCD mice, first body and liver weight between BY- and PBS-treated Mdr2$^{-/-}$ mice were compared, revealing no significant differences

(**Fig.32A**). While serum ALT levels were not reduced significantly in BY-L-treated mice, there was a significant 52.5% decrease of ALT following BY-H treatment (**Table 5**). Equally, serum AST and AP were significantly decreased by 43.9% and 36.7%, resp., in the BY-H treatment group (**Table 5**). Finally, there was a significant decrease of Hyp documenting a reduced collagen accumulation in BY-L-treated Mdr2$^{-/-}$ mice (**Fig.32B**).

Table 5. Metabolic parameters of Mdr2$^{-/-}$ mice with PBS and BY treatment

Mdr2$^{-/-}$ with PBS or BY treatment	PBS	BY-L	BY-H
Body weight (g)	23.19±0.58	21.90±0.37	21.65±0.47
ALT (U/l)	629.1±64.71	631.7±60.38	299.1±49.76 **
AST (U/l)	658.0±70.20	754.7±57.53	369.4±68.41*
AP (U/l)	815.1±79.89	707.0±47.58	516.0±48.51**

Mdr2$^{-/-}$ mice were treated with PBS, 0.4 mg/kg BY (BY-L) or 2 mg/kg BY (BY-H) for 4 weeks. At the start, every other week and at the time of sacrifice the body weight was recorded. The liver weight was determined at sacrifice. Data are expressed as means ± SEM. N=10 mice per group. *p < 0.05, **p < 0.01, and ***p < 0.001 versus PBS-treated mice at the same time point.

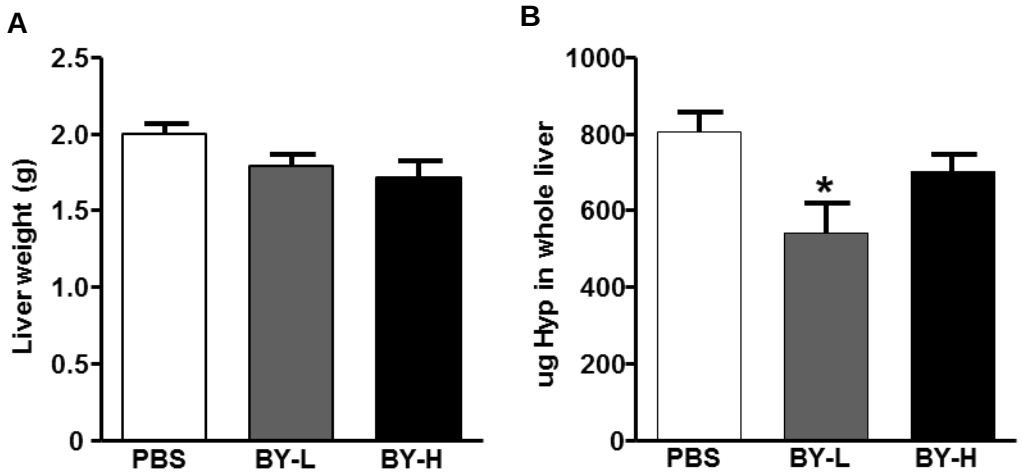

Fig.32 Analysis of liver weight and Hyp levels in Mdr2$^{-/-}$ mice that were treated with PBS or BY (**A**) BY treatment did not significantly reduce liver weight in Mdr2$^{-/-}$ mice. (**B**) BY-L treatment significantly reduced Hyp levels in Mdr2$^{-/-}$ livers. N=10 per group. *p < 0.05, **p < 0.01, and ***p < 0.001 versus PBS-treated mice at the same time point.

3.3.13 BY attenuates inflammation in Mdr2$^{-/-}$mice

To next analyze the effect of BY on monocytes/macrophages in liver sections and to determine the modulation of key inflammation-related genes after BY treatment of Mdr2$^{-/-}$ mice, immunohistochemistry and qPCR were performed. CD68^{+} cells were greatly decreased to 49.4% and 52.4% vs PBS-treated controls after BY-L and BY-H treatment, resp. (**Fig.33A,D**). Similarly, F4/80^{+} cells were reduced by 68.0% and 71.3% (**Fig.33B,D**). By contrast, expression of the anti-inflammatory Ym1 marker was

significantly increased 4.3 fold in BY-L- and 4.4 fold in BY-H-treated liver sections (**Fig.33C,D**).

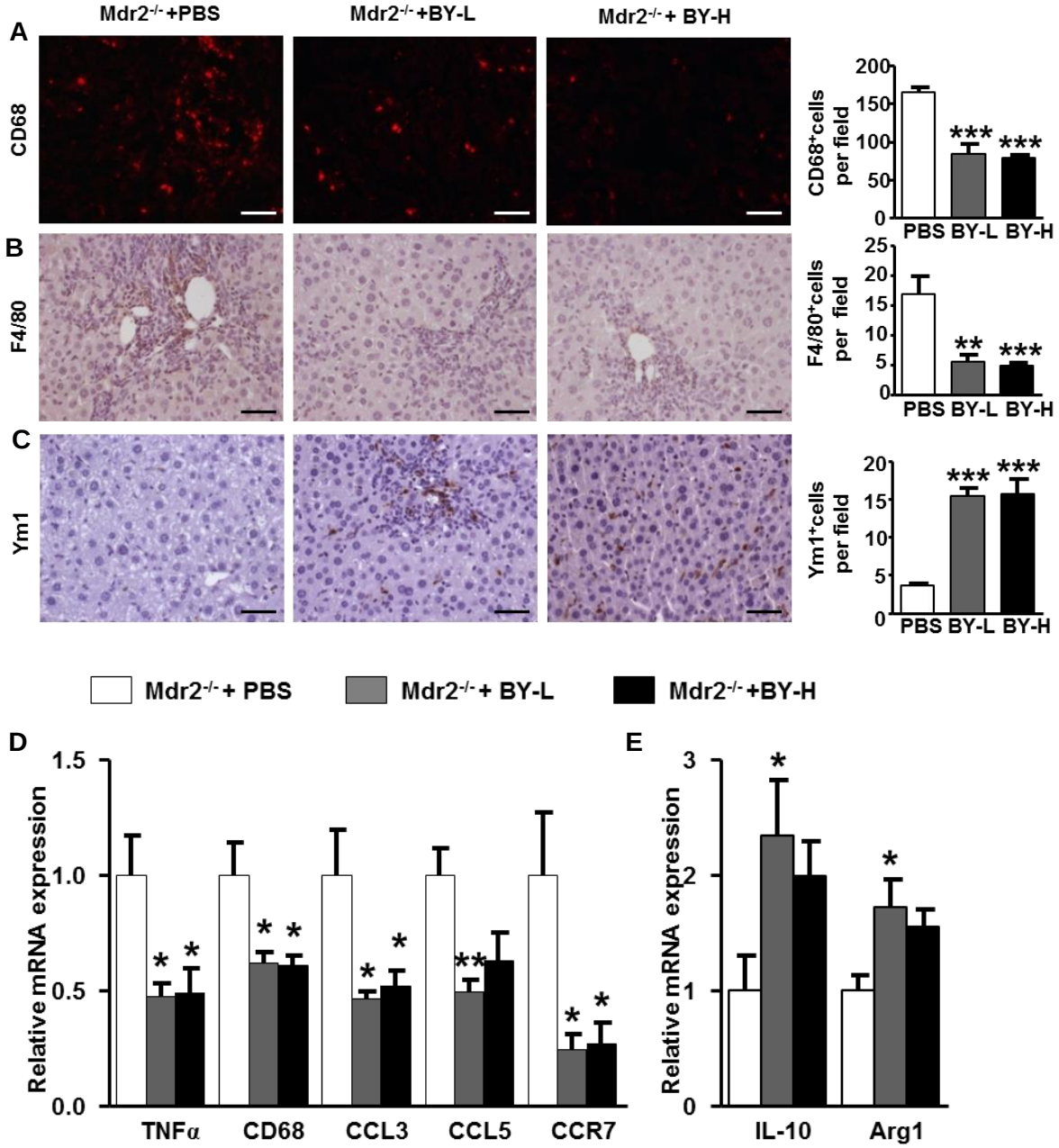

Fig.33 BY treatment improves parameters of hepatic inflammation in Mdr2$^{-/-}$ mice (**A-C**) Representative liver sections from mice were stained for the expression of CD68, F4/80 and Ym1. The bar diagrams on the right represent mean values ± SEM of CD68, F4/80 and Ym1. In each group 70 individual areas were analyzed. Scale bars indicate 50 µm. (**D**) BY treatment suppressed relative mRNA transcription for TNFα, CD68, CCL3, CCL5 and CCR7, and (**E**) up-regulated IL-10 and Arg1 mRNA levels. Data are shown as mean mRNA levels ± SEM and are represented relative to mRNA transcription of Gapdh. N=7 per group. *p< 0.05; **p< 0.01 and ***p< 0.001 versus PBS-treated mice at the same time point.

Further confirming the anti-inflammatory action of BY, BY-L and BY-H reduced transcript levels of pro-inflammatory TNFα >50%, and CD68 transcripts by almost 40% (**Fig.33E**). Similarly, transcripts for the M1 macrophage transcripts for CCL3, CCL5 and CCR7 were significantly suppressed, while anti-inflammatory IL-10 and Arg1 transcripts were up-regulated by BY-treatment (**Fig.33E**).

3.3.14 BY ameliorates hepatic fibrosis in Mdr2$^{-/-}$ mice

Liver sections were stained with Sirius Red, and for α-SMA and COL3. The deposition of fibrillar collagen was significantly upon treatment with BY (**Fig.34A,D**), as was the protein expression of α-SMA and deposition of COL3 in the BY-treated livers of fibrotic Mdr2$^{-/-}$ mice (**Fig.34B, C, D**).

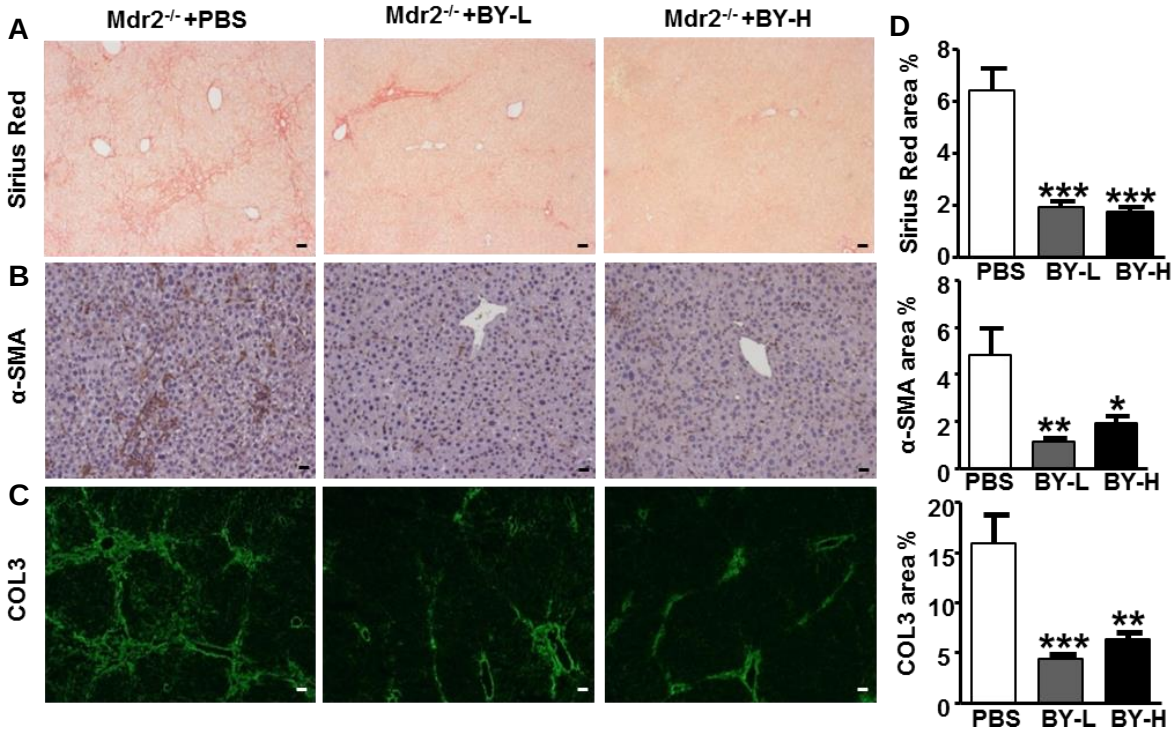

Fig.34 A**dministration of BY improves hepatic fibrosis in Mdr2$^{-/-}$ mice** (**A-C**) Representative liver sections stained for collagen deposition (Sirius red), α-SMA and COL3 expression (scale bars indicates 50 μm). (**D**) Statistical morphometric analysis of collagen deposition, α-SMA and COL3 deposition. Positive areas were scored by image analysis in ten random microscopic fields from each slide. Data are expressed as mean ± SEM (N=7 per group), *p < 0.05, **p < 0.01, and ***p < 0.001 versus PBS-treated mice at the same time point.

3.3.15 Effect of BY on liver fibrosis related gene expression

To obtain further information about the fibrosis related genes that are regulated by BY in Mdr2$^{-/-}$ mice, a spectrum of profibrogenic as well as putative fibrolytic mRNA

transcripts were quantified by qPCR. Importantly and directly documenting the anti-fibrotic effect of BY, transcript levels for all tested fibrosis-associated genes (α-SMA, COL1α1 and TGFβ1, the TGFβ1 dependent signal transducer Smad2 and Smad3) were down-regulated in BY-treated Mdr2$^{-/-}$ mice (**Fig.35A**). Treatment with BY also reduced the mRNA expression of putatively fibrolytic but also ECM remodeling matrix metalloproteinases and of the general MMP inhibitor TIMP-1 (**Fig.35B**).

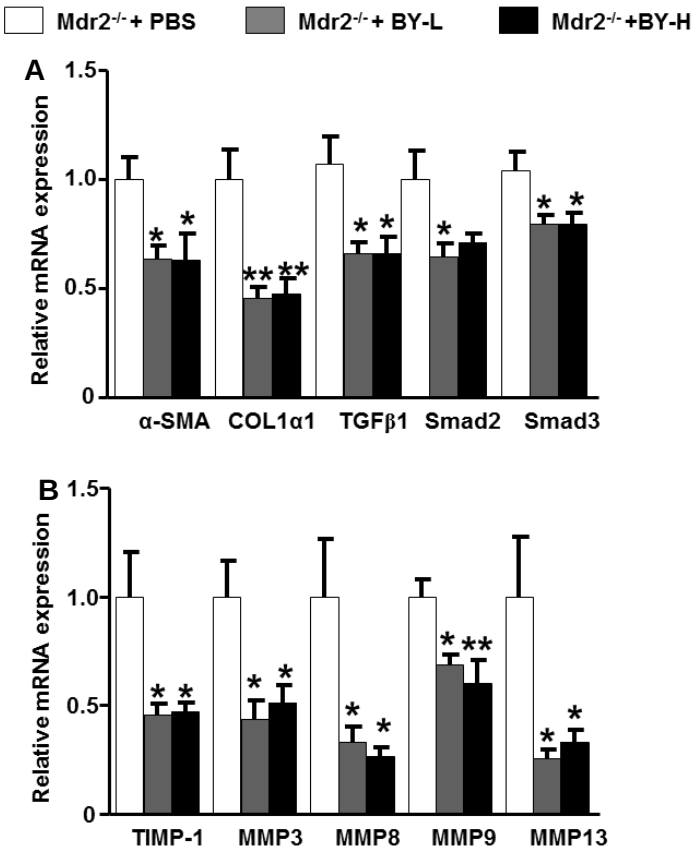

Fig.35 BY treatment reduces mRNA levels of key pro-fibrotic and MMP genes in Mdr2$^{-/-}$ mice (**A**) BY treatment reduced relative mRNA levels of profibrotic genes (α-SMA, COL1α1, TGFβ1, Smad2 and Smad3). (**B**) BY treatment also reduced relative mRNA expression of TIMP-1 and MMP3, 8, 9 and 13. Graphs show mean mRNA levels ± SEM and are represented relative to mRNA transcription of Gapdh. Data are expressed as mean ± SEM (N=7 per group), *p < 0.05, **p < 0.01, and ***p < 0.001 versus PBS-treated mice at the same time point.

4. Discussion

NAFLD is an increasing public health problem in Western and developing countries[170]. Most therapies for NAFLD and NASH aim at preventing or reversing hepatic injury induced by lipotoxicity. One possible therapeutic strategy is to correct hyperinsulinemia and IR, and to reduce body fat mass, in particular visceral adiposity. Physical exercise and weight loss, lifestyle and diet changes, insulin-sensitizing agents and anti-obesity surgery are important therapeutic regimes that can reduce disease burden. A more liver targeted approach is to prevent or reverse lipotoxicity by either suppressing oxidative stress / lipid peroxidation, or by using anti-apoptotic, anti-inflammatory or other hepato-protective agents. Moreover, in advanced disease and antifibrotic therapy is needed, to block progression or reverse fibrosis and cirrhosis. A combination of several of these strategies should provide a stage-adapted therapy. A most promising pharmacological approach is the use of DPP-4 inhibitors and GLP-1R agonists, both of which have already been approved for treatment of T2D[47]. The purpose of this study was therefore to experimentally evaluate the *in vivo* efficacy of these agents in diet-induced and genetically modified NASH and fibrosis mouse models.

4.1 Evaluation of DPP-4 and GLP-1R agonist therapies with the MCD diet model of NASH

In the present study and using a wide array of experimental setups, I demonstrated that the MCD NASH model recapitulates key features of liver fat accumulation, inflammation, fibrosis, and tissue damage. Notably, I found that all of these central features associated with NASH are ameliorated by systemic therapy with the DPP-4 inhibitors Linagliptin and Sitagliptin and especially by systemic application of the GLP-1R agonist BY. This beneficial therapeutic effect operated independently from insulin, because mice fed with the MCD diet are characterized by reduced levels of insulin[34]. Moreover, my work with the MCD mouse model demonstrated the occurrence of pronounced myeloid inflammation that is characterized by increased infiltration of inflammatory macrophages and monocytes into the liver that represents an initial as well as advanced step of the NASH pathologic cascade. Importantly, this thesis reports the first *in vivo* analysis of hepatic resident macrophages and infiltrating monocytes in MCD NASH mice that were treated with DPP-4 inhibitors and a GLP-1R agonist and,

in addition, also uncovers several mechanistic principles and pathways that promote our understanding of the mechanisms underlying the benefit of this therapeutics.

Several dietary models for NASH such as high fat diets develop experimental obesity and IR but generally lack pronounced steatohepatitis[171]. In the current study, I have used MCD diet-fed mice as a more appropriate animal model for the severe inflammatory aspects of NASH. Although this model has been extensively studied due to the morphological changes of the liver and the close resemblance to human NASH with regard to the induction of oxidative stress, hepatocyte lipoapoptosis, inflammation and fibrosis[33], it does not entirely reflect the metabolic syndrome of human NASH with its characteristic IR and obesity[40]. However, drug regulatory authorities such as the US Food and Drug Administration (FDA) consider this inflammatory liver phenotype as prime target for the development of novel pharmacological therapies for NASH. One reason is that there are already numerous medications that specifically address IR/T2Dand cardiovascular pathology. Therefore, the MCD model is the best approximation to test drugs that affect this pathological liver inflammation and fibrosis. My study demonstrates that the administration of the MCD diet to C57BL/6J mice for 4 and especially 8 weeks resulted in the classical and relevant hepatic phenotype of NASH when compared to the MCS control cohorts.

Firstly, this study confirmed that serum ALT and mRNA levels of TGFβ1 and TNFα were markedly increased in the MCD model. Similarly, mRNA levels for α-SMA, COL1α1, TIMP-1 and MMP family members (MMP3, MMP13) were all significantly increased in mice fed the MCD diet for 4 and especially 8 weeks. In addition, CD36, which is known to be enhanced upon MCD feeding and directly contributes to detrimental free fatty acid uptake in the liver, as well as increased hepatic triglyceride storage and secretion[172] were greatly up-regulated. Feeding the MCD diet also significantly increased mRNA levels of CCL3 (macrophage inflammatory protein-1α, MIP-1α), a member of the CC motif subfamily of chemokines that is involved in both acute and chronic macrophage-mediated inflammation[173]. I also found a steep increase in relative hepatic collagen accumulation, i.e., collagen per g of liver tissue, the central fibrosis related parameter that is linked to liver dysfunction, being 2-fold above that of MCS diet controls at 4 weeks and 2.5-fold at 8 weeks. Using the NAS scoring system, which is currently considered the gold standard for the histological assessment of the severity of apoptosis and inflammation in human NAFL/NASH,

clearly revealed that MCD mice had a much more advanced liver disease than controls. In fact, an 8 week MCD diet reached a NAS of 5.36 and a F3 fibrosis stage, caused also by increased hepatocyte ballooning, a sign of lipoapoptosis, and fibrosis, both of which are the strongest markers of disease severity and progression, even above scores of classical inflammation. Since the MCD model recapitulated several key features of human NASH, I used this system to better understand the molecular and cellular pathways involved in NASH and for studying the therapeutic effect of DPP-4 inhibitors and the GLP-1R agonist *in vivo*.

4.2 DPP-4 inhibitors and GLP-1R agonist improved steatosis

To analyze general parameters and to put any observed improvements in “hard” hepatic endpoints into a more therapeutic perspective, I first investigated weight loss. As a matter of fact, I found that treatment with DPP-4 inhibitors was weight-neutral, while the long-acting GLP-1R agonist BY induced liver weight loss in a dose-dependent manner. The weight loss observed with BY is in line with publications that report that higher doses of GLP-1R agonists like Liraglutide (3.0 mg) are efficient for weight reduction, even gaining recent approval for this indication[174]. The mechanisms underlying this weight loss are still incompletely understood. One possible explanation is a GLP-1R agonist-mediated reduction in gastric emptying that may be responsible for decreased appetite. Moreover, preclinical data show that GLP-1 reduces homeostatic and reward-associated food intake and, in humans, GLP-1 affected brain areas related to feeding and satiety[175]. In a recent study, liraglutide initially decreased central nervous activation, an effect that was not anymore observed after 12 weeks of treatment, thus suggesting that GLP-1R agonism in the central nervous may contribute to the induction of weight loss, but not necessarily to its maintenance[176]. Unfortunately, effects on gastric emptying were not measured in this study. From the perspective of biochemical parameters, I found that BY treatment did not affect ALT and triglyceride levels. These data suggest that DPP-4 inhibitors and BY have benefits on the liver independently from caloric restriction, appetite or (temporary) induction of weight loss.

These studies also indicate that DPP-4 inhibitors and BY can modestly and significantly, resp., improve the histological severity of steatosis and fibrosis. Excessive fat accumulation in the liver is an early step in the progression of NAFL to NASH and represents an independent risk factor for NASH. Most hepatic fat in NASH patients

derives from increased release of fat from adipose tissue via LPL and the subsequent enhanced uptake of free fatty acids by the liver[177]. In my study, the epididymal adipose tissue was significantly reduced after BY treatment, likely leading to a decreased release of fat from adipose tissue. Apart from assessing the histological fat semi-quantification via the NAS score in liver sections[160], I performed a more detailed examination of hepatocyte steatosis using a more quantitative method, i.e., Sudan III or Oil Red O staining. This approach confirmed my findings a significantly reduced liver fat accumulation by treatment of MCD mice with DPP-4 inhibitors or BY, apart from a significant attenuation of inflammation and hepatocyte ballooning.

These findings are supported by studies of others using DPP-4 or GLP-1 knock-out mice which showed attenuated hepatic steatosis that was accompanied by decreased mRNA levels of genes associated with fatty acid synthesis and improving insulin sensitivity[75,178]. In addition, GLP-1 signaling directly reduced hepatic lipogenesis through the cAMP/AMPK pathway even in non-insulin-resistant states, indicating that other mechanisms may exist independent from its effect on insulin signaling[179]. Interestingly, the data presented here demonstrate that DPP-4 inhibitors and BY significantly down-regulate mRNA level of SREBP-1c, a key lipogenic transcription factor, and its target genes FAS and ACC. All three tested drugs also significantly lowered transcript levels of LPL, which hydrolyzes triglycerides in lipoproteins, leads to enhance free fatty acid release and burdens the liver with potentially toxic free fatty acids from the periphery. These data show that treatment with DPP-4 inhibitors and especially BY improved hepatic steatosis and liver injury in MCD diet-fed mice, at least in part by a reduction of peripheral as well as hepatic fat accumulation via a decreased stimulation of fatty acid synthesis, and a subsequently reduced load of free fatty acids to the liver that may either be stored as hepatic triglycerides, released into the blood stream, or incur damage via hepatic oxidative stress and resultant lipotoxicity.

4.3 DPP-4 inhibitors and BY improve inflammation in MCD fed mice

The progression of the complex pathology of NAFL to NASH includes a variety of liver cells including hepatocytes, immune cells, especially macrophages, and hepatic stellate cells. Inflammatory mediators that are derived from the gut, adipose tissues and the liver itself play an important role for initiating and maintaining the development of NASH, in part by regulating lipid metabolism[21,22]. In this study I provide first and

direct *in vivo* evidence that DPP-4 inhibitors and BY attenuated the initiation and progression of NASH by modulating hepatic macrophages. The up-regulated expression of TNFα and IL-1β genes, another hallmark of NASH, was accordingly reduced in gliptin or BY treated animals. These findings highlight an important role and hitherto unknown beneficial therapeutic effect of DPP-4 inhibitors and BY on macrophage activation during NASH.

TNFα is a pro-inflammatory cytokine that plays an important role in the pathogenesis of numerous human diseases. In the liver, tissue macrophages including KCs and infiltrated monocytes are the primary source of TNFα[180]. My data demonstrate a close link between macrophage infiltration and activation and the local production of TNFα after MCD diet administration. IL-1β prominently initiates early steps in immunoinflammatory responses and is equally mostly secreted by macrophages, here via inflammasome activation[181]. Functionally, IL-1β e.g. stimulates the expression of adhesion molecules on endothelial cells to increase the transmigration of leukocytes. Moreover, KCs promote hepatic steatosis via an IL-1β-dependent mechanism[134]. Interestingly and suggesting a positive feedback circuit, IL-1β enhances the cytotoxic effect of TNFα on cultured hepatocytes[182]. In this respect my data show that DPP-4 inhibitors and BY greatly decreased mRNA levels of IL-1β and TNFα which were both highly up-regulated during MCD diet feeding. This suggests that DPP-4 inhibitors and BY reduced exaggerated Kupffer cell and infiltrating /monocyte-macrophage activation which in turn likely resulted in reduced hepatic lipid accumulation and liver injury and a decreased secretion of IL-1β and TNFα.

KC are tissue resident macrophages and represent the largest hematopoietic cell population within the liver. Several studies using clodronate liposomes or gadolinium chloride to specifically deplete KC in NASH showed a marked reduction of steatohepatitis[120,132,139,183]. In addition, in NASH KC display a pro-inflammatory M1 phenotype that suppresses fatty acid oxidation, increases triglyceride accumulation and compromises insulin responsiveness in hepatocytes[132,183]. Furthermore, it was shown that treatment with GLP-1 agonists reduced vascular and hepatic immune cell infiltration and inflammation of atherosclerotic lesions[111,184]. Complementary to this, GLP-1 supplementation with exendin-4 (the peptide of the BY-formulation) decreased the expression of iNOS, an M1-related macrophage gene in Raw 264.7 macrophages[185]. My results bring this knowledge one step further to show that *in vivo*

treatment of MCD diet-fed mice with DPP-4 inhibitors or BY significantly decreased the numbers of CD68 and F4/80 positive KC/macrophages. This observation was supported and expanded by my finding that DPP-4 inhibitors or BY treatment down-regulated the expression of CD68, TNFα and IL1-β and decreased M1 phenotype-associated CCL3 gene expression. Likewise, this pharmacological treatment induced a pronounced expression of the alternatively activated M2 macrophage markers Ym1 and Arg1 and induced the expression of the anti-inflammatory cytokine IL10. Notably, M2 macrophages with this phenotype are implicated as protective, anti-inflammatory and anti-fibrotic in NASH and other chronic diseases[153-155]. I also investigated the JNK and ERK1/2 signaling cascades, since their activation has been shown to underly the progression of hepatic inflammation by promoting M1-like macrophages[186]. I observed that MCD diet feeding significantly increased JNK, ERK1/2 and phosphorylated c-Jun, JNK and ERK1/2 expression. By contrast, BY more than gliptin treatment inhibited MCD diet-induced ERK expression and the phosphorylation of ERK1/2 in a dose-dependent manner. These results confirm that DPP-4 inhibitors and especially BY modulate macrophage phenotype towards a (beneficial) M2 polarization and suggest that the anti-inflammatory effect of these substances is prominently exerted via the associated inhibition of their ERK/MAPK signaling, which is a central mechanism of the progression of NASH.

Recent studies reported that changes in DC, apart from KC and monocytes-macrophages, play an important role in the progression of NAFLD[139,187]. These reports demonstrated a regulatory role for anti-inflammatory vs pro-inflammatory DC in NASH by limiting sterile inflammation through their role in clearance of apoptotic cells and necrotic debris, with similarities to the M1 and M2 macrophage paradigm. They also showed that deletion of DCs induced an up-regulation of Toll-like receptor expression and cytokine secretion in (other) innate immune effector cells in NASH, including neutrophils, KC, and inflammatory monocytes[187]. In line with these data, I detected an increase in the percentage of $CD11c^+$ DC in MCD steatotic livers when compared to normal livers. Though there were no any changes in the percentage of $CD11c^+$ cells per liver between livers of controls and DPP-4 inhibitor or BY treated mice, I observed a significant decrease in the percentage of $CD11c^+F4/80^+$ cells (inflammatory macrophages/DCs) in the drug treated vs control livers. Since there was no change in other DC populations, this result suggests that DPP-4 inhibitors and BY exert their

effect mainly on monocyte-derived macrophages DCs. In conclusion, my findings demonstrate that DPP-4 inhibitors and BY reduced the number of inflammatory monocytes/macrophages/DCs in the liver, an effect that is very likely to be key to the observed amelioration of NASH.

One of the main changes during liver injury is the recruitment of inflammatory monocytes and their differentiation toward tissue macrophages and DCs[148,188,189]. In the MCD model there was a significant increase in the mRNA levels for CD11b in the steatotic livers compared to control livers. Importantly, Linagliptin treatment significantly reduced CD11b expression in MCD livers. In diet-induced steatohepatitis, KC is the first innate cells to respond to hepatocyte injury and to adept an M1 macrophage phenotype, thereby promoting the recruitment of blood-derived $CD11b^{int}$ $Ly6C^{hi}$ monocytes through secretion of chemokines such as MCP-1 and TNFα[139]. The recruitment of these inflammatory M1-polarized $Ly6C^{hi}$ monocytes from the circulation is also greatly dependent on MCP-1 (CCL2) and its receptor CCR2[137]. While $CD11b^{+}Ly6C^{hi}$ cells were significantly increased in steatotic MCD livers, their numbers were greatly reduced by DPP-4 inhibitors and BY treatment. Moreover, $CD11b^{+}Ly6C^{lo}$ restorative (anti-inflammatory) monocytes-macrophages increased significantly by this treatment. In line with these data, it was previously shown that monocytes/macrophages lacking CX_3CR1, which is predominantly present on non-classical $Ly6C^{lo}$ monocytes, are prone to premature cell death after liver injury[155]. In the model of lacking CX_3CR1, which are also leads to prolonged inflammatory monocyte infiltration into the liver and results in enhanced liver fibrosis[155]. Another study also showed that GLP-1 induces M2 polarization of human macrophages in vitro via STAT3 activation[190]. Therefore, I hypothesized that DPP-4 inhibitors and the GLP-1R agonist might directly inhibit inflammatory signaling pathways like JAK-STAT which in turn may modulate macrophage polarization toward the anti-inflammatory M2 phenotype. Notably, in my studies, the GLP-1R agonist, but not the DPP-4 inhibitors, prominently promoted M2 polarization, whereas the number of restorative M2 ($CD11b^{+}Ly6C^{lo}$) macrophages was not affected by treatment with the DPP-4 inhibitors. I thus conclude that changes in macrophage polarization require potent and specific signaling through the GLP-1R, and that GLP-1 increase via the DPP-4 inhibitors is either too weak to generate such signal and/or the other effects of DPP-4 inhibition,

such as inhibition of chemokine cleavage may counteract the beneficial GLP-1 effects in regards to macrophage polarization.

4.4 DPP-4 inhibitors and BY improve fibrosis in the MCD and Mdr2$^{-/-}$ mouse models

The current understanding of the mechanisms of progression of NASH to fibrosis and cirrhosis favors a model in which steatosis and then steatohepatitis are induced as a result of excess free fatty acids, which in conjunction with mitochondrial dysfunction generate toxic lipid products that cause inflammation, hepatocyte growth arrest and apoptosis, leading to the subsequent activation of HSC that produce excess ECM[191]. The key component in hepatic fibrosis is thus the activation of HSC that are characterized by α-SMA expression and excess collagen production[192]. Importantly and highlighting the therapeutic potential of the tested DPP-4 inhibitors and BY in NASH and fibrosis in general, I found that the increased Sirius red area, α-SMA and collagen type III expression in the livers of MCD diet-fed mice were significantly decreased upon treatment. Consistent with these histomorphometric results, RT-PCR analysis revealed decreased expression of major genes related to fibrogenesis, such as α-SMA, COL1α1 TIMP-1 and TGFβ1 upon systemic DPP-4 inhibition and BY administration. These results indicate that DPP-4 inhibitors and BY induce anti-fibrogenic effects, which due to a lowered activation of HSC during the course of fibrogenic processes.

As a matter of fact, HSC activation can be induced by multiple factors, including predominantly TNFα and TGFβ1[191,193,194]. Here, apart from TGFβ1, increased production of TNFα by activated KC potently augments TIMP-1 expression in activated HSC. In this line, my study demonstrates an upregulation of TIMP-1 levels in MCD diet-fed mice that was reduced after DPP-4 inhibitors and BY treatment, along with a decrease in both cytokines. The relevance of TIMP-1 is also supported by a study reporting that the administration of anti-TIMP-1 antibodies attenuated liver fibrosis and decreased HSC activation[195]. Likewise, blockade of macrophage infiltration by mutated form of MCP-1 inhibited the activation of HSC and the development liver fibrosis in active fibrogenic inflammation in the dimethylnitrosamine (DMN)-treated rats, an established model of liver fibrosis with a pathology closely resembling that of human cirrhosis[196]. Although inflammation rapidly decreased after termination of injury, in my

study observed a sustained influx of Ly6C^{hi} proinflammatory monocytes-macrophages. However, in a study of spontaneous fibrosis regression in mice after discontinuation of the hepatotoxic CCL4, the depletion of macrophages increased myofibroblast numbers leading to blockade of regression[147]. This indicates that macrophages are profibrotic during active inflammation but can adopt a protective (restorative) and fibrolytic phenotype once the aggressive stimulus is removed. In my studies treatment with GLP-1 drugs always acted beneficially in terms of fibrosis, due to their clear activity in generating restorative macrophage phenotype.

Previous studies identified JNK as an important regulator of hepatocyte apoptosis, hepatic inflammatory cell recruitment and liver fibrosis in NASH[197]. My data support this view and demonstrate that MCD feeding induced JNK pathway activation via phospho-JNK and simultaneously demonstrate that treatment with BY decreases protein levels of p-JNK. In addition, BY exposure elicited a significant reduction of c-Jun and phosphorylated c-Jun. Attenuation of JNK activation was previously reported in high fat diet-fed mice treated with a peroxisome proliferator-activated receptor-α agonist[197] and in mice fed the MCD diet receiving α-lipoic acid[198]. JNK stimulation has also been linked to fibrogenesis through PDGF induction of Smad3[199], a signal transducer linked to fibrogenic TGFβ-signaling. My data directly suggest that JNK signaling may be an important executer for linking hepatic (and likely systemic) BY effects with the down-regulation of chronic inflammation and hepatic fibrogenesis. This discovery suggests that the JNK pathway represents a novel and specific target for GLP-1R agonist effects in patients with NASH.

4.5 GLP-1R agonist versus DPP-4 inhibitors

Two types of GLP-1 based therapies were studied: The first group consists of incretin mimetics like BY that bind to the GLP-1 receptor and mimic the action of GLP-1. The therapeutic effect of these GLP-1 receptor agonists works by exceeding the actions of endogenous GLP-1 on metabolism and digestion, on changes in intestinal mucosal proliferation, gallbladder motility, and hepatic glucose and lipid production[200]. The second group consists of DPP-4 inhibitors that prolong endogenously produced GLP-1 activity, and the activity of other cytokines, chemokines and hormones that are degraded by DPP-4. Thus apart from GLP-1, DPP-4 can cleave multiple substrates,

such as brain-derived natriuretic peptide, substance P, neuropeptide Y, peptide YY, high-mobility group protein B1, and stromal-derived factor (SDF)-1 α[57].

In the clinic both these drug classes are used as anti-hyperglycaemic agents and several of them have been approved for the treatment of T2D. The first available GLP-1R agonist, exenatide, was based on a peptide extracted from saliva of the gila monster (*Heloderma suspectum*). Subsequently, synthetic forms, more homologous to human GLP-1, were developed. The crucial difference between endogenous GLP-1 and GLP-1R agonists is the susceptibility for degradation by DPP-4. Current GLP-1R agonists are resistant to degradation, leading to prolonged half-lives of 2–160 h instead of only a few minutes. Combined with a high dose administration, this results in 6–10 times supranatural serum levels[201]. Based on their half-lives, GLP-1R agonists are classified as short-acting agents (e.g., exenatide and lixisenatide, given twice daily) and long-acting agents (albiglutide, dulaglutide and bydureon, i.e., pegylated exenatide once weekly and liraglutide, once daily). Thus the GLP-1R agonists are administered subcutaneously, ranging from twice daily to once weekly, but other routes are being investigated[202].

DPP-4 inhibitors are taken orally, once or twice daily, while once weekly formulations are currently being developed[203]. They inhibit degradation of target proteins by 80–97%, with half-live times of 2–40 h and maintain GLP-1 at postprandial levels[201]. However, as mentioned above, DPP-4 not only degrades GLP-1, but several other cytokines, chemokines like macrophage inflammatory protein-1α (MIP-1α/CCL3), and notably enteroendocrine hormones (incretins), including glucose dependent insulinotropic peptide (GIP), glucagon-like peptide 2 (GLP-2), and peptide YY (PYY)[57]. GIP has been shown to amplify the effect of insulin on target tissues. In adipose tissue, GIP has been reported to increase insulin receptor affinity, stimulate fatty acid synthesis, enhance insulin-stimulated incorporation of fatty acids into triglycerides, and increase the sensitivity of insulin stimulated glucose transport[204]. CCL3 is a 7.8 kDa CC chemokine which is strongly expressed by numerous cell types including T cells, macrophages, neutrophils, endothelial and also stellate cells upon injury[141]. Hence, DPP-4 inhibitors have a wider range of actions than GLP-1R agonists. Since beneficial activity of GLP-1 agonism was less pronounced with the gliptins than with the more GLP-1R specific direct agonists, it may be assumed that DDP-4 inhibitors generate

factors that neutralize some of the beneficial effects on steatosis, inflammation and fibrosis brought about by pure GLP-1 agonism.

GLP-1 induces several metabolic changes in the liver, promoting lower glucose and lipid levels. Independent from insulin and glucagon, GLP-1 stimulates hepatic glycogen storage, while suppressing gluconeogenesis[205,206]. It increases mitochondrial degradation of fatty acids and inhibits triglyceride production[207,208]. In addition, GLP-1 influences bile metabolism[209]. Thus it lowers bile acid production and increases their excretion, thereby lowering the bile acid pool and thus potentially toxic bile acid exposure of hepatocytes[210]. *In vitro*, GLP-1 and the GLP-1R agonist exendin-4 increase cholangiocyte proliferation and reduce apoptosis[69]. Moreover, a single dose of exenatide decreased CCK-induced gallbladder contractions in healthy humans[200]. Taken together, these biliary effects may potentially prevent or ameliorate actions of toxic bile acids that in the extreme can lead to secondary biliary cirrhosis in mice or patients with cholangiopathies. An example is a deficiency in the canalicular phospholipid flippase (Mdr2/Abcb4$^{-/-}$ mice, or the equivalent of familial progressive intrahepatic cholestasis type 4, PFIC-3, in man), with the spontaneous development of bile acid induced liver injury, due to the absence of phospholipid from bile[211], and subsequent evolution of biliary fibrosis resembling primary sclerosing cholangitis (PSC), an autoimmune disease of the biliary ductules [212]. Therefore, the Mdr2$^{-/-}$ mouse is a good animal model for human FPIC-3 and PSC and the resultant liver fibrosis and cirrhosis[213]. The pathology of Mdr2$^{-/-}$ mice is characterized as a sequence of events that include disruption of tight junctions and basement membranes of bile ducts, and bile leakage to the portal tract. These features trigger a multistep process that ultimately leads to the formation of periportal biliary fibrosis[214]. I used this pure biliary fibrosis model to analyze the potential direct antifibrotic effect of the GLP-1 drugs. Interestingly, while the GLP-1R agonist BY significantly reduced inflammatory cytokines, fibrosis and Sirius red stainable collagen, the DPP-4 inhibitors only showed a non-significant reduction of inflammation-related gene expression and had no effect on fibrosis parameters. Therefore as shown in the MCD diet NASH model, the direct agonists were more effective that the DPP-4 inhibitors also in ameliorating biliary fibrosis that is unrelated to hepatic metabolic derangement, though less dramatically.

4.6 Conclusion

Taken together, the experiments and studies performed in this thesis provide novel information on the metabolic derangements and subsequent inflammatory and fibrogenic pathways that are triggered in livers of MCD diet-fed mice. Importantly, this is a first in-depth mechanistic and efficacy study on the relative beneficial activities of two DPP-4 inhibitors vs a long-term GLP-1R agonists in the treatment of this common disease, with an increasing prevalence in most countries. In particular, this work provides important new insight into the pharmacological possibilities, via GLP-1 agonism, of decreasing fat accumulation, inflammation, apoptosis and fibrosis, all of which represent key features of NASH. Most liver injuries are known to trigger the activation of the resident Kupffer cell/macrophage population that quickly releases pro-inflammatory and profibrotic mediators such as TNFα, IL-1β and TGFβ1. Based on my findings and also supported by the current literature, I propose that this pathogenic cascade, predominantly in resident Kupffer cells and freshly recruited macrophages, can be targeted by DPP-4 inhibitors and especially GLP-1R agonists. Mechanistically my data also suggest that in addition to the modulation of the classical GLP-1 receptor activity, BY suppressed the JNK and ERK signaling pathways which are centrally involved in macrophage and hepatocyte inflammation and resultant fibrosis. Moreover, the beneficial effect of DPP-4 inhibitors and GLP-1R agonists might be further enhanced by additional therapeutic interventions like the targeting of pro-inflammatory chemokines and their receptors. This should be most efficient during early phases of inflammation and should mechanistically prevent the recruitment of inflammatory cells, mainly macrophages, to the liver. Thus DPP-4 inhibitors and GLP-1R uniformly suppressed all disease-typical features of steatosis, inflammation and fibrosis progression in the used models

This work therefore supports the view that targeting GPL-1 signaling in macrophages to treat NASH and liver fibrosis, apart from the desired insulinotropic and anti-obesity effects, will be a promising therapy for all aspects of the disease. Notably, these agents are already in clinical use for their pure metabolic effects, and therefore clinical trials in Patients with NASH will be of low risk.

5. References

1 Alberti, K. G. *et al.* Harmonizing the metabolic syndrome: a joint interim statement of the International Diabetes Federation Task Force on Epidemiology and Prevention; National Heart, Lung, and Blood Institute; American Heart Association; World Heart Federation; International Atherosclerosis Society; and International Association for the Study of Obesity. *Circulation* **120**, 1640-1645, doi:10.1161/CIRCULATIONAHA.109.192644 (2009).

2 Weston, S. R. *et al.* Racial and ethnic distribution of nonalcoholic fatty liver in persons with newly diagnosed chronic liver disease. *Hepatology* **41**, 372-379, doi:10.1002/hep.20554 (2005).
3 Blachier, M., Leleu, H., Peck-Radosavljevic, M., Valla, D. C. & Roudot-Thoraval, F. The burden of liver disease in Europe: a review of available epidemiological data. *Journal of hepatology* **58**, 593-608, doi:10.1016/j.jhep.2012.12.005 (2013).
4 Fan, J. G. *et al.* What are the risk factors and settings for non-alcoholic fatty liver disease in Asia-Pacific? *Journal of gastroenterology and hepatology* **22**, 794-800, doi:10.1111/j.1440-1746.2007.04952.x (2007).
5 Hashimoto, E., Taniai, M. & Tokushige, K. Characteristics and diagnosis of NAFLD/NASH. *Journal of gastroenterology and hepatology* **28 Suppl 4**, 64-70, doi:10.1111/jgh.12271 (2013).
6 Gross, L. S., Li, L., Ford, E. S. & Liu, S. Increased consumption of refined carbohydrates and the epidemic of type 2 diabetes in the United States: an ecologic assessment. *The American journal of clinical nutrition* **79**, 774-779 (2004).
7 Adams, L. A. *et al.* The natural history of nonalcoholic fatty liver disease: a population-based cohort study. *Gastroenterology* **129**, 113-121 (2005).
8 Bugianesi, E. Review article: steatosis, the metabolic syndrome and cancer. *Alimentary pharmacology & therapeutics* **22 Suppl 2**, 40-43, doi:10.1111/j.1365-2036.2005.02594.x (2005).
9 Misra, V. L., Khashab, M. & Chalasani, N. Nonalcoholic fatty liver disease and cardiovascular risk. *Current gastroenterology reports* **11**, 50-55 (2009).
10 Li, Y., Xu, C., Yu, C., Xu, L. & Miao, M. Association of serum uric acid level with non-alcoholic fatty liver disease: a cross-sectional study. *Journal of hepatology* **50**, 1029-1034, doi:10.1016/j.jhep.2008.11.021 (2009).
11 Chitturi, S., Wong, V. W. & Farrell, G. Nonalcoholic fatty liver in Asia: Firmly entrenched and rapidly gaining ground. *Journal of gastroenterology and hepatology* **26 Suppl 1**, 163-172, doi:10.1111/j.1440-1746.2010.06548.x (2011).
12 Fan, J. G. & Farrell, G. C. Epidemiology of non-alcoholic fatty liver disease in China. *Journal of hepatology* **50**, 204-210, doi:10.1016/j.jhep.2008.10.010 (2009).
13 Papandreou, D., Rousso, I. & Mavromichalis, I. Update on non-alcoholic fatty liver disease in children. *Clinical nutrition* **26**, 409-415, doi:10.1016/j.clnu.2007.02.002 (2007).
14 Comar, K. M. & Sterling, R. K. Review article: Drug therapy for non-alcoholic fatty liver disease. *Alimentary pharmacology & therapeutics* **23**, 207-215, doi:10.1111/j.1365-2036.2006.02751.x (2006).
15 Marchesini, G. *et al.* Nonalcoholic fatty liver, steatohepatitis, and the metabolic syndrome. *Hepatology* **37**, 917-923, doi:10.1053/jhep.2003.50161 (2003).
16 Greenfield, V., Cheung, O. & Sanyal, A. J. Recent advances in nonalcholic fatty liver disease. *Current opinion in gastroenterology* **24**, 320-327, doi:10.1097/MOG.0b013e3282fbccf2 (2008).
17 Williams, C. D. *et al.* Prevalence of nonalcoholic fatty liver disease and nonalcoholic steatohepatitis among a largely middle-aged population utilizing ultrasound and liver biopsy: a prospective study. *Gastroenterology* **140**, 124-131, doi:10.1053/j.gastro.2010.09.038 (2011).
18 Ekstedt, M. *et al.* Long-term follow-up of patients with NAFLD and elevated liver enzymes. *Hepatology* **44**, 865-873, doi:10.1002/hep.21327 (2006).
19 Targher, G., Day, C. P. & Bonora, E. Risk of cardiovascular disease in patients with nonalcoholic fatty liver disease. *The New England journal of medicine* **363**, 1341-1350, doi:10.1056/NEJMra0912063 (2010).
20 Schuppan, D., Gorrell, M. D., Klein, T., Mark, M. & Afdhal, N. H. The challenge of developing novel pharmacological therapies for non-alcoholic steatohepatitis. *Liver international : official journal of the International Association for the Study of the Liver* **30**, 795-808, doi:10.1111/j.1478-3231.2010.02264.x (2010).
21 Day, C. P. & James, O. F. Steatohepatitis: a tale of two "hits"? *Gastroenterology* **114**, 842-845 (1998).

22 Tilg, H. & Moschen, A. R. Evolution of inflammation in nonalcoholic fatty liver disease: the multiple parallel hits hypothesis. *Hepatology* **52**, 1836-1846, doi:10.1002/hep.24001 (2010).
23 Angulo, P. Nonalcoholic fatty liver disease. *The New England journal of medicine* **346**, 1221-1231, doi:10.1056/NEJMra011775 (2002).
24 de Luca, C. & Olefsky, J. M. Inflammation and insulin resistance. *FEBS letters* **582**, 97-105, doi:10.1016/j.febslet.2007.11.057 (2008).
25 Berlanga, A., Guiu-Jurado, E., Porras, J. A. & Auguet, T. Molecular pathways in non-alcoholic fatty liver disease. *Clinical and experimental gastroenterology* **7**, 221-239, doi:10.2147/CEG.S62831 (2014).
26 Tomeno, W. *et al.* Emerging drugs for non-alcoholic steatohepatitis. *Expert opinion on emerging drugs* **18**, 279-290, doi:10.1517/14728214.2013.811232 (2013).
27 Sozio, M. S., Liangpunsakul, S. & Crabb, D. The role of lipid metabolism in the pathogenesis of alcoholic and nonalcoholic hepatic steatosis. *Seminars in liver disease* **30**, 378-390, doi:10.1055/s-0030-1267538 (2010).
28 Ibrahim, M. A., Kelleni, M. & Geddawy, A. Nonalcoholic fatty liver disease: current and potential therapies. *Life sciences* **92**, 114-118, doi:10.1016/j.lfs.2012.11.004 (2013).
29 Tiniakos, D. G., Vos, M. B. & Brunt, E. M. Nonalcoholic fatty liver disease: pathology and pathogenesis. *Annual review of pathology* **5**, 145-171, doi:10.1146/annurev-pathol-121808-102132 (2010).
30 Kucera, O. & Cervinkova, Z. Experimental models of non-alcoholic fatty liver disease in rats. *World journal of gastroenterology : WJG* **20**, 8364-8376, doi:10.3748/wjg.v20.i26.8364 (2014).
31 Anstee, Q. M. & Goldin, R. D. Mouse models in non-alcoholic fatty liver disease and steatohepatitis research. *International journal of experimental pathology* **87**, 1-16, doi:10.1111/j.0959-9673.2006.00465.x (2006).
32 Fan, J. G. & Qiao, L. Commonly used animal models of non-alcoholic steatohepatitis. *Hepatobiliary & pancreatic diseases international : HBPD INT* **8**, 233-240 (2009).
33 Leclercq, I. A. *et al.* CYP2E1 and CYP4A as microsomal catalysts of lipid peroxides in murine nonalcoholic steatohepatitis. *The Journal of clinical investigation* **105**, 1067-1075, doi:10.1172/JCI8814 (2000).
34 Larter, C. Z., Yeh, M. M., Williams, J., Bell-Anderson, K. S. & Farrell, G. C. MCD-induced steatohepatitis is associated with hepatic adiponectin resistance and adipogenic transformation of hepatocytes. *Journal of hepatology* **49**, 407-416, doi:10.1016/j.jhep.2008.03.026 (2008).
35 Dela Pena, A. *et al.* NF-kappaB activation, rather than TNF, mediates hepatic inflammation in a murine dietary model of steatohepatitis. *Gastroenterology* **129**, 1663-1674, doi:10.1053/j.gastro.2005.09.004 (2005).
36 Yu, J. *et al.* COX-2 induction in mice with experimental nutritional steatohepatitis: Role as pro-inflammatory mediator. *Hepatology* **43**, 826-836, doi:10.1002/hep.21108 (2006).
37 McCuskey, R. S. *et al.* Hepatic microvascular dysfunction during evolution of dietary steatohepatitis in mice. *Hepatology* **40**, 386-393, doi:10.1002/hep.20302 (2004).
38 Gao, D. *et al.* Oxidative DNA damage and DNA repair enzyme expression are inversely related in murine models of fatty liver disease. *American journal of physiology. Gastrointestinal and liver physiology* **287**, G1070-1077, doi:10.1152/ajpgi.00228.2004 (2004).
39 Koteish, A. & Mae Diehl, A. Animal models of steatohepatitis. *Best practice & research. Clinical gastroenterology* **16**, 679-690 (2002).
40 Rinella, M. E. *et al.* Mechanisms of hepatic steatosis in mice fed a lipogenic methionine choline-deficient diet. *Journal of lipid research* **49**, 1068-1076, doi:10.1194/jlr.M800042-JLR200 (2008).
41 George, J. *et al.* Lipid peroxidation, stellate cell activation and hepatic fibrogenesis in a rat model of chronic steatohepatitis. *Journal of hepatology* **39**, 756-764 (2003).
42 Grubb, S. C., Churchill, G. A. & Bogue, M. A. A collaborative database of inbred mouse strain characteristics. *Bioinformatics* **20**, 2857-2859, doi:10.1093/bioinformatics/bth299 (2004).

43 Rangnekar, A. S., Lammert, F., Igolnikov, A. & Green, R. M. Quantitative trait loci analysis of mice administered the methionine-choline deficient dietary model of experimental steatohepatitis. *Liver international : official journal of the International Association for the Study of the Liver* **26**, 1000-1005, doi:10.1111/j.1478-3231.2006.01314.x (2006).

44 Yamazaki, Y. *et al.* Interstrain differences in susceptibility to non-alcoholic steatohepatitis. *Journal of gastroenterology and hepatology* **23**, 276-282, doi:10.1111/j.1440-1746.2007.05150.x (2008).

45 Pogribny, I. P. *et al.* Hepatic epigenetic phenotype predetermines individual susceptibility to hepatic steatosis in mice fed a lipogenic methyl-deficient diet. *Journal of hepatology* **51**, 176-186, doi:10.1016/j.jhep.2009.03.021 (2009).

46 Kirsch, R. *et al.* Rodent nutritional model of non-alcoholic steatohepatitis: species, strain and sex difference studies. *Journal of gastroenterology and hepatology* **18**, 1272-1282 (2003).

47 Samson, S. L. & Bajaj, M. Potential of incretin-based therapies for non-alcoholic fatty liver disease. *Journal of diabetes and its complications* **27**, 401-406, doi:10.1016/j.jdiacomp.2012.12.005 (2013).

48 McCaughan, G. W. *et al.* Molecular pathogenesis of liver disease: an approach to hepatic inflammation, cirrhosis and liver transplant tolerance. *Immunological reviews* **174**, 172-191 (2000).

49 Gorrell, M. D., Gysbers, V. & McCaughan, G. W. CD26: a multifunctional integral membrane and secreted protein of activated lymphocytes. *Scandinavian journal of immunology* **54**, 249-264 (2001).

50 Ogata, S. *et al.* Identification of the active site residues in dipeptidyl peptidase IV by affinity labeling and site-directed mutagenesis. *Biochemistry* **31**, 2582-2587 (1992).

51 Aertgeerts, K. *et al.* Crystal structure of human dipeptidyl peptidase IV in complex with a decapeptide reveals details on substrate specificity and tetrahedral intermediate formation. *Protein science : a publication of the Protein Society* **13**, 412-421, doi:10.1110/ps.03460604 (2004).

52 Lambeir, A. M., Durinx, C., Scharpe, S. & De Meester, I. Dipeptidyl-peptidase IV from bench to bedside: an update on structural properties, functions, and clinical aspects of the enzyme DPP IV. *Critical reviews in clinical laboratory sciences* **40**, 209-294, doi:10.1080/713609354 (2003).

53 Kazafeos, K. Incretin effect: GLP-1, GIP, DPP4. *Diabetes research and clinical practice* **93 Suppl 1**, S32-36, doi:10.1016/S0168-8227(11)70011-0 (2011).

54 Qi, S. Y., Riviere, P. J., Trojnar, J., Junien, J. L. & Akinsanya, K. O. Cloning and characterization of dipeptidyl peptidase 10, a new member of an emerging subgroup of serine proteases. *The Biochemical journal* **373**, 179-189, doi:10.1042/BJ20021914 (2003).

55 Ajami, K., Abbott, C. A., McCaughan, G. W. & Gorrell, M. D. Dipeptidyl peptidase 9 has two forms, a broad tissue distribution, cytoplasmic localization and DPIV-like peptidase activity. *Biochimica et biophysica acta* **1679**, 18-28, doi:10.1016/j.bbaexp.2004.03.010 (2004).

56 Chen, T. *et al.* Molecular characterization of a novel dipeptidyl peptidase like 2-short form (DPL2-s) that is highly expressed in the brain and lacks dipeptidyl peptidase activity. *Biochimica et biophysica acta* **1764**, 33-43, doi:10.1016/j.bbapap.2005.09.013 (2006).

57 Kim, N. H., Yu, T. & Lee, D. H. The nonglycemic actions of dipeptidyl peptidase-4 inhibitors. *BioMed research international* **2014**, 368703, doi:10.1155/2014/368703 (2014).

58 Mentlein, R. Dipeptidyl-peptidase IV (CD26)--role in the inactivation of regulatory peptides. *Regulatory peptides* **85**, 9-24 (1999).

59 Shioda, T. *et al.* Anti-HIV-1 and chemotactic activities of human stromal cell-derived factor 1alpha (SDF-1alpha) and SDF-1beta are abolished by CD26/dipeptidyl peptidase IV-mediated cleavage. *Proceedings of the National Academy of Sciences of the United States of America* **95**, 6331-6336 (1998).

60 Zaruba, M. M. *et al.* Synergy between CD26/DPP-IV inhibition and G-CSF improves cardiac function after acute myocardial infarction. *Cell stem cell* **4**, 313-323, doi:10.1016/j.stem.2009.02.013 (2009).
61 Huang, C. Y. *et al.* Dipeptidyl peptidase-4 inhibitor improves neovascularization by increasing circulating endothelial progenitor cells. *British journal of pharmacology* **167**, 1506-1519, doi:10.1111/j.1476-5381.2012.02102.x (2012).
62 Fadini, G. P. *et al.* The oral dipeptidyl peptidase-4 inhibitor sitagliptin increases circulating endothelial progenitor cells in patients with type 2 diabetes: possible role of stromal-derived factor-1alpha. *Diabetes care* **33**, 1607-1609, doi:10.2337/dc10-0187 (2010).
63 Balaban, Y. H. *et al.* Dipeptidyl peptidase IV (DDP IV) in NASH patients. *Annals of hepatology* **6**, 242-250 (2007).
64 Fleischer, B. CD26: a surface protease involved in T-cell activation. *Immunology today* **15**, 180-184, doi:10.1016/0167-5699(94)90316-6 (1994).
65 Loster, K., Zeilinger, K., Schuppan, D. & Reutter, W. The cysteine-rich region of dipeptidyl peptidase IV (CD 26) is the collagen-binding site. *Biochemical and biophysical research communications* **217**, 341-348, doi:10.1006/bbrc.1995.2782 (1995).
66 Yang, J. *et al.* Increase in DPP-IV in the intestine, liver and kidney of the rat treated with high fat diet and streptozotocin. *Life sciences* **81**, 272-279, doi:10.1016/j.lfs.2007.04.040 (2007).
67 Lakatos, P. L. *et al.* Elevated serum dipeptidyl peptidase IV (CD26, EC 3.4.14.5) activity in experimental liver cirrhosis. *European journal of clinical investigation* **30**, 793-797 (2000).
68 Itou, M. *et al.* Altered expression of glucagon-like peptide-1 and dipeptidyl peptidase IV in patients with HCV-related glucose intolerance. *Journal of gastroenterology and hepatology* **23**, 244-251, doi:10.1111/j.1440-1746.2007.05183.x (2008).
69 Marzioni, M. *et al.* Exendin-4, a glucagon-like peptide 1 receptor agonist, protects cholangiocytes from apoptosis. *Gut* **58**, 990-997, doi:10.1136/gut.2008.150870 (2009).
70 Richter, B., Bandeira-Echtler, E., Bergerhoff, K. & Lerch, C. Emerging role of dipeptidyl peptidase-4 inhibitors in the management of type 2 diabetes. *Vascular health and risk management* **4**, 753-768 (2008).
71 Yilmaz, Y. *et al.* Dipeptidyl peptidase IV inhibitors: therapeutic potential in nonalcoholic fatty liver disease. *Medical science monitor : international medical journal of experimental and clinical research* **15**, HY1-5 (2009).
72 Shirakawa, J. *et al.* Diet-induced adipose tissue inflammation and liver steatosis are prevented by DPP-4 inhibition in diabetic mice. *Diabetes* **60**, 1246-1257, doi:10.2337/db10-1338 (2011).
73 Kern, M. *et al.* Linagliptin improves insulin sensitivity and hepatic steatosis in diet-induced obesity. *PloS one* **7**, e38744, doi:10.1371/journal.pone.0038744 (2012).
74 Itou, M., Kawaguchi, T., Taniguchi, E., Oriishi, T. & Sata, M. Dipeptidyl Peptidase IV Inhibitor Improves Insulin Resistance and Steatosis in a Refractory Nonalcoholic Fatty Liver Disease Patient: A Case Report. *Case reports in gastroenterology* **6**, 538-544, doi:10.1159/000341510

000341510 (2012).
75 Ding, X., Saxena, N. K., Lin, S., Gupta, N. A. & Anania, F. A. Exendin-4, a glucagon-like protein-1 (GLP-1) receptor agonist, reverses hepatic steatosis in ob/ob mice. *Hepatology* **43**, 173-181, doi:10.1002/hep.21006 (2006).
76 Pocai, A. *et al.* Glucagon-like peptide 1/glucagon receptor dual agonism reverses obesity in mice. *Diabetes* **58**, 2258-2266, doi:10.2337/db09-0278 (2009).
77 Miura, K., Kitahara, Y. & Yamagishi, S. Combination therapy with nateglinide and vildagliptin improves postprandial metabolic derangements in Zucker fatty rats. *Hormone and metabolic research = Hormon- und Stoffwechselforschung = Hormones et metabolisme* **42**, 731-735, doi:10.1055/s-0030-1261929 (2010).

78 Heise, T. *et al.* Pharmacokinetics, pharmacodynamics and tolerability of multiple oral doses of linagliptin, a dipeptidyl peptidase-4 inhibitor in male type 2 diabetes patients. *Diabetes, obesity & metabolism* **11**, 786-794, doi:10.1111/j.1463-1326.2009.01046.x (2009).
79 Klein, T. *et al.* Linagliptin alleviates hepatic steatosis and inflammation in a mouse model of non-alcoholic steatohepatitis. *Medical molecular morphology* **47**, 137-149, doi:10.1007/s00795-013-0053-9 (2014).
80 Jung, Y. A. *et al.* Sitagliptin attenuates methionine/choline-deficient diet-induced steatohepatitis. *Diabetes research and clinical practice* **105**, 47-57, doi:10.1016/j.diabres.2014.04.028 (2014).
81 Dobrian, A. D. *et al.* Dipeptidyl peptidase IV inhibitor sitagliptin reduces local inflammation in adipose tissue and in pancreatic islets of obese mice. *American journal of physiology. Endocrinology and metabolism* **300**, E410-421, doi:10.1152/ajpendo.00463.2010 (2011).
82 Iwasaki, T. *et al.* Sitagliptin as a novel treatment agent for non-alcoholic Fatty liver disease patients with type 2 diabetes mellitus. *Hepato-gastroenterology* **58**, 2103-2105, doi:10.5754/hge11263 (2011).
83 Yilmaz, Y. *et al.* Effects of sitagliptin in diabetic patients with nonalcoholic steatohepatitis. *Acta gastro-enterologica Belgica* **75**, 240-244 (2012).
84 Drucker, D. J. Biological actions and therapeutic potential of the glucagon-like peptides. *Gastroenterology* **122**, 531-544 (2002).
85 Fehmann, H. C., Goke, R. & Goke, B. Cell and molecular biology of the incretin hormones glucagon-like peptide-I and glucose-dependent insulin releasing polypeptide. *Endocrine reviews* **16**, 390-410, doi:10.1210/edrv-16-3-390 (1995).
86 Drucker, D. J. Minireview: the glucagon-like peptides. *Endocrinology* **142**, 521-527, doi:10.1210/endo.142.2.7983 (2001).
87 Holst, J. J. Glucagon-like peptide-1: from extract to agent. The Claude Bernard Lecture, 2005. *Diabetologia* **49**, 253-260, doi:10.1007/s00125-005-0107-1 (2006).
88 Baggio, L. L. & Drucker, D. J. Biology of incretins: GLP-1 and GIP. *Gastroenterology* **132**, 2131-2157, doi:10.1053/j.gastro.2007.03.054 (2007).
89 Le, T. A. & Loomba, R. Management of Non-alcoholic Fatty Liver Disease and Steatohepatitis. *Journal of clinical and experimental hepatology* **2**, 156-173, doi:10.1016/S0973-6883(12)60104-2 (2012).
90 Delzenne, N. *et al.* Gastrointestinal targets of appetite regulation in humans. *Obesity reviews : an official journal of the International Association for the Study of Obesity* **11**, 234-250, doi:10.1111/j.1467-789X.2009.00707.x (2010).
91 Mayo, K. E. *et al.* International Union of Pharmacology. XXXV. The glucagon receptor family. *Pharmacological reviews* **55**, 167-194, doi:10.1124/pr.55.1.6 (2003).
92 Gupta, N. A. *et al.* Glucagon-like peptide-1 receptor is present on human hepatocytes and has a direct role in decreasing hepatic steatosis in vitro by modulating elements of the insulin signaling pathway. *Hepatology* **51**, 1584-1592, doi:10.1002/hep.23569 (2010).
93 Amori, R. E., Lau, J. & Pittas, A. G. Efficacy and safety of incretin therapy in type 2 diabetes: systematic review and meta-analysis. *Jama* **298**, 194-206, doi:10.1001/jama.298.2.194 (2007).
94 Stonehouse, A., Okerson, T., Kendall, D. & Maggs, D. Emerging incretin based therapies for type 2 diabetes: incretin mimetics and DPP-4 inhibitors. *Current diabetes reviews* **4**, 101-109 (2008).
95 Uccellatore, A., Genovese, S., Dicembrini, I., Mannucci, E. & Ceriello, A. Comparison Review of Short-Acting and Long-Acting Glucagon-like Peptide-1 Receptor Agonists. *Diabetes therapy : research, treatment and education of diabetes and related disorders* **6**, 239-256, doi:10.1007/s13300-015-0127-x (2015).
96 Mojsov, S., Weir, G. C. & Habener, J. F. Insulinotropin: glucagon-like peptide I (7-37) co-encoded in the glucagon gene is a potent stimulator of insulin release in the perfused rat pancreas. *The Journal of clinical investigation* **79**, 616-619, doi:10.1172/JCI112855 (1987).

97 Kreymann, B., Williams, G., Ghatei, M. A. & Bloom, S. R. Glucagon-like peptide-1 7-36: a physiological incretin in man. *Lancet* **2**, 1300-1304 (1987).
98 Holst, J. J., Orskov, C., Nielsen, O. V. & Schwartz, T. W. Truncated glucagon-like peptide I, an insulin-releasing hormone from the distal gut. *FEBS letters* **211**, 169-174 (1987).
99 Nielsen, L. L., Young, A. A. & Parkes, D. G. Pharmacology of exenatide (synthetic exendin-4): a potential therapeutic for improved glycemic control of type 2 diabetes. *Regulatory peptides* **117**, 77-88 (2004).
100 Kieffer, T. J., McIntosh, C. H. & Pederson, R. A. Degradation of glucose-dependent insulinotropic polypeptide and truncated glucagon-like peptide 1 in vitro and in vivo by dipeptidyl peptidase IV. *Endocrinology* **136**, 3585-3596, doi:10.1210/endo.136.8.7628397 (1995).
101 Ritzel, U. *et al.* A synthetic glucagon-like peptide-1 analog with improved plasma stability. *The Journal of endocrinology* **159**, 93-102 (1998).
102 Juhl, C. B. *et al.* Bedtime administration of NN2211, a long-acting GLP-1 derivative, substantially reduces fasting and postprandial glycemia in type 2 diabetes. *Diabetes* **51**, 424-429 (2002).
103 Madsbad, S. Exenatide and liraglutide: different approaches to develop GLP-1 receptor agonists (incretin mimetics)--preclinical and clinical results. *Best practice & research. Clinical endocrinology & metabolism* **23**, 463-477, doi:10.1016/j.beem.2009.03.008 (2009).
104 Norris, S. L., Lee, N., Thakurta, S. & Chan, B. K. Exenatide efficacy and safety: a systematic review. *Diabetic medicine : a journal of the British Diabetic Association* **26**, 837-846, doi:10.1111/j.1464-5491.2009.02790.x (2009).
105 Pye, S. R. *et al.* Late-Onset Hypogonadism and Mortality in Aging Men. *J Clin Endocr Metab* **99**, 1357-1366, doi:10.1210/jc.2013-2052 (2014).
106 Lee, J. *et al.* Exendin-4 improves steatohepatitis by increasing Sirt1 expression in high-fat diet-induced obese C57BL/6J mice. *PloS one* **7**, e31394, doi:10.1371/journal.pone.0031394 (2012).
107 Trevaskis, J. L. *et al.* Glucagon-like peptide-1 receptor agonism improves metabolic, biochemical, and histopathological indices of nonalcoholic steatohepatitis in mice. *American journal of physiology. Gastrointestinal and liver physiology* **302**, G762-772, doi:10.1152/ajpgi.00476.2011 (2012).
108 Svegliati-Baroni, G. *et al.* Glucagon-like peptide-1 receptor activation stimulates hepatic lipid oxidation and restores hepatic signalling alteration induced by a high-fat diet in nonalcoholic steatohepatitis. *Liver international : official journal of the International Association for the Study of the Liver* **31**, 1285-1297, doi:10.1111/j.1478-3231.2011.02462.x (2011).
109 Mells, J. E. *et al.* Glp-1 analog, liraglutide, ameliorates hepatic steatosis and cardiac hypertrophy in C57BL/6J mice fed a Western diet. *American journal of physiology. Gastrointestinal and liver physiology* **302**, G225-235, doi:10.1152/ajpgi.00274.2011 (2012).
110 Sharma, S., Mells, J. E., Fu, P. P., Saxena, N. K. & Anania, F. A. GLP-1 analogs reduce hepatocyte steatosis and improve survival by enhancing the unfolded protein response and promoting macroautophagy. *PloS one* **6**, e25269, doi:10.1371/journal.pone.0025269 (2011).
111 Wang, Y. *et al.* Exendin-4 decreases liver inflammation and atherosclerosis development simultaneously by reducing macrophage infiltration. *British journal of pharmacology* **171**, 723-734, doi:10.1111/bph.12490 (2014).
112 Kenny, P. R. *et al.* Exenatide in the treatment of diabetic patients with non-alcoholic steatohepatitis: a case series. *The American journal of gastroenterology* **105**, 2707-2709, doi:10.1038/ajg.2010.363 (2010).
113 DeYoung, M. B., MacConell, L., Sarin, V., Trautmann, M. & Herbert, P. Encapsulation of exenatide in poly-(D,L-lactide-co-glycolide) microspheres produced an investigational long-acting once-weekly formulation for type 2 diabetes. *Diabetes technology & therapeutics* **13**, 1145-1154, doi:10.1089/dia.2011.0050 (2011).

114 Buse, J. B. *et al.* Exenatide once weekly versus liraglutide once daily in patients with type 2 diabetes (DURATION-6): a randomised, open-label study. *Lancet* **381**, 117-124, doi:10.1016/S0140-6736(12)61267-7 (2013).
115 Drucker, D. J. *et al.* Exenatide once weekly versus twice daily for the treatment of type 2 diabetes: a randomised, open-label, non-inferiority study. *Lancet* **372**, 1240-1250, doi:10.1016/S0140-6736(08)61206-4 (2008).
116 Blevins, T. *et al.* DURATION-5: exenatide once weekly resulted in greater improvements in glycemic control compared with exenatide twice daily in patients with type 2 diabetes. *The Journal of clinical endocrinology and metabolism* **96**, 1301-1310, doi:10.1210/jc.2010-2081 (2011).
117 Hotamisligil, G. S. Inflammation and metabolic disorders. *Nature* **444**, 860-867, doi:10.1038/nature05485 (2006).
118 Malaguarnera, L. *et al.* Chitotriosidase gene expression in Kupffer cells from patients with non-alcoholic fatty liver disease. *Gut* **55**, 1313-1320, doi:10.1136/gut.2005.075697 (2006).
119 Tomita, K. *et al.* Tumour necrosis factor alpha signalling through activation of Kupffer cells plays an essential role in liver fibrosis of non-alcoholic steatohepatitis in mice. *Gut* **55**, 415-424, doi:10.1136/gut.2005.071118 (2006).
120 Rivera, C. A. *et al.* Toll-like receptor-4 signaling and Kupffer cells play pivotal roles in the pathogenesis of non-alcoholic steatohepatitis. *Journal of hepatology* **47**, 571-579, doi:10.1016/j.jhep.2007.04.019 (2007).
121 Mantovani, A. *et al.* The chemokine system in diverse forms of macrophage activation and polarization. *Trends in immunology* **25**, 677-686, doi:10.1016/j.it.2004.09.015 (2004).
122 Lumeng, C. N., Bodzin, J. L. & Saltiel, A. R. Obesity induces a phenotypic switch in adipose tissue macrophage polarization. *The Journal of clinical investigation* **117**, 175-184, doi:10.1172/JCI29881 (2007).
123 Boorsma, C. E., Draijer, C. & Melgert, B. N. Macrophage heterogeneity in respiratory diseases. *Mediators of inflammation* **2013**, 769214, doi:10.1155/2013/769214 (2013).
124 Odegaard, J. I. *et al.* Macrophage-specific PPARgamma controls alternative activation and improves insulin resistance. *Nature* **447**, 1116-1120, doi:10.1038/nature05894 (2007).
125 Louvet, A. *et al.* Cannabinoid CB2 receptors protect against alcoholic liver disease by regulating Kupffer cell polarization in mice. *Hepatology* **54**, 1217-1226, doi:10.1002/hep.24524 (2011).
126 Ouchi, N., Parker, J. L., Lugus, J. J. & Walsh, K. Adipokines in inflammation and metabolic disease. *Nature reviews. Immunology* **11**, 85-97, doi:10.1038/nri2921 (2011).
127 Dey, A., Allen, J. & Hankey-Giblin, P. A. Ontogeny and polarization of macrophages in inflammation: blood monocytes versus tissue macrophages. *Frontiers in immunology* **5**, 683, doi:10.3389/fimmu.2014.00683 (2014).
128 Ji, Y. *et al.* Activation of natural killer T cells promotes M2 Macrophage polarization in adipose tissue and improves systemic glucose tolerance via interleukin-4 (IL-4)/STAT6 protein signaling axis in obesity. *The Journal of biological chemistry* **287**, 13561-13571, doi:10.1074/jbc.M112.350066 (2012).
129 Cintra, D. E. *et al.* Interleukin-10 is a protective factor against diet-induced insulin resistance in liver. *Journal of hepatology* **48**, 628-637, doi:10.1016/j.jhep.2007.12.017 (2008).
130 Wan, J. *et al.* M2 Kupffer cells promote M1 Kupffer cell apoptosis: a protective mechanism against alcoholic and nonalcoholic fatty liver disease. *Hepatology* **59**, 130-142, doi:10.1002/hep.26607 (2014).
131 Odegaard, J. I. *et al.* Alternative M2 activation of Kupffer cells by PPARdelta ameliorates obesity-induced insulin resistance. *Cell metabolism* **7**, 496-507, doi:10.1016/j.cmet.2008.04.003 (2008).
132 Huang, W. *et al.* Depletion of liver Kupffer cells prevents the development of diet-induced hepatic steatosis and insulin resistance. *Diabetes* **59**, 347-357, doi:10.2337/db09-0016 (2010).

133 Miura, K. *et al.* Toll-like receptor 9 promotes steatohepatitis by induction of interleukin-1beta in mice. *Gastroenterology* **139**, 323-334 e327, doi:10.1053/j.gastro.2010.03.052 (2010).
134 Stienstra, R. *et al.* Kupffer cells promote hepatic steatosis via interleukin-1beta-dependent suppression of peroxisome proliferator-activated receptor alpha activity. *Hepatology* **51**, 511-522, doi:10.1002/hep.23337 (2010).
135 Haukeland, J. W. *et al.* Systemic inflammation in nonalcoholic fatty liver disease is characterized by elevated levels of CCL2. *Journal of hepatology* **44**, 1167-1174, doi:10.1016/j.jhep.2006.02.011 (2006).
136 Weisberg, S. P. *et al.* CCR2 modulates inflammatory and metabolic effects of high-fat feeding. *The Journal of clinical investigation* **116**, 115-124, doi:10.1172/JCI24335 (2006).
137 Miura, K., Yang, L., van Rooijen, N., Ohnishi, H. & Seki, E. Hepatic recruitment of macrophages promotes nonalcoholic steatohepatitis through CCR2. *American journal of physiology. Gastrointestinal and liver physiology* **302**, G1310-1321, doi:10.1152/ajpgi.00365.2011 (2012).
138 Baeck, C. *et al.* Pharmacological inhibition of the chemokine CCL2 (MCP-1) diminishes liver macrophage infiltration and steatohepatitis in chronic hepatic injury. *Gut* **61**, 416-426, doi:10.1136/gutjnl-2011-300304 (2012).
139 Tosello-Trampont, A. C., Landes, S. G., Nguyen, V., Novobrantseva, T. I. & Hahn, Y. S. Kuppfer cells trigger nonalcoholic steatohepatitis development in diet-induced mouse model through tumor necrosis factor-alpha production. *The Journal of biological chemistry* **287**, 40161-40172, doi:10.1074/jbc.M112.417014 (2012).
140 Xu, L., Kitade, H., Ni, Y. & Ota, T. Roles of Chemokines and Chemokine Receptors in Obesity-Associated Insulin Resistance and Nonalcoholic Fatty Liver Disease. *Biomolecules* **5**, 1563-1579, doi:10.3390/biom5031563 (2015).
141 Seki, E. *et al.* CCR1 and CCR5 promote hepatic fibrosis in mice. *The Journal of clinical investigation* **119**, 1858-1870 (2009).
142 Kitade, H. *et al.* CCR5 plays a critical role in obesity-induced adipose tissue inflammation and insulin resistance by regulating both macrophage recruitment and M1/M2 status. *Diabetes* **61**, 1680-1690, doi:10.2337/db11-1506 (2012).
143 Wu, H. *et al.* T-cell accumulation and regulated on activation, normal T cell expressed and secreted upregulation in adipose tissue in obesity. *Circulation* **115**, 1029-1038, doi:10.1161/CIRCULATIONAHA.106.638379 (2007).
144 Kirovski, G. *et al.* Hepatic steatosis causes induction of the chemokine RANTES in the absence of significant hepatic inflammation. *International journal of clinical and experimental pathology* **3**, 675-680 (2010).
145 Mantovani, A., Bonecchi, R. & Locati, M. Tuning inflammation and immunity by chemokine sequestration: decoys and more. *Nature reviews. Immunology* **6**, 907-918, doi:10.1038/nri1964 (2006).
146 Pellicoro, A., Ramachandran, P., Iredale, J. P. & Fallowfield, J. A. Liver fibrosis and repair: immune regulation of wound healing in a solid organ. *Nature reviews. Immunology* **14**, 181-194, doi:10.1038/nri3623 (2014).
147 Duffield, J. S. *et al.* Selective depletion of macrophages reveals distinct, opposing roles during liver injury and repair. *The Journal of clinical investigation* **115**, 56-65, doi:10.1172/JCI22675 (2005).
148 Ramachandran, P. *et al.* Differential Ly-6C expression identifies the recruited macrophage phenotype, which orchestrates the regression of murine liver fibrosis. *Proceedings of the National Academy of Sciences of the United States of America* **109**, E3186-3195, doi:10.1073/pnas.1119964109 (2012).
149 Cheng, K., Yang, N. & Mahato, R. I. TGF-beta1 gene silencing for treating liver fibrosis. *Molecular pharmaceutics* **6**, 772-779, doi:10.1021/mp9000469 (2009).

150 Galastri, S. *et al.* Lack of CC chemokine ligand 2 differentially affects inflammation and fibrosis according to the genetic background in a murine model of steatohepatitis. *Clinical science* **123**, 459-471, doi:10.1042/CS20110515 (2012).
151 Brancato, S. K. & Albina, J. E. Wound macrophages as key regulators of repair: origin, phenotype, and function. *The American journal of pathology* **178**, 19-25, doi:10.1016/j.ajpath.2010.08.003 (2011).
152 Dooley, S. & ten Dijke, P. TGF-beta in progression of liver disease. *Cell and tissue research* **347**, 245-256, doi:10.1007/s00441-011-1246-y (2012).
153 Aoyama, T., Inokuchi, S., Brenner, D. A. & Seki, E. CX3CL1-CX3CR1 interaction prevents carbon tetrachloride-induced liver inflammation and fibrosis in mice. *Hepatology* **52**, 1390-1400, doi:10.1002/hep.23795 (2010).
154 Pesce, J. T. *et al.* Arginase-1-expressing macrophages suppress Th2 cytokine-driven inflammation and fibrosis. *PLoS pathogens* **5**, e1000371, doi:10.1371/journal.ppat.1000371 (2009).
155 Karlmark, K. R. *et al.* The fractalkine receptor CX(3)CR1 protects against liver fibrosis by controlling differentiation and survival of infiltrating hepatic monocytes. *Hepatology* **52**, 1769-1782, doi:10.1002/hep.23894 (2010).
156 Thomas, L., Tadayyon, M. & Mark, M. Chronic treatment with the dipeptidyl peptidase-4 inhibitor BI 1356 [(R)-8-(3-amino-piperidin-1-yl)-7-but-2-ynyl-3-methyl-1-(4-methyl-quinazolin-2-yl methyl)-3,7-dihydro-purine-2,6-dione] increases basal glucagon-like peptide-1 and improves glycemic control in diabetic rodent models. *The Journal of pharmacology and experimental therapeutics* **328**, 556-563, doi:10.1124/jpet.108.143966 (2009).
157 Connelly, K. A. *et al.* Dipeptidyl peptidase-4 inhibition improves left ventricular function in chronic kidney disease. *Clinical and investigative medicine. Medecine clinique et experimentale* **37**, E172 (2014).
158 Reagan-Shaw, S., Nihal, M. & Ahmad, N. Dose translation from animal to human studies revisited. *FASEB journal : official publication of the Federation of American Societies for Experimental Biology* **22**, 659-661, doi:10.1096/fj.07-9574LSF (2008).
159 Popov, Y. *et al.* Halofuginone induces matrix metalloproteinases in rat hepatic stellate cells via activation of p38 and NFkappaB. *The Journal of biological chemistry* **281**, 15090-15098, doi:10.1074/jbc.M600030200 (2006).
160 Kleiner, D. E. *et al.* Design and validation of a histological scoring system for nonalcoholic fatty liver disease. *Hepatology* **41**, 1313-1321, doi:10.1002/hep.20701 (2005).
161 Popov, Y., Patsenker, E., Fickert, P., Trauner, M. & Schuppan, D. Mdr2 (Abcb4)-/- mice spontaneously develop severe biliary fibrosis via massive dysregulation of pro- and antifibrogenic genes. *Journal of hepatology* **43**, 1045-1054, doi:10.1016/j.jhep.2005.06.025 (2005).
162 Vizzutti, F. *et al.* Curcumin limits the fibrogenic evolution of experimental steatohepatitis. *Laboratory investigation; a journal of technical methods and pathology* **90**, 104-115, doi:10.1038/labinvest.2009.112 (2010).
163 Standish, R. A., Cholongitas, E., Dhillon, A., Burroughs, A. K. & Dhillon, A. P. An appraisal of the histopathological assessment of liver fibrosis. *Gut* **55**, 569-578, doi:10.1136/gut.2005.084475 (2006).
164 Wynn, T. A. Common and unique mechanisms regulate fibrosis in various fibroproliferative diseases. *The Journal of clinical investigation* **117**, 524-529, doi:10.1172/JCI31487 (2007).
165 Bamboat, Z. M. *et al.* Conventional DCs reduce liver ischemia/reperfusion injury in mice via IL-10 secretion. *The Journal of clinical investigation* **120**, 559-569, doi:10.1172/JCI40008 (2010).
166 Jiao, J. *et al.* Dendritic cell regulation of carbon tetrachloride-induced murine liver fibrosis regression. *Hepatology* **55**, 244-255, doi:10.1002/hep.24621 (2012).
167 Hume, D. A. Macrophages as APC and the dendritic cell myth. *Journal of immunology* **181**, 5829-5835 (2008).

168 Bertola, A. *et al.* Identification of adipose tissue dendritic cells correlated with obesity-associated insulin-resistance and inducing Th17 responses in mice and patients. *Diabetes* **61**, 2238-2247, doi:10.2337/db11-1274 (2012).
169 Kluwe, J. *et al.* Modulation of hepatic fibrosis by c-Jun-N-terminal kinase inhibition. *Gastroenterology* **138**, 347-359, doi:10.1053/j.gastro.2009.09.015 (2010).
170 Carbone, L. J., Angus, P. W. & Yeomans, N. D. Incretin-based therapies for the treatment of nonalcoholic fatty liver disease: A systematic review and meta-analysis. *Journal of gastroenterology and hepatology*, doi:10.1111/jgh.13026 (2015).
171 Collins, S., Martin, T. L., Surwit, R. S. & Robidoux, J. Genetic vulnerability to diet-induced obesity in the C57BL/6J mouse: physiological and molecular characteristics. *Physiology & behavior* **81**, 243-248, doi:10.1016/j.physbeh.2004.02.006 (2004).
172 Koonen, D. P. *et al.* Increased hepatic CD36 expression contributes to dyslipidemia associated with diet-induced obesity. *Diabetes* **56**, 2863-2871, doi:10.2337/db07-0907 (2007).
173 Maurer, M. & von Stebut, E. Macrophage inflammatory protein-1. *The international journal of biochemistry & cell biology* **36**, 1882-1886, doi:10.1016/j.biocel.2003.10.019 (2004).
174 Pi-Sunyer, X. *et al.* A Randomized, Controlled Trial of 3.0 mg of Liraglutide in Weight Management. *The New England journal of medicine* **373**, 11-22, doi:10.1056/NEJMoa1411892 (2015).
175 van Bloemendaal, L., Ten Kulve, J. S., la Fleur, S. E., Ijzerman, R. G. & Diamant, M. Effects of glucagon-like peptide 1 on appetite and body weight: focus on the CNS. *The Journal of endocrinology* **221**, T1-16, doi:10.1530/JOE-13-0414 (2014).
176 Ten Kulve, J. S. *et al.* Liraglutide Reduces CNS Activation in Response to Visual Food Cues Only After Short-term Treatment in Patients With Type 2 Diabetes. *Diabetes care* **39**, 214-221, doi:10.2337/dc15-0772 (2016).
177 Donnelly, K. L. *et al.* Sources of fatty acids stored in liver and secreted via lipoproteins in patients with nonalcoholic fatty liver disease. *The Journal of clinical investigation* **115**, 1343-1351, doi:10.1172/JCI23621 (2005).
178 Conarello, S. L. *et al.* Mice lacking dipeptidyl peptidase IV are protected against obesity and insulin resistance. *Proceedings of the National Academy of Sciences of the United States of America* **100**, 6825-6830, doi:10.1073/pnas.0631828100 (2003).
179 Ben-Shlomo, S. *et al.* Glucagon-like peptide-1 reduces hepatic lipogenesis via activation of AMP-activated protein kinase. *Journal of hepatology* **54**, 1214-1223, doi:10.1016/j.jhep.2010.09.032 (2011).
180 Su, G. L. Lipopolysaccharides in liver injury: molecular mechanisms of Kupffer cell activation. *American journal of physiology. Gastrointestinal and liver physiology* **283**, G256-265, doi:10.1152/ajpgi.00550.2001 (2002).
181 Szabo, G. & Csak, T. Inflammasomes in liver diseases. *Journal of hepatology* **57**, 642-654, doi:10.1016/j.jhep.2012.03.035 (2012).
182 Petrasek, J., Dolganiuc, A., Csak, T., Kurt-Jones, E. A. & Szabo, G. Type I interferons protect from Toll-like receptor 9-associated liver injury and regulate IL-1 receptor antagonist in mice. *Gastroenterology* **140**, 697-708 e694, doi:10.1053/j.gastro.2010.08.020 (2011).
183 Lanthier, N. *et al.* Kupffer cell depletion prevents but has no therapeutic effect on metabolic and inflammatory changes induced by a high-fat diet. *FASEB journal : official publication of the Federation of American Societies for Experimental Biology* **25**, 4301-4311, doi:10.1096/fj.11-189472 (2011).
184 Burgmaier, M. *et al.* Glucagon-like peptide-1 (GLP-1) and its split products GLP-1(9-37) and GLP-1(28-37) stabilize atherosclerotic lesions in apoe(-)/(-) mice. *Atherosclerosis* **231**, 427-435, doi:10.1016/j.atherosclerosis.2013.08.033 (2013).
185 Chang, S. Y. *et al.* Exendin-4 inhibits iNOS expression at the protein level in LPS-stimulated Raw264.7 macrophage by the activation of cAMP/PKA pathway. *Journal of cellular biochemistry* **114**, 844-853, doi:10.1002/jcb.24425 (2013).

186 Zhou, D. *et al.* Macrophage polarization and function with emphasis on the evolving roles of coordinated regulation of cellular signaling pathways. *Cellular signalling* **26**, 192-197, doi:10.1016/j.cellsig.2013.11.004 (2014).
187 Henning, J. R. *et al.* Dendritic cells limit fibroinflammatory injury in nonalcoholic steatohepatitis in mice. *Hepatology* **58**, 589-602, doi:10.1002/hep.26267 (2013).
188 Liaskou, E. *et al.* Monocyte subsets in human liver disease show distinct phenotypic and functional characteristics. *Hepatology* **57**, 385-398, doi:10.1002/hep.26016 (2013).
189 Zimmermann, H. W. *et al.* Functional contribution of elevated circulating and hepatic non-classical CD14CD16 monocytes to inflammation and human liver fibrosis. *PloS one* **5**, e11049, doi:10.1371/journal.pone.0011049 (2010).
190 Shiraishi, D., Fujiwara, Y., Komohara, Y., Mizuta, H. & Takeya, M. Glucagon-like peptide-1 (GLP-1) induces M2 polarization of human macrophages via STAT3 activation. *Biochemical and biophysical research communications* **425**, 304-308, doi:10.1016/j.bbrc.2012.07.086 (2012).
191 Seki, E. *et al.* TLR4 enhances TGF-beta signaling and hepatic fibrosis. *Nature medicine* **13**, 1324-1332, doi:10.1038/nm1663 (2007).
192 Yavrom, S. *et al.* Peroxisome proliferator-activated receptor gamma suppresses proximal alpha1(I) collagen promoter via inhibition of p300-facilitated NF-I binding to DNA in hepatic stellate cells. *The Journal of biological chemistry* **280**, 40650-40659, doi:10.1074/jbc.M510094200 (2005).
193 Tilg, H. *et al.* Anti-tumor necrosis factor-alpha monoclonal antibody therapy in severe alcoholic hepatitis. *Journal of hepatology* **38**, 419-425 (2003).
194 Chitturi, S. & Farrell, G. C. Etiopathogenesis of nonalcoholic steatohepatitis. *Seminars in liver disease* **21**, 27-41 (2001).
195 Parsons, C. J. *et al.* Antifibrotic effects of a tissue inhibitor of metalloproteinase-1 antibody on established liver fibrosis in rats. *Hepatology* **40**, 1106-1115, doi:10.1002/hep.20425 (2004).
196 Imamura, M., Ogawa, T., Sasaguri, Y., Chayama, K. & Ueno, H. Suppression of macrophage infiltration inhibits activation of hepatic stellate cells and liver fibrogenesis in rats. *Gastroenterology* **128**, 138-146 (2005).
197 Larter, C. Z. *et al.* Peroxisome proliferator-activated receptor-alpha agonist, Wy 14,643, improves metabolic indices, steatosis and ballooning in diabetic mice with non-alcoholic steatohepatitis. *Journal of gastroenterology and hepatology* **27**, 341-350, doi:10.1111/j.1440-1746.2011.06939.x (2012).
198 Min, A. K. *et al.* Alpha-lipoic acid attenuates methionine choline deficient diet-induced steatohepatitis in C57BL/6 mice. *Life sciences* **90**, 200-205, doi:10.1016/j.lfs.2011.11.012 (2012).
199 Yoshida, K. & Matsuzaki, K. Differential Regulation of TGF-beta/Smad Signaling in Hepatic Stellate Cells between Acute and Chronic Liver Injuries. *Frontiers in physiology* **3**, 53, doi:10.3389/fphys.2012.00053 (2012).
200 Keller, J. *et al.* Effect of exenatide on cholecystokinin-induced gallbladder emptying in fasting healthy subjects. *Regulatory peptides* **179**, 77-83, doi:10.1016/j.regpep.2012.08.005 (2012).
201 DeFronzo, R. A. *et al.* Effects of exenatide versus sitagliptin on postprandial glucose, insulin and glucagon secretion, gastric emptying, and caloric intake: a randomized, cross-over study. *Current medical research and opinion* **24**, 2943-2952, doi:10.1185/03007990802418851 (2008).
202 Meier, J. J. & Nauck, M. A. Incretin-based therapies: where will we be 50 years from now? *Diabetologia* **58**, 1745-1750, doi:10.1007/s00125-015-3608-6 (2015).
203 Scheen, A. J. Once-weekly DPP-4 inhibitors: do they meet an unmet need? *The lancet. Diabetes & endocrinology* **3**, 162-164, doi:10.1016/S2213-8587(14)70270-0 (2015).
204 Yip, R. G. & Wolfe, M. M. GIP biology and fat metabolism. *Life sciences* **66**, 91-103 (2000).

205 Dardevet, D. *et al.* Insulin-independent effects of GLP-1 on canine liver glucose metabolism: duration of infusion and involvement of hepatoportal region. *American journal of physiology. Endocrinology and metabolism* **287**, E75-81, doi:10.1152/ajpendo.00035.2004 (2004).
206 Seghieri, M. *et al.* Direct effect of GLP-1 infusion on endogenous glucose production in humans. *Diabetologia* **56**, 156-161, doi:10.1007/s00125-012-2738-3 (2013).
207 Panjwani, N. *et al.* GLP-1 receptor activation indirectly reduces hepatic lipid accumulation but does not attenuate development of atherosclerosis in diabetic male ApoE(-/-) mice. *Endocrinology* **154**, 127-139, doi:10.1210/en.2012-1937 (2013).
208 Parlevliet, E. T. *et al.* GLP-1 receptor activation inhibits VLDL production and reverses hepatic steatosis by decreasing hepatic lipogenesis in high-fat-fed APOE*3-Leiden mice. *PloS one* **7**, e49152, doi:10.1371/journal.pone.0049152 (2012).
209 Hermansen, K. *et al.* Liraglutide suppresses postprandial triglyceride and apolipoprotein B48 elevations after a fat-rich meal in patients with type 2 diabetes: a randomized, double-blind, placebo-controlled, cross-over trial. *Diabetes, obesity & metabolism* **15**, 1040-1048, doi:10.1111/dom.12133 (2013).
210 Ben-Shlomo, S. *et al.* Dipeptidyl peptidase 4-deficient rats have improved bile secretory function in high fat diet-induced steatosis. *Digestive diseases and sciences* **58**, 172-178, doi:10.1007/s10620-012-2353-7 (2013).
211 Smit, J. J. *et al.* Homozygous disruption of the murine mdr2 P-glycoprotein gene leads to a complete absence of phospholipid from bile and to liver disease. *Cell* **75**, 451-462 (1993).
212 Fickert, P. *et al.* Ursodeoxycholic acid aggravates bile infarcts in bile duct-ligated and Mdr2 knockout mice via disruption of cholangioles. *Gastroenterology* **123**, 1238-1251 (2002).
213 Jacquemin, E. Role of multidrug resistance 3 deficiency in pediatric and adult liver disease: one gene for three diseases. *Seminars in liver disease* **21**, 551-562, doi:10.1055/s-2001-19033 (2001).
214 Fickert, P. *et al.* Regurgitation of bile acids from leaky bile ducts causes sclerosing cholangitis in Mdr2 (Abcb4) knockout mice. *Gastroenterology* **127**, 261-274 (2004).